AN EFFICIENT METHOD FOR FUNDAMENTAL FREQUENCY ESTIMATION OF PERIODIC SIGNALS WITH HARMONICS

A THESIS SUBMITTED TO
THE GRADUATE SCHOOL OF NATURAL AND APPLIED SCIENCES
OF
MIDDLE EAST TECHNICAL UNIVERSITY

BY

UTKU ÇELEBİ

IN PARTIAL FULFILLMENT OF THE REQUIREMENTS
FOR
THE DEGREE OF MASTER OF SCIENCE
IN
ELECTRICAL AND ELECTRONICS ENGINEERING

AUGUST 2020

Approval of the thesis:

AN EFFICIENT METHOD FOR FUNDAMENTAL FREQUENCY ESTIMATION OF PERIODIC SIGNALS WITH HARMONICS

submitted by **UTKU ÇELEBİ** in partial fulfillment of the requirements for the degree of **Master of Science in Electrical and Electronics Engineering Department, Middle East Technical University** by,

Prof. Dr. Halil Kalıpçılar
Dean, Graduate School of **Natural and Applied Sciences** ______________

Prof. Dr. İlkay Ulusoy
Head of Department, **Electrical and Electronics Engineering** ______________

Prof. Dr. Çağatay Candan
Supervisor, **Electrical and Electronics Engineering, METU** ______________

Examining Committee Members:

Prof. Dr. Orhan Arıkan
Electrical and Electronics Engineering, Bilkent University ______________

Prof. Dr. Çağatay Candan
Electrical and Electronics Engineering, METU ______________

Prof. Dr. Umut Orguner
Electrical and Electronics Engineering, METU ______________

Prof. Dr. Tolga Mete Duman
Electrical and Electronics Engineering, Bilkent University ______________

Assist. Prof. Dr. Gökhan Muzaffer Güvensen
Electrical and Electronics Engineering, METU ______________

Date: ______________

I hereby declare that all information in this document has been obtained and presented in accordance with academic rules and ethical conduct. I also declare that, as required by these rules and conduct, I have fully cited and referenced all material and results that are not original to this work.

Name, Surname: Utku Çelebi

Signature :

ABSTRACT

AN EFFICIENT METHOD FOR FUNDAMENTAL FREQUENCY ESTIMATION OF PERIODIC SIGNALS WITH HARMONICS

Çelebi, Utku

M.S., Department of Electrical and Electronics Engineering

Supervisor: Prof. Dr. Çağatay Candan

August 2020, 100 pages

A computationally efficient method for the fundamental frequency estimation of a group of harmonically related complex sinusoids is given. To this aim, an efficient frequency estimation method for single tone complex sinusoids is adapted to the harmonic frequency estimation problem. The main idea of the suggested Fast Fourier Transform based method is the frequency estimation of individual complex sinusoids after the removal of the interference due to other harmonics. After several iterations of estimation and interference cancellation, the frequency estimates of each harmonic component are fused to obtain the fundamental frequency estimate. In addition to this, the model order selection, that is the estimation of the number of harmonics, is also discussed. The proposed method is applied on the direction of arrival problem for a single far-field source with harmonics. A theoretical study of the suggested scheme and its verification by computer experiments are provided.

Keywords: Frequency estimation, Pitch frequency estimation, Fundamental frequency estimation, Periodic signals.

ÖZ

HARMONİK İŞARETLERİN HASSAS TEMEL FREKANS KESTİRİMİ İÇİN DÜŞÜK İŞLEM YÜKLÜ BİR YÖNTEM

Çelebi, Utku

Yüksek Lisans, Elektrik ve Elektronik Mühendisliği Bölümü

Tez Yöneticisi: Prof. Dr. Çağatay Candan

Ağustos 2020 , 100 sayfa

Harmonik ilişkili bir grup karmaşık sinüzoidin temel frekansının kestirimi için düşük hesaplama yüküne sahip bir yöntem verilmektedir. Bu amaç doğrultusunda, tek tonlu sinüzoidlerin frekans kestirimi problemi için geliştirilen bir yöntem harmonik duruma uyarlanmaktadır. Önerilen Hızlı Fourier Dönüşümü tabanlı yöntemin ana fikri, karmaşık sinüzoidlerin birbirleri üzerine girişimlerini ortadan kaldırarak, her bir karmaşık sinüzoidin frekansını ayrı ayrı kestirmek ve bu sonuçlarını birleştirerek temel frekans kestirimi elde etmektir. Buna ek olarak, harmonik sayısının kestirimi problemine de değinilmiştir. Önerilen yöntem, uzak alandaki kaynağın harmonikleri ile birlikte gözlemlendiği durumda, yön bulma problemi üzerinde uygulanmıştır. Önerilen kestiricinin başarımı kuramsal olarak incelenmiş ve benzetim sonuçlarıyla doğrulanmıştır.

Anahtar Kelimeler: Frekans kestirim, Temel frekans kestirimi, Periyodik işaretler.

To my loved ones.

ACKNOWLEDGMENTS

I want to thank my supervisor Çağatay Candan, for his endless support and guidance. He always provided me with his time and interest. I did see him trying to help me when I needed, even in the situations that are out of his responsibilities. I am grateful, and very glad to have him as the supervisor of my thesis.

I want to thank my mother and my friends Esen Özbay and Özlem Tuğfe Demir for always listening, helping and supporting me.

I want to thank the Scientific and Technological Research Council of Turkey (TÜBİTAK) through the financial support they provided through 2210-A National Scholarship Programme for MSc Students.

TABLE OF CONTENTS

LIST OF TABLES

TABLES

LIST OF FIGURES

FIGURES

LIST OF ALGORITHMS

ALGORITHMS

LIST OF ABBREVIATIONS

ABBREVIATIONS	
ACRB	Asymptotic Cramer-Rao Bound
AIC	Akaike Information Criteria
ALB	Approximate Lower Bound
CRB	Cramer-Rao Bound
DFT	Discrete Fourier Transform
DOA	Direction of Arrival
DTFT	Discrete-Time Fourier Transform
ESPRIT	Estimation of Signal Parameters via Rotational Invariance Technique
EVD	Eigenvalue Decomposition
FFT	Fast Fourier Transform
FIM	Fisher Information Matrix
HCRB	Hybrid Cramer-Rao Bound
HMUSIC	Harmonically Constrained MUSIC
MDL	Minimum Description Length Criterion
MLE	Maximum Likelihood Estimation
MSE	Mean Squared Error
MUSIC	Multiple Signal Classification
PDF	Probability Density Function
PSNR	Pseudo Signal to Noise Ratio
RMSE	Root Mean Square Error
SNR	Signal to Noise Ratio
SVD	Singular Value Decomposition

ULA	Uniform Linear Array

CHAPTER 1

INTRODUCTION

The topic of this thesis is the fundamental frequency estimation of periodic signals observed under additive white Gaussian noise. Frequency estimation problem is of major concern in many applications such as spectrum estimation, radar signal processing, direction of arrival estimation, speech processing and more [1]. The frequency estimation problem can be posed either for the complex exponential signal ($Ae^{j(\omega n+\phi)}$) or real-valued sinusoids ($A\cos(\omega n + \phi)$). The complex exponential signals arise as the low-pass equivalent of band-pass signals and heavily utilized in radar signal processing (Doppler frequency shift estimation), direction of arrival estimation (spatial frequency estimation) and spectrum estimation problems. The real-valued sinusoids can be considered as the time-domain samples of a periodic signal without any downconversion operation. Real-valued sinusoids arise in speech/music processing, underwater acoustics, instrumentation and measurement problems such as analog-to-digital converter (ADC) testing, waveform generators etc. Although both problems are similar, the frequency estimators for real-valued sinusoids are not, in general, straightforward extensions of the ones for complex exponentials. In this thesis, our focus is taking one more step in this line of research and examining the fundamental frequency estimation of periodic signal with several harmonics. Our goal is to develop frequency estimators for periodic signals which are efficient both in the computational sense and also in the statistical sense, i.e. operating close to the Cramer-Rao performance lower bound.

Before delving into the specifics of the problem, we would like to provide some general information on topics related with estimation theory. Statistical signal processing can be defined as the useful information retrieval from noisy observations. The input, that is the observed signal, is distorted by noise due to natural sources, such as the thermal noise, or due to man-made sources. The noise term is stochastically modelled; while the signal or parameter of interest can be non-random (deterministic) or random. There are various approaches for both non-random parameter estimation or random-parameter (Bayesian) estimation which differ from each other in computational complexity and estimation accuracy.

The maximum likelihood (ML) estimator is a well known non-random parameter estimation method. ML estimator is known to be asymptotically efficient, i.e. asymptotically achieves the Cramer Rao Lower Bound (CRB). For the frequency estimation problem, the ML estimator for the complex-exponential model is simply the peak detector in the Discrete-Time Fourier Transform (DTFT) magnitude spectrum of the input; when the input is assumed to be observed under white Gaussian noise [2]. In practice, the DTFT samples are calculated by using the Discrete Fourier Transform (DFT). For multiple sinusoidal sources with unknown frequencies, the frequency estimation problem becomes a peak detection (the likelihood maxima) via a multi-dimensional search. The complexity of a multi-dimensional search is exponentially increasing in the number of dimensions and, in general, prohibitively complex. One of major goals is to develop frequency estimators (spectrum estimators) with a good performance at a reasonable complexity. ML estimators are generally considered as the performance benchmark. Their efficient implementation or the development of reduced complexity ML-like estimators is an ever-present goal of signal processing applications. We also note that in spite of their benchmark status, but the optimality of ML estimator is only asymptotically valid.

In addition to the ML estimator, there are several sub-spaced based methods which try to make use of the auto-correlation matrix of the input for the spectrum estimation. These methods decompose the signal into noise/signal space via eigenvalue decomposition (EVD) or singular value decomposition (SVD). These methods are sub-optimal; but computationally less demanding. A major drawback of these methods is their need of autocorrelation matrix; hence the problem of auto-correlation matrix estimation arises for their usage. The most well known sub-space methods are ESPRIT (Estimation of Signal Parameters via Rotational Invariance Technique) [3] and MUSIC (Multiple Signal Classification) [4]. Their main advantage is their ability to resolve multiple sources with a slight increase in computation complexity.

In recent years, computationally efficient frequency estimation methods are proposed for single tone complex exponentials [5–14]. The performance of these estimators are as good as MLE and their computation load is very low. These methods, also called fine frequency estimation techniques, are based on the DFT domain representation of the input signal and developing an invariant function to the nuisance parameters of the problem, which are the amplitude and phase of the complex exponential for the problem of interest [15]. The first stage of fine frequency estimators is the coarse frequency estimation by finding the peak location over a coarse grid in the DTFT spectra. Then, in the second stage, the fine frequency estimation is made by using an invariant function. In the fine frequency estimation stage, two/three DFT samples calculated in the first stage are used as the input of the invariant function. The main computational burden of methods in this class is the DFT calculation in the first stage. Hence, these estimators are considered to have very low implementation complexity.

The fine frequency estimation of the real-valued sinusoids, that is the development of similar low complexity estimators, is a bit more complicated. A real-valued sinusoid is composed of two complex valued sinusoids ($\cos(\omega n + \phi) = (e^{j(\omega n+\phi)} + e^{-j(\omega n+\phi)})/2$) and in DFT domain, the interference of each complex exponential on the other one complicates the problem. Fine frequency estimation methods are much more abundant for the complex exponential case in the literature. To convert the real valued frequency estimation problem to its complex exponential counterpart, some iterative interference cancellation procedures are developed [16, 17]. These procedures are based on iteratively estimating the frequency and then removing the interference term and repeating the frequency estimation with interference removed or reduced input. This approach is also related to the RELAX algorithm [18] and can also be applied when multiple complex sinusoids are observed.

In this thesis, the main topic is the frequency estimation of periodic signals with multiple harmonics. More specifically, the fundamental frequency estimation (also called pitch estimation) of a group of harmonically related sinusoids is the main goal. Fundamental frequency estimation is used in many applications, e.g, tuning of the musical instruments, classification and identifications of the audio based signals, separation of the signals coming from different sources, transcription of the recorded music, etc. An important reference on this topic is the book titled Multi-Pitch Estimation [19]. The ML estimator with different implementations are available in the literature [20–22]. Methods based on the autocorrelation function of the input, filtering methods [23–25] and subspace methods [26, 27] are proposed. The most well known subspace based methods are MUSIC [28–30] and ESPRIT [31–33]. All of these methods require computationally demanding operations such as grid search, autocorrelation matrix estimation, eigenvalue value decomposition etc. Also, in recent studies, atomic norm techniques [34–38] that utilize the sparsity of the superimposed sinusoidal signals are proposed for the frequency estimation and the main goal is to get optimal frequency estimates by resolving grid mismatch problem. Frequency estimation methods based on the atomic norm optimization are also called gridless frequency estimation methods in the literature. These methods are in principle similar to the methods studied in this thesis; yet, they require orders of magnitude (more than 100 folds) more computation than the methods called as low-complexity methods in this thesis. Hence, in this study, we don't go into detail about atomic norm denoising concept, since this topic is not the subject of this study. However, in Appendix B, brief discussion about the computational complexity of atomic norm based methods together with one of the successful fine frequency estimators (AM algorithm [8]) is given. Simply, in this thesis work, our goal is to extend the low complexity fine frequency methods given for the complex exponentials to the fundamental frequency estimation problem.

For the fundamental frequency estimation problem, a viable approach is using the successive interference cancellation procedures along with conventional fine-frequency estimators for the complex exponential signals. We follow this approach in this study, that is the frequencies of harmonically related complex exponentials are estimated individually after successively eliminating the interference due to other harmonics. The individual estimates are fused to get a final estimate. Also, the case when the number of harmonics is not known a-priori is also examined through a model order estimation formulation. Finally, an application of the fundamental frequency estimation to the fundamental *spatial* frequency estimation is given within the context of direction of arrival (DOA) estimation of periodic signals.

1.1 The Outline of the Thesis

In Chapter 2, the system model is described and some preliminary information on single tone frequency estimation with complex exponentials is given. In Section 2.4, the motivation for the fine frequency estimation methods is explained and an analysis for a well-known fine frequency estimation method in the literature, namely Aboutanios-Mulgrew (AM) method, [8] is given.

In Chapter 3, the fundamental frequency estimation problem is studied. Joint estimation of fundamental frequency and model order (total number of harmonics) is discussed. In Section 3.5, the proposed method is given.

In Chapter 4, the proposed method is applied on the direction of arrival problem with a uniform linear array. The problem is the angular localization of a single source with harmonics in a multipath-free environment. The advantages of utilizing higher other harmonics in the direction of arrival problem are studied.

In Chapter 5, the numerical comparisons of the proposed method with other methods are given. The performance of the method with and without model order selection (known model order) is investigated for different scenarios. Results for the directional of arrival estimation application are given.

1.2 Contributions

The following are the publications related with the thesis study:

- U. Celebi and C. Candan, "A computationally efficient fine frequency estimation method for harmonic signals" in 2020 28th Signal Processing and Communications Applications Conference (SIU), pp. 1–4, 2020. [39]

- C. Candan and U. Çelebi, "Invariant function approach for gridless and non-iterative maximum likelihood parameter estimation and its application to frequency estimation of real-valued sinusoids" Elsevier Signal Processing (under review), 2020. [15]

In addition, the following is the list of analysis results on the AM method [8]:

- Section 2.5.1 Number of Iterations to Reach Cramer-Rao Bound,
- Section 2.5.2 Approximate MSE Lower Bound and Gross Error Analysis,
- Section 2.5.3 Asymptotic MSE Analysis at High SNR.

The analysis of AM method given in Sections 2.5.1, 2.5.2 and 2.5.3 are alternative derivations of the results given in the AM paper [8, 16]. The final results of the presented derivations agree with earlier findings and they are easier to utilize.

CHAPTER 2

FREQUENCY ESTIMATION OF COMPLEX EXPONENTIALS

This chapter presents the problem of frequency estimation for complex exponential signals. The chapter is organized as follows: In Section 2.1, some preliminary definitions are given. In Section 2.2, the maximum likelihood estimator, which is the benchmark estimator, for the problem is given. In Section 2.3, the Cramer-Rao lower bound for the problem is given and some discussions on the limitations of the grid-search based estimators is discussed. In Section 2.4, a class of low complexity estimators, known as fine frequency estimators, are described. Finally, a theoretical analysis of Aboutanios-Mulgrew (AM), a member of fine frequency estimators class, is given in Section 2.5. Theoretical results given in this section are utilized in the next chapter on the fundamental frequency estimation problem.

2.1 Preliminaries

A complex sinusoid signal of unknown amplitude, phase and frequency is observed under white complex Gaussian noise:

$$r[n] = Ae^{j(2\pi f n+\phi)} + w[n], \quad n = \{0, \dots, N-1\}. \tag{2.1}$$

where N is number of samples, A and ϕ are the amplitude and the phase of the complex sinusoid signal. The frequency variable f in equation (2.1) is the normalized frequency defined in $[0, 1)$ and can be expressed as $f = \frac{(k_p+\delta)}{N}$ in terms of N-point DFT bins where k_p is an integer in $[0, N-1]$ and δ is a real number in $(-0.5, 0.5)$. It is assumed that noise $w[n]$ is circularly symmetric white complex Gaussian distributed noise with zero mean and σ_w^2 variance, $w[n] \sim \mathcal{CN}(0, \sigma_w^2)$. The signal-to-noise ratio (SNR) is A^2/σ_w^2.

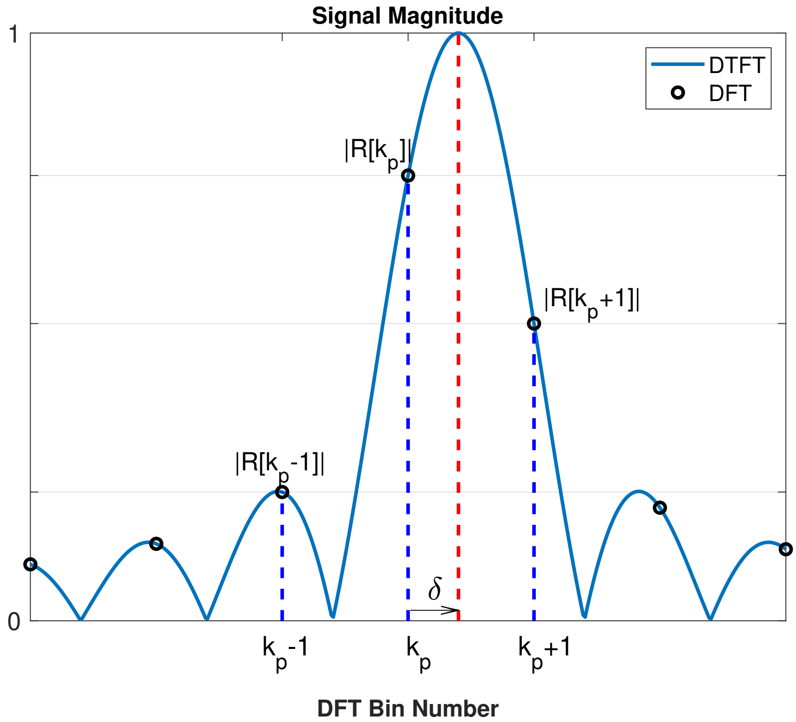

Figure 2.1: Magnitude DTFT and DFT magnitude spectrum of the complex sinusoidal signal with frequency $\omega = \frac{2\pi(k_p+\delta)}{N}$.

The N-point DFT of the input is,

$$\begin{aligned}
R[k] =& \sum_{n=0}^{N-1} r[n] e^{-\frac{j2\pi kn}{N}}, \\
=& Ae^{j\phi} \frac{1 - e^{j2\pi(k_p - k + \delta)}}{1 - e^{j\frac{2\pi}{N}(k_p - k + \delta)}} + W[k], \\
=& Ae^{j\phi} e^{j\frac{\pi}{N}(k_p - k + \delta)(N-1)} \frac{\sin(\pi(k_p - k + \delta))}{\sin(\frac{\pi}{N}(k_p - k + \delta))} + W[k],
\end{aligned} \tag{2.2}$$

where $W[k] = \sum_{n=0}^{N-1} w[n] e^{-\frac{j2\pi kn}{N}}$ and $k = 0, \ldots, N-1$. In Figure 2.1, DTFT and DFT magnitude spectrum of the complex sinusoidal signal with frequency $\frac{2\pi(k_p+\delta)}{N}$ are shown. We know that N-point DFT of a signal corresponds to the sampled version of its continuous DTFT spectra. As the DFT size N increases, the DFT spectra approaches to the DTFT result. Also, when δ is equal to zero, the DFT samples are all zero except the value at the DFT bin with the index $k = k_p$. The statistical characterization of the noise term after DFT operation, $W[k]$, can be given as follows,

$$
\begin{aligned}
E\{W[l]W[m]\} &= E\left\{\sum_{n=0}^{N-1}\left(e^{-\frac{j2\pi ln}{N}}w[n]\right)\sum_{q=0}^{N-1}\left(e^{-\frac{j2\pi mq}{N}}w[q]\right)\right\}, \\
&= \sum_{n=0}^{N-1} e^{-\frac{j2\pi(l+m)n}{N}} E\{w^2[n]\} = 0.
\end{aligned} \tag{2.3}
$$

$$
\begin{aligned}
E\{W[l]W^*[m]\} &= E\left\{\sum_{n=0}^{N-1}\left(e^{-\frac{j2\pi ln}{N}}w[n]\right)\sum_{q=0}^{N-1}\left(e^{\frac{j2\pi mq}{N}}w^*[q]\right)\right\}, \\
&= \sum_{n=0}^{N-1} e^{-\frac{j2\pi(l-m)n}{N}} E\{|w[n]|^2\}, \\
&= N\sigma_w^2\delta[l-m].
\end{aligned} \tag{2.4}
$$

where (l, m) are integers in the range of $[0, N-1]$. We should note that $E\{w^2[n]\} = E\{a^2 + 2jab - b^2\} = 0$ where a is the real part and the b is the imaginary part of the noise term $\omega[n]$. It is important to note that after DFT operation the noise term keeps its white Gaussian properties, that is $W[k] \sim \mathcal{CN}(0, N\sigma_w^2)$; since DFT is a linear operation, that is DFT operation can be represented with an unitary matrix $\mathbf{S}_{N\times N}$ and $\mathbf{SS}^H = N\mathbf{I}_{N\times N}$. In equation (2.4), the terms l, m can have non-integer values and as long as their difference is an integer. Note that, when the difference $l-m$ is a non-zero integer, two random variables $W[l]$ and $W[m]$ are independent.

The expression in (2.3) isn't the conventional representation of the second order characteristic of the random variables. However, by using this expressions in (2.3) and (2.4), we can show that real and imaginary parts of given random terms are independent when the difference $l-m$ is a non-zero integer. In [40], more detailed information about the circularly symmetry properties of the vectors generated by the jointly Gaussian random variables and the statistical properties of real and the imaginary parts of these random variables are given. Simply, the following derivation results are important while analyzing the MSE of the AM algorithm in Section 2.5.3.

$$
\begin{aligned}
E\Big\{ \text{Real}\{W[l]\}\,\text{Real}\{W[m]\} \Big\} &= E\left\{\frac{W[l]+W^*[l]}{2}\frac{W[k]+W^*[k]}{2}\right\}, \\
&= \frac{N}{2}\sigma_w^2\delta[l-m].
\end{aligned} \tag{2.5}
$$

$$E\{ \text{Imag}\{W[l]\} \text{Imag}\{W[m]\} \} = E\left\{\frac{W[l]-W^*[l]}{2j}\frac{W[k]-W^*[k]}{2j}\right\}, \\ = \frac{N}{2}\sigma_w^2\delta[l-m]. \tag{2.6}$$

$$E\{ \text{Real}\{W[l]\} \text{Imag}\{W[m]\} \} = E\left\{\frac{W[l]+W^*[l]}{2}\frac{W[k]-W^*[k]}{2j}\right\}, \\ = 0. \tag{2.7}$$

2.2 Maximum Likelihood Estimation (MLE)

The main idea of MLE is to maximize the value of probability density function (pdf) evaluated at the observation vector (the likelihood) over its non-random unknown parameters, (see equation (2.1)). In this context, the parameters of the sinusoid are considered as deterministic unknowns; hence, noise is the only random term. The maximum likelihood estimate of non-random signal parameters is shown with vector $\widehat{\boldsymbol{\psi}} = [\widehat{A}\ \widehat{f}\ \widehat{\phi}]^T$ and $\widehat{\boldsymbol{\psi}}$ maximizes the joint distribution function of observations, that is $p(\mathbf{r};\boldsymbol{\psi})$ for a given $\mathbf{r}$. For white complex Gaussian noise case with zero mean and σ_w^2 variance, the joint distribution function of observations in (2.1) can be given as,

$$p(\mathbf{r};\boldsymbol{\psi}) = \frac{1}{(\pi\sigma_w^2)^N}\exp\left[-\frac{1}{\sigma_w^2}\sum_{n=0}^{N-1}|r[n]-Ae^{j(2\pi f+\phi)}|^2\right]. \tag{2.8}$$

and for the maximum likelihood estimation, simply, we can minimize

$$J(A,f,\phi) = \sum_{n=0}^{N-1}|r[n]-Ae^{j(2\pi f+\phi)}|^2. \tag{2.9}$$

It is well known that the maximum likelihood (ML) estimates of the parameters of the complex sinusoid are [2],

$$\begin{aligned} \widehat{f} &= \arg\max_f \left|\sum_{n=0}^{N-1} r[n]e^{-j2\pi fn}\right|^2, \\ \widehat{A} &= \frac{1}{N}\left|\sum_{n=0}^{N-1} r[n]e^{-j2\pi\widehat{f}n}\right|^2, \\ \widehat{\phi} &= \arctan\frac{\text{Imag}(\sum_{n=0}^{N-1} r[n]e^{-j2\pi\widehat{f}n})}{\text{Real}(\sum_{n=0}^{N-1} r[n]e^{-j2\pi\widehat{f}n})}. \end{aligned} \tag{2.10}$$

As can be seen from (2.10), the maximum likelihood frequency estimate is the peak location of the DTFT spectra (see Figure 2.1) where f is a real number in the range $[0, 1)$ and estimates of amplitude and the phase follow from simple calculations given the frequency estimate. Clearly, a poor frequency estimate affects the estimation accuracy of other parameters. However the periodogram samples calculated via DFT can be computationally demanding in some scenarios. Typically, M-point DFT is required to achieve a frequency resolution of $1/M$. This may lead to a dramatic increase in the number of DFT points to reach the Cramer-Rao bound (CRB) at high SNR. As an example, to achieve the accuracy of $1/(100 \times N)$, at least $100 \times N$-point DFT calculations are needed. We would like to remind that the achievable accuracy is lower bounded by CRB and this bound can be utilized to set the search grid a-priori, given the operational SNR.

Some specific DFT implementations such as the chirp z-transformation can be utilized to reduce the DFT calculation complexity, [41, p.780-785]. Yet, even with chirp z-transform implementation, the maximization takes place over a grid with granularity and eventually suffers from high complexity as SNR increases. An alternative to grid-search is the usage of Newton-Raphson type, that is the general purpose numerical optimization routines for the likelihood maximization. In fact, the suggested computationally efficient fine-frequency estimators in this thesis can be considered as very specific implementation of Newton-Raphson type estimators for the frequency estimation problem.

2.3 Cramer-Rao Bound (CRB)

The Cramer-Rao Bound (CRB) is a lower bound on the mean square error of an unbiased estimate of a non-random parameter, [2]. It is derived by the calculation of Fisher information matrix, followed by its inversion. The parameter vector is $\boldsymbol{\psi} = [A\ f\ \phi]^T$. The elements of the Fisher information matrix can be written as,

$$\begin{aligned} \mathbf{I}[\boldsymbol{\psi}]_{ij} &= -\,\mathbb{E}\left[\frac{\partial^2 \ln p(\mathbf{r};\boldsymbol{\psi})}{\partial \boldsymbol{\psi}_i \partial \boldsymbol{\psi}_j}\right], \\ &= \frac{2}{\sigma_w^2}\,\mathrm{Real}\left[\sum_{n=0}^{N-1}\left(\frac{\partial A e^{j(2\pi f n+\phi)}}{\partial \psi_i}\right)^* \frac{\partial A e^{j(2\pi f n+\phi)}}{\partial \psi_j}\right], \end{aligned} \tag{2.11}$$

where ψ_i is the i'th element of the vector $\boldsymbol{\psi}$ and $\mathbb{E}(x)$ represents the expected value of a random variable, x. The result in (2.11) is the simplified version of the Fisher information matrix valid for the Gaussian case [2].

The Fisher information matrix for the frequency estimation problem can be explicitly written as,

$$\mathbf{I}[\boldsymbol{\psi}] = \frac{2}{\sigma_w^2}\begin{bmatrix} N & 0 & 0 \\ 0 & A^2\sum_0^{N-1}(2\pi n)^2 & A^2\sum_0^{N-1}2\pi n \\ 0 & A^2\sum_0^{N-1}2\pi n & NA^2 \end{bmatrix}, \tag{2.12}$$

where A is the amplitude, f is the frequency and ϕ is the phase. As noted in [2, p.57], upon the inversion of the Fisher information matrix, the 2nd row and 2nd column entry becomes the CRB of the frequency estimates.

The Cramer Rao Lower Bounds (CRB) of these parameters are,

$$\begin{aligned} \mathrm{var}(\widehat{f}) &\geq \mathbf{I}^{-1}[\boldsymbol{\psi}]_{22} = \frac{6}{(2\pi)^2 N(N^2-1)\mathrm{SNR}}, \\ \mathrm{var}(\widehat{A}) &\geq \mathbf{I}^{-1}[\boldsymbol{\psi}]_{11} = \frac{\sigma_w^2}{2N}, \\ \mathrm{var}(\widehat{\phi}) &\geq \mathbf{I}^{-1}[\boldsymbol{\psi}]_{33} = \frac{2N-1}{N(N+1)\mathrm{SNR}}. \end{aligned} \tag{2.13}$$

Throughout the thesis work, the main parameter to be estimated is the frequency in terms of DFT bin $(k_p + \delta)$. More specifically, the frequency $2\pi f$ in (2.1) corresponds to the radial frequency with the units of radians per sample. The variable $f \in [0, 1)$ is the normalized frequency. If the number of observations is given as N as in (2.1), then $f = \frac{(k_p+\delta)}{N}$ and $(k_p + \delta) \in [0, N)$ is the frequency in DFT bins.

To convert CRB to the unit of DFT bins, we need to multiply the expression in (2.13) with N^2. Therefore, the CRB of the frequency in terms of DFT bins can be written as $N^2\mathbf{I}^{-1}[\boldsymbol{\psi}]_{22} = \frac{6N}{(2\pi)^2(N^2-1)\mathrm{SNR}}$.

Also, to compare the performance of the estimators, the root mean squared error

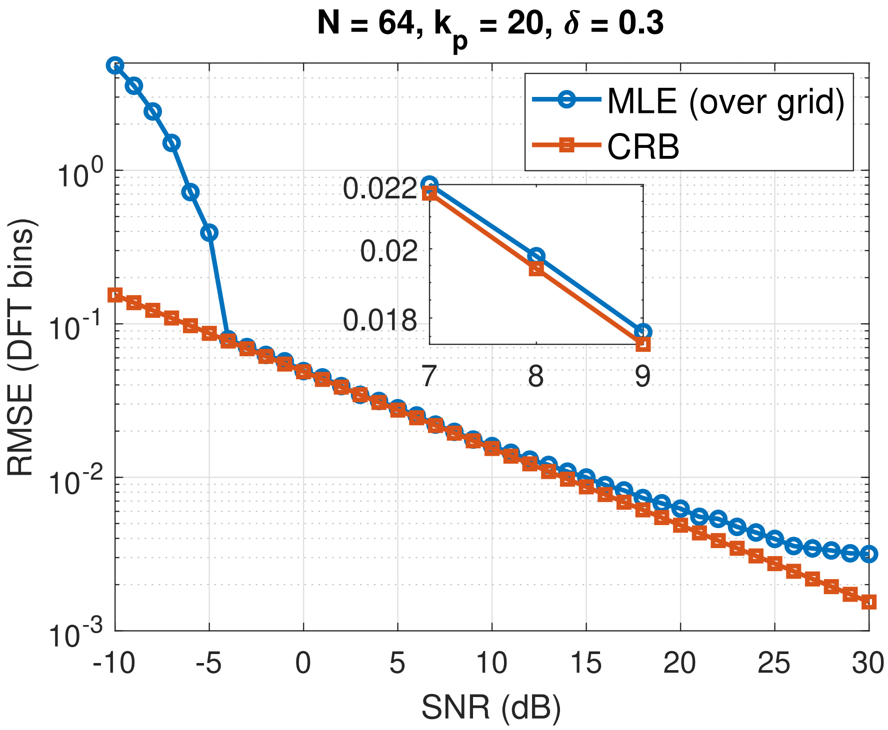

Figure 2.2: RMSE vs SNR plot for MLE with frequency $\omega = \frac{2\pi(20+0.3)}{64}$.

(RMSE) is estimated via Monte Carlo simulations as follows,

$$\text{RMSE} = \sqrt{\frac{1}{\text{\#trials}} \sum_{t=1}^{\text{\#trials}} (\text{true frequency} - \text{estimated-frequency-at-}i\text{'th-trial})^2}. \tag{2.14}$$

Here, true and estimated frequencies are also expressed in terms of DFT bins and RMSE result is compared with the square root of the CRB expression $\sqrt{\frac{6N}{(2\pi)^2(N^2-1)\text{SNR}}}$.

Next, we focus on the relation between the MLE and CRB of the complex sinusoids. The MLE results in (2.10) are asymptotically efficient which means the performance of the estimator reaches the CRB when the number of samples N goes to infinity. In Figure 2.2, performance of the ML estimator is presented with $N = 64$ samples for the frequency of $f = \frac{20+0.3}{64}$. In this example, the DFT size for the MLE is 2^{13} which corresponds to the precision of the grid search, that is the resolution of the frequency estimate, $(\triangle f = 1/2^{13})$.

At low SNR region, there is little information due to strong noise, therefore detection of the peak at the true DFT bin k_p becomes more difficult. In this example (Figure 2.2), the selected grid with 2^{13} points in $[0, 1)$ interval remains applicable until a threshold SNR around 12 dB. However, it is clear that the grid spacing should be reduced as SNR increases to continue tracking the CRB. Otherwise, estimator faces an error-floor due to poor grid spacing. However, from the viewpoint of computational complexity, it may not be easy to increase the number of grid points. For example, in Figure 2.2, CRB is equal to 3×10^{-3} at around 25 dB SNR in terms of DFT bins. To achieve the CRB, the grid spacing should be selected smaller than 3×10^{-3}. Let's choose the grid spacing as $3 \times 10^{-3}/2$ and since $N = 64$, total number of grids needed in this example is $\frac{64}{3\times10^{-3}/2} = 42667$. For higher SNR values, this number increases dramatically. Knowing that the computational cost of the N'-point FFT calculation is in the order of $N' \log_2 N'$ (for the given example $N' = 42667$), computational complexity of MLE increases significantly to achieve the CRB.

Let's assume that the grid spacing is N/N' in terms of DFT bins, that is N'-point DFT is evaluated. If the true frequency value is at around the mid point of two consecutive DFT samples, we know that the frequency resolution of the ML estimator is not enough to get an accurate estimate and bias term arises in the estimation. This bias term can be written as,

$$\text{bias}^2 = (\delta')^2 = \left(k_p + \delta - \text{floor}\left((k_p + \delta)\frac{N'}{N}\right)\frac{N}{N'}\right)^2. \tag{2.15}$$

If $N' = N$, it is easy to see that the expression in (2.15) is δ^2. For different numbers of N', the difference between the true frequency and the DFT sample with the largest magnitude is called δ' and it can be calculated as in equation (2.15). Intuitively, if $N' > N$, we can get a DFT sample closer to the true frequency and we get smaller error floor $(\delta' < \delta)$.

Now, we know that for high SNR values, the performance of the MLE is restricted by the frequency resolution. If the CRB value is as much as grid spacing, we take the effect of the bias as negligible. Using this simple reasoning, we can write the following relation to find a SNR threshold so that ML estimator performs optimal (reaches CRB) without suffering from bias:

$$\text{var}(\widehat{f}N) = \frac{6}{(2\pi)^2 N \text{SNR}_T} = \frac{N^2}{(N')^2} \rightarrow \text{SNR}_T = \frac{3(N')^2}{2\pi^2 N^3}. \tag{2.16}$$

Figures 2.3 and 2.4 illustrates the performance of MLE with $N = 32$ samples for the

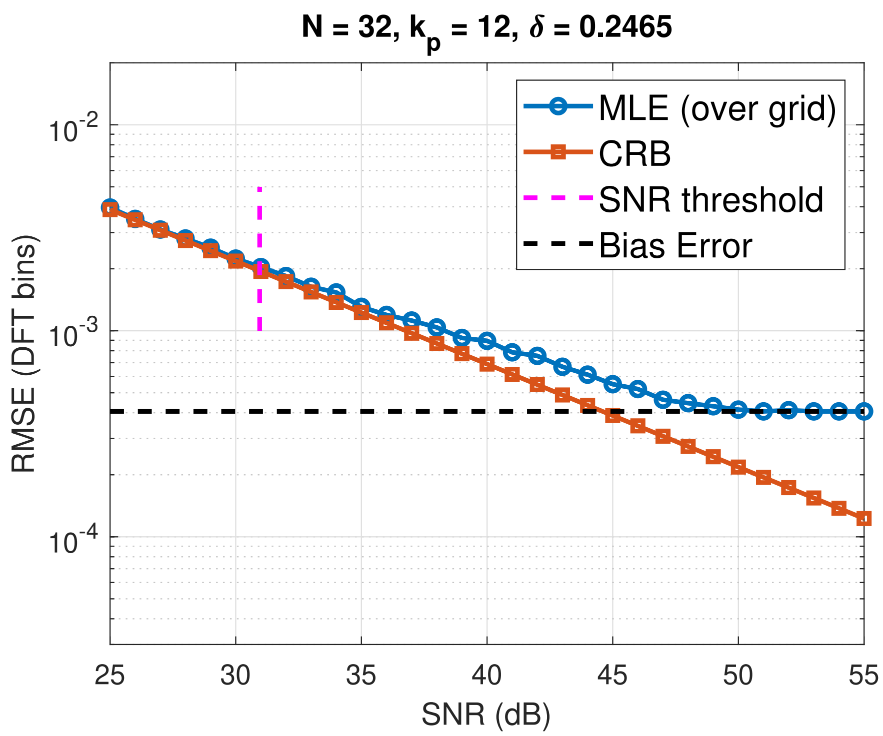

Figure 2.3: RMSE vs SNR plot for MLE with frequency $\omega = \frac{2\pi(12+0.2465)}{32}$.

frequency of $f = \frac{12+0.2465}{32}$ and $N = 64$ samples for the frequency of $f = \frac{21+0.1345}{64}$ respectively. Theoretical bias error and SNR threshold are shown in these figures for $N' = 2^{14}$. The simulation results verifies the derivations in (2.15) and (2.16).

These practical limitations of grid based maximization methods are the motivations for the fine frequency estimation methods developed in the next section.

2.4 Fine Frequency Estimation Methods

As described in the previous section, the computational complexity of maximum likelihood estimator becomes an increasing burden at high SNR. Fine frequency estimators described in this section present a solution to this problem. The main goal of fine frequency estimators is to get an accurate frequency estimate closely tracking the CRB without utilizing a dense grid.

The fine frequency estimators have two stages which are the coarse frequency estimation stage and fine frequency estimation stage. First stage aims to detect $k_p \in$

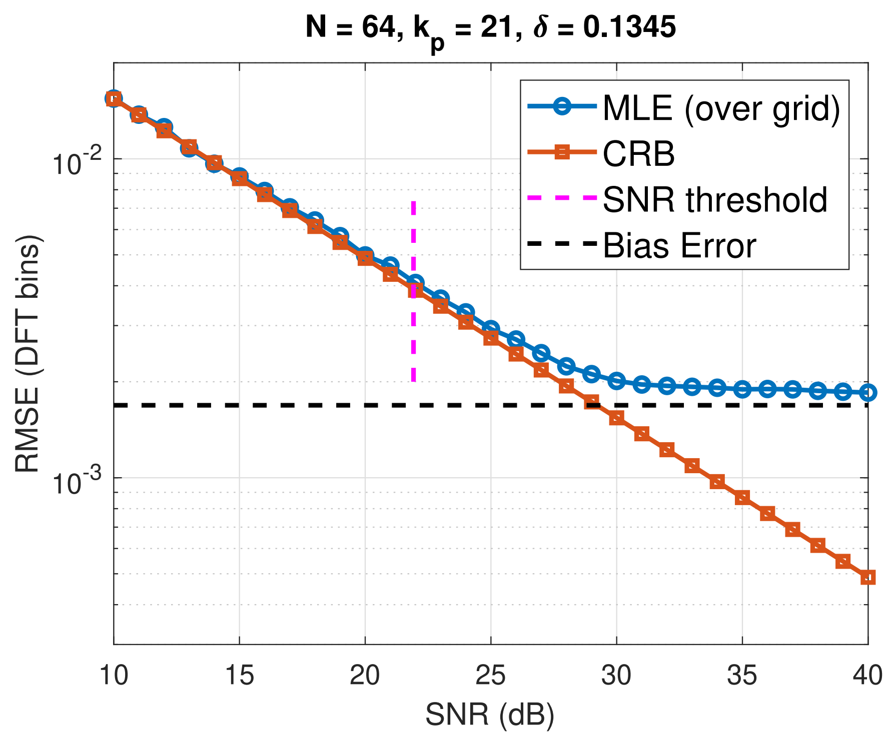

Figure 2.4: RMSE vs SNR plot for MLE with frequency $\omega = \frac{2\pi(21+0.1345)}{64}$.

$\{0, \ldots, N-1\}$; while the second one estimates $\delta \in (-0.5, 0.5)$. The second stage unknown δ is considered as the fine part of frequency $f = \frac{k_p+\delta}{N}$.

2.4.1 Coarse Frequency Estimation Stage (First Stage)

The first stage uses N-point DFT of N-point input $r[n]$ given in (2.2) for detection. The coarse estimate on f, that is $\widehat{k}_p$, is generated by locating the DFT bin (k_p) with the largest magnitude as shown in equation (2.17):

$$\widehat{k}_p = \arg\max_{k_p} \left| \sum_{n=0}^{N-1} r[n] e^{-j2\pi \frac{k_p}{N} n} \right|^2 . \tag{2.17}$$

The success of the first stage is vital for the overall success of the method. An erroneous detection in the first step creates gross errors. A more detailed discussion of gross error is given in Chapter 2.5.2.

2.4.2 Fine Frequency Estimation Stage (Second Stage)

In the second stage, the fractional part of the frequency (δ) is estimated. For this purpose, the DFT bin where the peak occurs $(R[\widehat{k}_p])$ and its neighbours are used for the estimation of δ. Several fine frequency estimation methods are available in the literature for both real and complex valued sinusoids. These methods differ in the number of DFT bins they utilize and the non-linear expression for the estimation of δ in the fine frequency estimation stage.

The main interest of this section is the estimation of the fine frequency part in the high SNR region. Hence, throughout this section, we assume that the first stage is error free.

We describe two fine frequency estimation methods in the literature. The first one is Jacobsen's method after biased correction [6] and its expression is

$$\widehat{\delta}_1 = \frac{\tan \pi/N}{\pi/N} \operatorname{Real}\left\{ \frac{R[k_p - 1] - R[k_p + 1]}{2R[k_p] - R[k_p - 1] - R[k_p + 1]} \right\}. \tag{2.18}$$

We would like to remind that k_p in (2.18) is an unknown of the problem. Here we assume that the value of k_p is correctly estimated in the first stage, that is $\widehat{k}_p = k_p$. The ratio in the argument of the real part operator in (2.18) is a non-linear function of the input due to division operation. In the absence of noise, the ratio is, trivially, invariant to unknown amplitude and phase of complex exponential signal. Hence, the right hand side of (2.18) depends only on δ in the absence of noise. This also explains the labeling of the left hand side of the same equation. We call the functions of several arguments with no dependency on some arguments as the invariant functions [15].

By using elementary mathematical manipulations, in the absence of noise, the expression in (2.18) can be simplified as [7],

$$\begin{aligned} \widehat{\delta}_1 &= \tan(\pi\delta/N) \frac{\sin(2\pi/N)}{2\sin^2(\pi/N)}, \\ &\approx \frac{\tan(\pi\delta/N)}{\pi/N}. \end{aligned} \tag{2.19}$$

Another fine frequency estimator is developed by Aboutanios and Mulgrew (AM) [8] and its expression is

$$\widehat{\delta}_2 = \frac{1}{2} \operatorname{Real}\left\{ \frac{R[k_p + 0.5] + R[k_p - 0.5]}{R[k_p + 0.5] - R[k_p - 0.5]} \right\}. \tag{2.20}$$

Ignoring the noise term on $R[k]$, we can simplify the expression in (2.20) as follows:

$$
\begin{aligned}
\widehat{\delta}_2 =& \frac{1}{2}\,\text{Real}\left\{\frac{\frac{1+e^{j2\pi\delta}}{1-e^{j\frac{2\pi}{N}(\delta-0.5)}}+\frac{1+e^{j2\pi\delta}}{1-e^{j\frac{2\pi}{N}(\delta+0.5)}}}{\frac{1+e^{j2\pi\delta}}{1-e^{j\frac{2\pi}{N}(\delta-0.5)}}-\frac{1+e^{j2\pi\delta}}{1-e^{j\frac{2\pi}{N}(\delta+0.5)}}}\right\}\\
=& \frac{1}{2}\,\text{Real}\left\{\frac{2-2e^{j\frac{2\pi}{N}\delta}\cos(\frac{\pi}{N})}{-j2e^{j\frac{2\pi}{N}\delta}\sin(\frac{\pi}{N})}\right\},\\
=& \frac{1}{2}\,\text{Real}\left\{\frac{1}{-je^{j\frac{2\pi}{N}\delta}\sin(\frac{\pi}{N})}-j\cot(\frac{\pi}{N})\right\},\\
=& \frac{\sin(\frac{2\pi}{N}\delta)}{2\sin(\frac{\pi}{N})}\approx\frac{\sin(\frac{2\pi}{N}\delta)}{2\pi/N}.
\end{aligned}
\tag{2.21}
$$

Having only δ and N dependency in the final expression, as in (2.19) and (2.21), is a requirement for fine frequency estimators. It is clear that this dependency is non-linear. Note from (2.19) and (2.21) that both $\widehat{\delta}_1$ and $\widehat{\delta}_2$ are not equal true δ even in the absence of noise. This results in a biased estimate at sufficiently high SNR conditions. Equation (2.22) gives the bias of estimators $\widehat{\delta}_1$ and and $\widehat{\delta}_2$:

$$
\begin{aligned}
\frac{\tan(\pi\delta/N)}{\pi/N} =& \delta\underbrace{+\frac{1}{3}\left(\frac{\pi}{N}\right)^2\delta^3+\frac{2}{15}\left(\frac{\pi}{N}\right)^4\delta^5+...}_{\text{bias term}}\\
\frac{\sin(2\pi\delta/N)}{2\pi/N} =& \delta\underbrace{-\frac{1}{6}\left(\frac{2\pi}{N}\right)^2\delta^3+\frac{1}{120}\left(\frac{2\pi}{N}\right)^4\delta^5+...}_{\text{bias term}}
\end{aligned}
\tag{2.22}
$$

The bias term can be negligible for high N or small δ; however, it is possible to remove the bias by inverting the non-linear expression causing the bias. For the Jacobsen estimator, the bias can be removed by using an inverse function [7] as fallows,

$$
\widehat{\delta}_1^{\text{Final}} = \frac{\tan^{-1}(\pi\widehat{\delta}_1/N)}{\pi/N}. \tag{2.23}
$$

In AM method [8], an iterative approach is proposed to reduce/remove the bias. The parameter δ is estimated iteratively and after each iteration, by using the previous result, new spectrum samples are calculated as shown in equation (2.24).

$$
\begin{aligned}
R_{\text{AM}}^{(i+1)}[k] =& \sum_{n=0}^{N-1} Ae^{j2\pi\frac{k_p+\delta}{N}n+\phi}e^{-j2\pi\frac{k+\widehat{\delta}_2^{(i)}}{N}n}+W[k],\\
=& Ae^{j\phi}\frac{1-e^{j2\pi(k_p-k+\delta-\widehat{\delta}_2^{(i)})}}{1-e^{j\frac{2\pi}{N}(k_p-k+\delta-\widehat{\delta}_2^{(i)})}}+W[k].
\end{aligned}
\tag{2.24}
$$

Algorithm 1: AM method

Input : $r[n]$: N samples of noisy complex sinusoid

Output: $\widehat{\omega} = \frac{2\pi}{N}(\widehat{k}_p + \widehat{\delta})$ rad./sample

$R[k] = fft(r[n], N)$ (N-point FFT calculation).

$\widehat{k}_p = \underset{1 \le k < N}{\arg\max} \, |R[k]|^2$.

Set $\widehat{\delta}^{(0)} = 0$.

for $i = 0$: maximum iteration $- 1$

$\quad R_{\text{AM}}^{(i)}[k] = \sum_{n=0}^{N-1} r[n] e^{-j2\pi \frac{k+\widehat{\delta}^{(i)}}{N} n}$, $k = \widehat{k}_p \pm 0.5$.

$\quad \widehat{\delta}^{(i+1)} = \frac{1}{2} \operatorname{Real} \left\{ \frac{R_{\text{AM}}^{(i)}[\widehat{k}_p+0.5] + R_{\text{AM}}^{(i)}[\widehat{k}_p-0.5]}{R_{\text{AM}}^{(i)}[\widehat{k}_p+0.5] - R_{\text{AM}}^{(i)}[\widehat{k}_p-0.5]} \right\} + \widehat{\delta}^{(i)}$.

end for

Return $\widehat{\omega} = \frac{2\pi}{N}(\widehat{k}_p + \widehat{\delta})$

Here $\widehat{\delta}_2^{(i)}$ is the δ estimate of AM method at i'th iteration and $\widehat{\delta}_2^{(0)}$ is the initial value of δ. For the iterative bias reduction, the final expression in (2.21) can be rewritten as,

$$\widehat{\delta}_2^{(i+1)} - \widehat{\delta}_2^{(i)} = \frac{\sin(\frac{2\pi}{N}(\delta - \widehat{\delta}_2^{(i)}))}{2\sin(\frac{\pi}{N})}. \tag{2.25}$$

It can be seen that the argument of sine function in (2.25) contains the difference of δ and its estimate at the ith iteration. Hence, the argument of sine function approaches zero as the iterations progress. This leads to the reduction/removal of bias term in (2.22) which is clearly absent for $\delta = 0$. With the bias removal iterations, AM iterations become

$$\begin{aligned} \widehat{\delta}_2^{(i+1)} &= \frac{1}{2} \operatorname{Real} \left\{ \frac{R_{\text{AM}}^{(i)}[k_p + 0.5] + R_{\text{AM}}^{(i)}[k_p - 0.5]}{R_{\text{AM}}^{(i)}[k_p + 0.5] - R_{\text{AM}}^{(i)}[k_p - 0.5]} \right\} + \widehat{\delta}_2^{(i)}, \quad &\text{(General Case)} \\ \widehat{\delta}_2^{(i+1)} &= \frac{\sin(\frac{2\pi}{N}(\delta - \widehat{\delta}_2^{(i)}))}{2\sin(\frac{\pi}{N})} + \widehat{\delta}_2^{(i)}. &\text{(Noiseless Case)} \end{aligned} \tag{2.26}$$

An algorithm listing of AM method is given in Algorithm Table 1. In the latter parts of this chapter, we also provide some analysis results on the AM method.

Figures 2.5 and 2.6 illustrates the performance of the fine frequency estimation methods mentioned in this section with $N = 32$ samples for the frequency of $f = \frac{15+0.2345}{32}$ and $N = 64$ samples for the frequency of $f = \frac{38+0.3456}{64}$ respectively. The algorithms

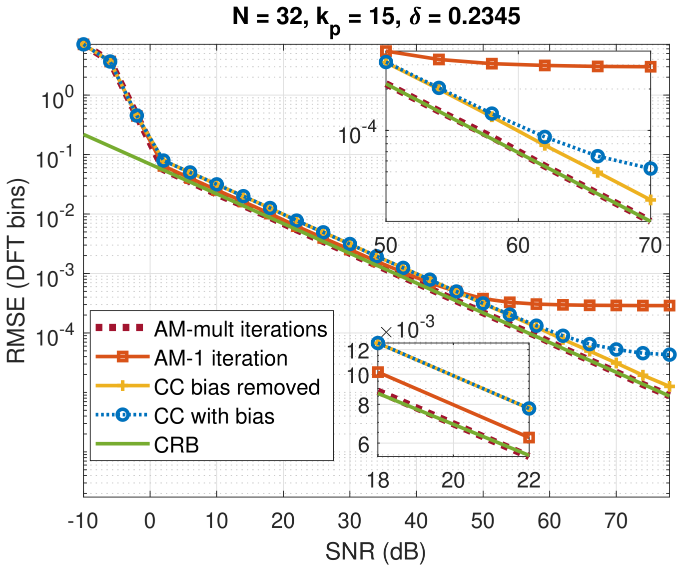

Figure 2.5: Comparison of different fine frequency estimation methods with frequency $\omega = \frac{2\pi(15+0.2345)}{32}$.

in (2.18), (2.20), (2.23) and (2.26) are called respectively CC with bias, AM-1 iteration, CC bias removed and AM-mult iterations in these figures. The curves labelled as AM-mult iterations shows the performance of the AM estimator with multiple iterations. For AM-1 iteration and CC with bias, at high SNR, the error floor occurs due to bias. The success of the bias removal operations are illustrated in curves labelled as CC bias removed and AM-mult iterations. AM-mult iterations has the best performance and it is a nearly an optimal estimator with a low computational cost ($N = \{32, 64\}$ point FFT computation and basic mathematical operations in this case). We utilize the AM method for the fundamental frequency estimation problem in Chapter 3. We give a study of AM method in the next section to better understand its performance.

2.5 Some Results on Aboutanios-Mulgrew Estimator

This section gives a theoretical analysis of Aboutanios-Mulgrew (AM) estimator [8]. First, by using the fixed point theorem [42], we investigate convergence properties of AM estimator and the number of iterations needed to achieve a performance on the order of CRB. After that, the gross error is defined to characterize the errors

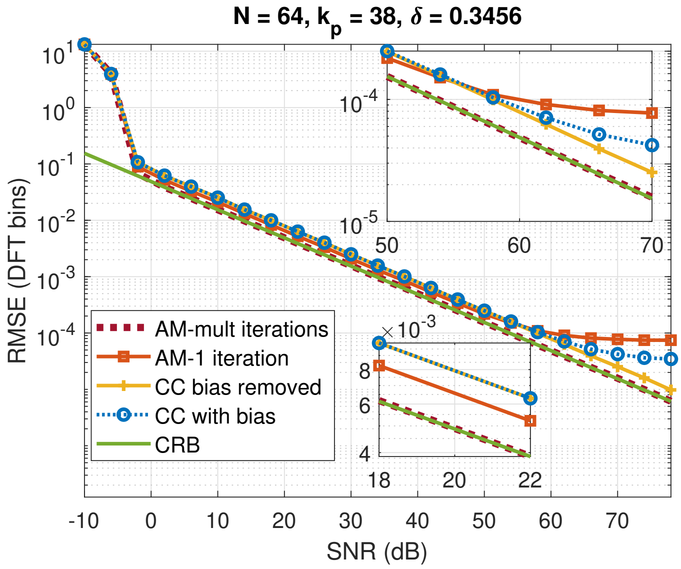

Figure 2.6: Comparison of different fine frequency estimation methods with frequency $\omega = \frac{2\pi(38+0.3456)}{64}$.

encountered at low SNR. Finally, we extend the analysis by characterizing the MSE of the estimator at high SNR.

2.5.1 Number of Iterations to Reach Cramer-Rao Bound

In iterative computations, such as AM algorithm, the main approach is to use the output of the previous iteration as the input of the next one. The iteration results can be considered as the elements of a sequence x_n in the form,

$$x_{n+1} = g(x_n), \qquad n = 0, 1, 2, 3, \ldots \tag{2.27}$$

where x_0 is the initial point and x_n is the n'th iteration result. A fixed point, x_f, of a function $g(x)$ is an element of its domain which is mapped to itself, i.e, $g(x_f) = x_f$. Existence of a fixed point and the convergence rate to the fixed point are both theoretical and practical interests in all similar iterative schemes. To investigate the convergence properties of the AM estimator, we use the Banach Fixed-Point theorem which can be stated as follows [42]:

Theorem 1 *If the function $g(x) : S \to S$ executes a contractive mapping with a constant, $\lambda \in [0, 1)$, the following results hold,* *1. A unique fixed point, $x_f \in S$, exists such that*

$$g(x_f) = x_f. \tag{2.28}$$

2. For any sequence, $\{x_n\} \subseteq S$ with any initial guess, $x_0 \in S$, converges to x_f such that

$$x_{n+1} = g(x_n) \rightarrow x_f \quad \textit{where} \quad n \rightarrow \infty. \tag{2.29}$$

3. The valid bounds related to the distance between the iteration results and fixed point are,

$$\begin{aligned} ||x_n - x_f|| &\leq \frac{\lambda^n}{1-\lambda}||x_0 - x_1||, \\ ||x_n - x_f|| &\leq \frac{\lambda}{1-\lambda}||x_{n-1} - x_n||, \\ ||x_n - x_f|| &\leq \lambda||x_{n-1} - x_f||. \end{aligned} \tag{2.30}$$

To determine whether a function or an operator is contractive, the following condition should be satisfied,

$$||g(x) - g(y)|| \leq \lambda||x - y|| \quad x, y \in S \quad \text{and} \quad \lambda \in [0, 1). \tag{2.31}$$

To show the convergence of AM iterations in the absence of noise, we will show that the non-linear expression of the AM estimator in (2.26) is contractive. The AM estimator relation from (2.26) can be considered as a mapping $g(\cdot)$ with $g(\widehat{\delta})$: $(-0.5, 0.5) \rightarrow (-0.5, 0.5)$,

$$\widehat{\delta}^{(i+1)} = g(\widehat{\delta}^{(i)}) = \frac{\sin(\frac{2\pi}{N}(\delta - \widehat{\delta}^{(i)}))}{2\sin(\frac{\pi}{N})} + \widehat{\delta}^{(i)}, \tag{2.32}$$

where δ is the true value and $\widehat{\delta}^{(i)}$ is the estimated value of δ at i'th iteration. The Taylor series expansion of the function $g(\widehat{\delta})$ around the point δ is,

$$g(\widehat{\delta}) \approx \delta + g'(\delta)(\widehat{\delta} - \delta) + \frac{g''(\delta)}{2}(\widehat{\delta} - \delta)^2 + \text{h.o.t.} \tag{2.33}$$

where $g'(\delta) = \frac{-\pi}{N\sin(\pi/N)} + 1$, $g''(\delta) = 0$ and $g'''(\delta) = \frac{4\pi^3}{N^3\sin(\pi/N)}$.

From the expansion, we can see that the values of the higher order terms much more smaller than the first term for large values of N. Hence, by ignoring the higher order terms we get,

$$g(\widehat{\delta}) \approx \delta + g'(\delta)(\widehat{\delta} - \delta), \tag{2.34}$$

and for any $\widehat{\delta}_1, \widehat{\delta}_2 \in (-0.5, 0.5)$ values, we can write the expression,

$$g(\widehat{\delta}_1) - g(\widehat{\delta}_2) = g'(\delta)(\widehat{\delta}_1 - \widehat{\delta}_2), \tag{2.35}$$

where $g'(\delta) = \frac{-\pi}{N\sin(\pi/N)} + 1$.

If the term $|g'(\delta)|$ is in the range of $[0, 1)$, then we can say that the function in (2.32) is contradictive. The function $g'(\delta)$ depends only N. Figure 2.7 shows that $g'(\delta) = b(N)$ is an increasing function and only by looking the boundaries, we can determine the range of the possible values of $g'(\delta)$ for different values of N.

$$\begin{aligned} &g'(\delta) \to 0 && N \to \infty, \\ &g'(\delta) = -\pi/2 + 1 = -0.5708 && N = 2. \end{aligned} \tag{2.36}$$

Also the derivative of the $g'(\delta) = b(N)$ is always greater than 0 when $N \geq 2$.

$$\begin{aligned} b'(N) &= \frac{\pi}{N^2\sin(\pi/N)} - \frac{\pi^2\cos(\pi/N)}{N^3\sin^2(\pi/N)}, \\ &= \frac{\pi}{N^2\sin(\pi/N)}\left(1 - \frac{\pi\cos(\pi/N)}{N\sin(\pi/N)}\right) \quad > 0, \end{aligned} \tag{2.37}$$

Finally, the values of $|g'(\delta)|$ is in the required interval, that is $|g'(\delta)| \in (0, 0.5708] \subset [0, 1)$ so that $g(\widehat{\delta})$ is a contractive function. Besides, it easy to see that δ is the fixed point for the contractive function in (2.32). That proves that the AM algorithm converges to a fixed point.

Next, we examine the convergence rate. By using the results in (2.32) and (2.34), we have the following approximate relation,

$$\widehat{\delta}^{(i+1)} \approx \delta + g'(\delta)(\widehat{\delta}^{(i)} - \delta). \tag{2.38}$$

Hence for large values of N, the convergence rate is

$$\text{convergence rate } \triangleq \frac{|\widehat{\delta}^{(i+1)} - \delta|}{|\widehat{\delta}^{(i)} - \delta|} = |g'(\delta)| = \frac{\pi}{N\sin(\pi/N)} - 1. \tag{2.39}$$

We know that the mean square error of AM estimator is on the order of CRB at high SNR. Hence, AM iterations can be repeated until the difference between the final estimate $\widehat{\delta}$ and the true δ value is on the order of square root of CRB in terms of DFT

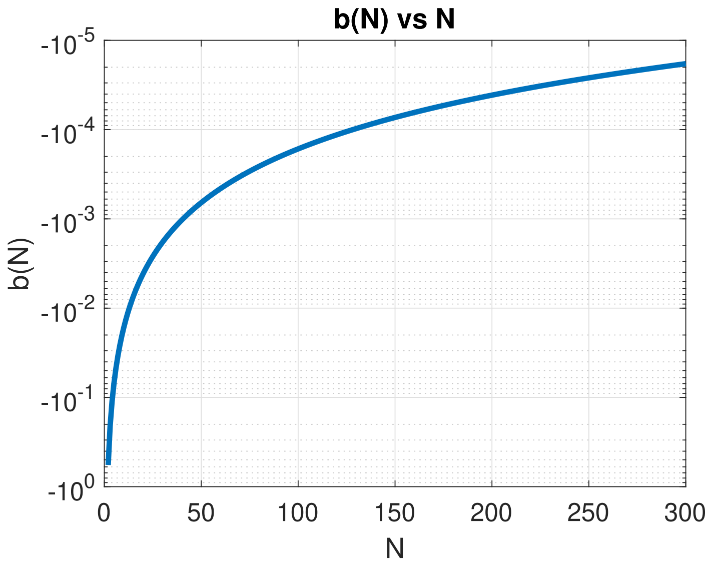

Figure 2.7: $g'(\delta) = b(N)$ vs N

bins (see Section 2.3). Since the convergence rate is given as $|g'(\delta)| = \frac{\pi}{N\sin(\pi/N)} - 1$, we can get the number of iterations to reach the CRB level as

$$|\widehat{\delta} - \delta_0||g'(\delta)|^n \leq \sqrt{\text{CRB}}. \tag{2.40}$$

Here n is the number of iterations and δ_0 is the initial point. We know δ is limited to range of -0.5 to 0.5. For the worst case condition of $|\widehat{\delta} - \delta_0| = 1$, the maximum number of iterations to reach CRB is

$$n(\text{SNR}) \geq \frac{\log\sqrt{\text{CRB}}}{\log|g'(\delta)|} = \frac{\log\sqrt{\frac{6N}{(N^2-1)(2\pi)^2\text{SNR}}}}{\log\left(\frac{\pi}{N\sin(\pi/N)} - 1\right)}. \tag{2.41}$$

In Figures 2.8 and 2.9, the performance of the AM is illustrated with $N = 64$ samples for the frequency $f = \frac{20+0.4}{64}$ and $N = 32$ samples for the frequency $f = \frac{20-0.4}{32}$, respectively, for different number of iterations. In these figures, also SNR threshold is presented by using the equation (2.41) for a given number of iterations. As can be observed from the figures, the insufficient number of iterations causes an error floor as the SNR increases. With the help of expression (2.41), it is possible to choose the number of iterations to avoid error floor.

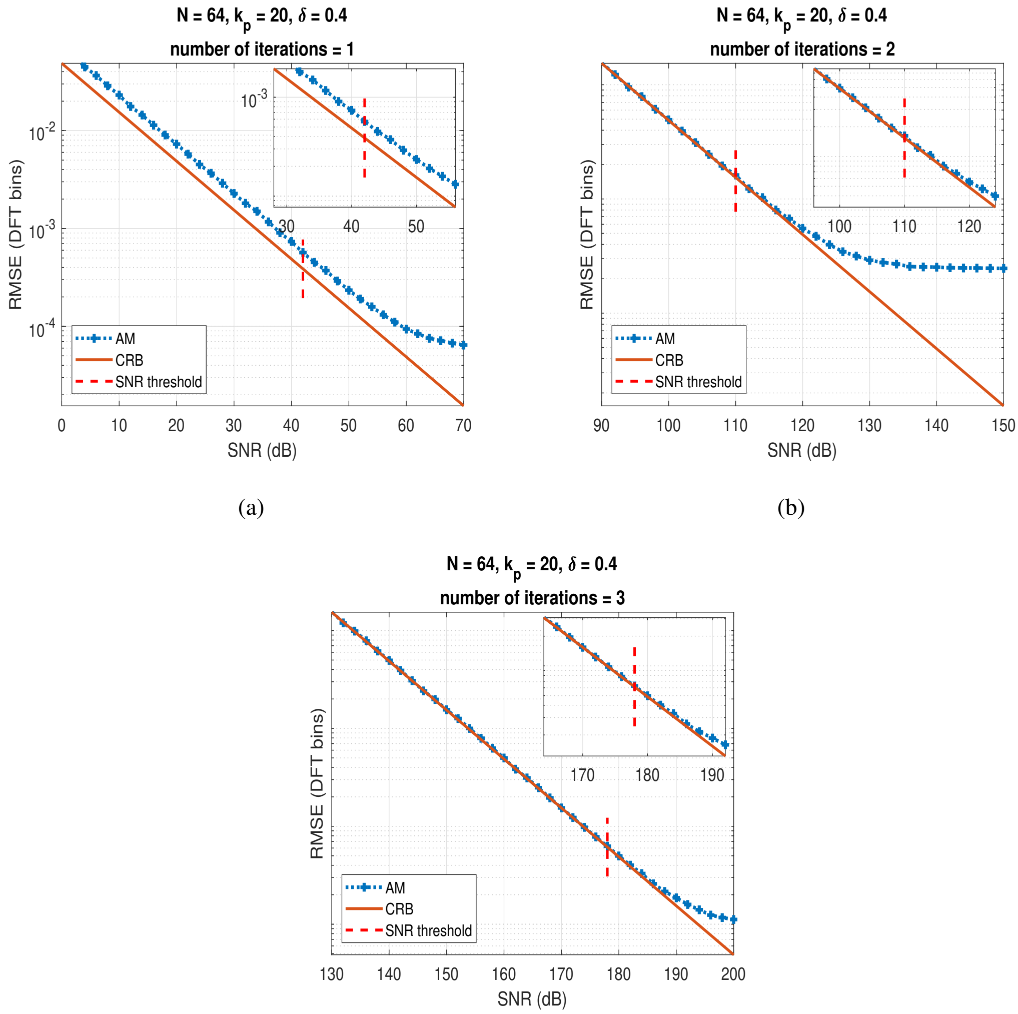

(c)

Figure 2.8: AM algorithm simulation results for different iterations where $N = 64$ and $f = \frac{20+0.4}{64}$: (a) 1 iteration, (b) 2 iterations, (c) 3 iterations.

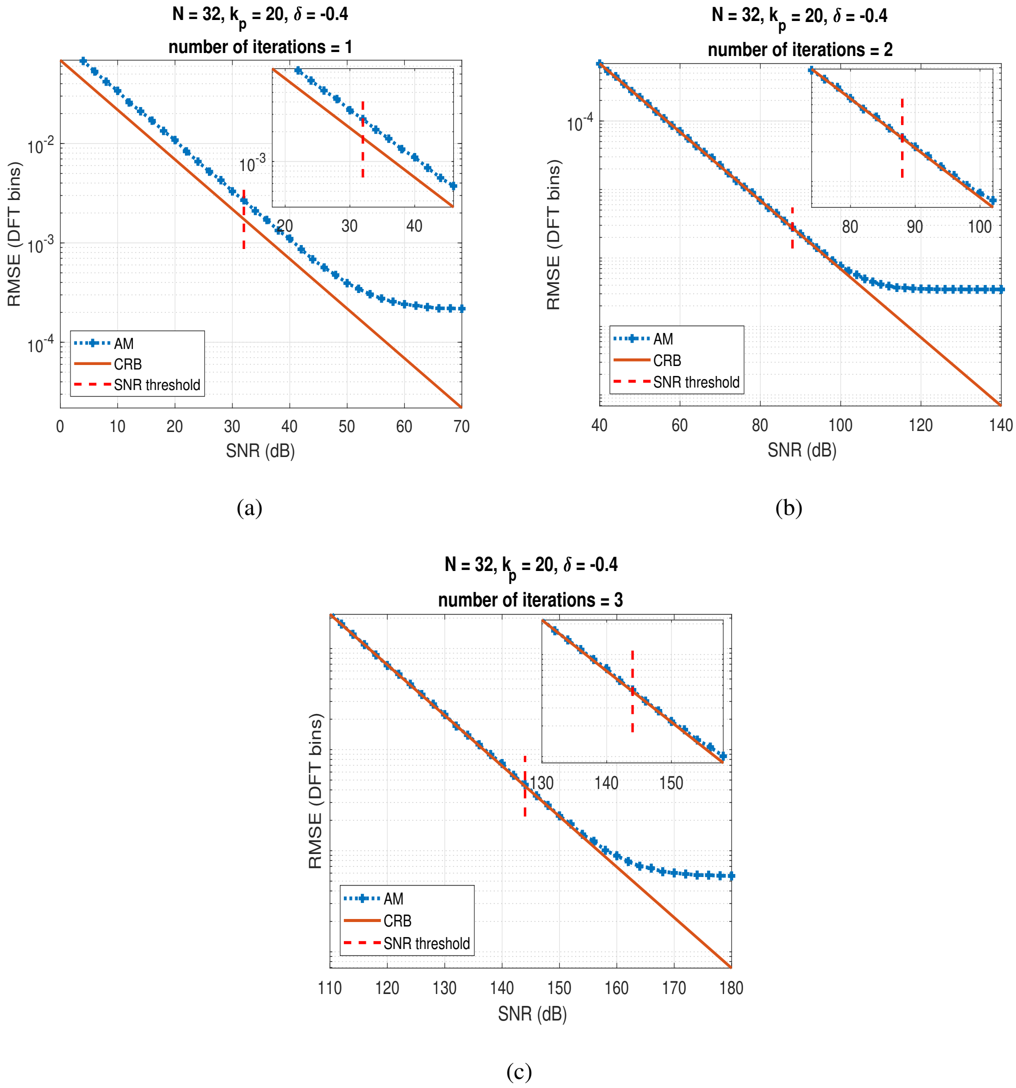

(a) (b) (c)

Figure 2.9: AM algorithm simulation results for different iterations where $N = 32$ and $f = \frac{20-0.4}{32}$: (a) 1 iteration, (b) 2 iterations, (c) 3 iterations.

2.5.2 Approximate MSE lower bound and Gross Error Analysis

When the peak location in the coarse frequency estimation stage is detected at the DFT bins whose indices are different from $k_p - 1, k_p, k_p + 1$, that is two or more DFT bins away from the true bin; a large error, what is called gross error, occurs. The fine frequency estimation stage is of little use in the presence of gross errors. The gross error problem is very similar to the error event for the non-coherent frequency shift keying (FSK) detection. Detailed analysis and an upper bound for the gross error can be found in [7]. In this part, we give an approximate lower bound on the gross error and we analyze the effect of the different values of δ on the gross error.

When we calculate the DFT of the input signal in (2.1), the noise term at each DFT bin is iid complex white Gaussian noise, shown as $W[k]$, with zero mean and $N\sigma_w^2$ variance. It is important to remember that all DFT bins except the one with index k_p sample the zeros of periodic sinc function when $\delta = 0$. Hence the bins with index $k \neq k_p$ contain the linear combinations of noise; but do not carry any information about signal of interest (see expression in (2.2)). Hence, the magnitude of DFT bin with index k_p is Rician distributed and the other DFT bins are Rayleigh distributed random variables when $\delta = 0$ (also see Figure 2.1):

$$\begin{aligned} \text{Rician PDF: } f_{\text{ric}}(x) &= \frac{2x}{N\sigma_w^2} \exp\left(\frac{-(x^2 + A^2N^2)}{N\sigma_w^2}\right) I_0\left(\frac{2Ax}{\sigma_w^2}\right) \\ \text{Rayleigh PDF: } f_{\text{ray}}(x) &= \frac{2x}{N\sigma_w^2} \exp\left(\frac{-x^2}{N\sigma_w^2}\right) \end{aligned} \tag{2.42}$$

Here I_0 is the modified Bessel function of the first kind with order zero, A is the magnitude, N is the number of samples and σ_w^2 is the noise variance. We calculate the probability that $R_{k_p} \triangleq |R[k_p]|$ is the largest value among all DFT bins. This probability, $P\{Z \triangleq \max\{R_0, \ldots, R_{N-1}\} = R_{k_p}\}$ can be written as,

$$P\{Z = R_{k_p}\} = \int_{\infty}^{\infty} P\{Z = x|\ R_{k_p} = x\} f_{\text{ric}}(x) dx \tag{2.43}$$

where

$$\begin{aligned} P\{Z = x|\ R_{k_p} = x\} =& P\{R_0 < x, \ldots, R_{k_p-1} < x, R_{k_p+1} < x, \ldots, R_{N-1} < x | R_{k_p} = x\}, \\ =& P\{R_0 < x\} \ldots P\{R_{k_p-1} < x\} P\{R_{k_p+1} < x\} \ldots P\{R_{N-1} < x\}, \\ =& \left(F_{\text{ray}}(x)\right)^{N-1}, \end{aligned} \tag{2.44}$$

and $F_{\text{ray}}(x) = 1 - \exp\left(\frac{-x^2}{N\sigma_w^2}\right)$ is the cumulative distribution function (CDF) of Rayleigh pdf. Finding a closed form solution of the equation (2.43) is a non-trivial task; but it is possible to use the numerical integration routines of MATLAB to calculate this probability. Specific for the $\delta = 0$ case, $P\{Z \triangleq \max\{R_0, \ldots, R_{N-1}\} = R_k; k \neq k_p\}$ can be written as

$$P\{Z = R_k\} = \frac{1 - P\{Z = R_{k_p}\}}{N-1}, \qquad k \neq k_p \quad (\delta = 0) \tag{2.45}$$

since $R_k^{k \neq k_p}$ are iid random variables when $\delta = 0$.

As mentioned earlier, if the detected bin in the first stage is two or more DFT bins away from the true bin, k_p, the fine frequency estimation is of little use/purpose. We assume very low SNR operational conditions and assume that the estimate conditioned on the gross error event as uniformly distributed in the gross error interval, as shown below:

$$f_{\text{gross}}(x) = \begin{cases} \frac{1}{N-3}, & 0 \leq x \leq k_p - 1.5 \\ 0, & k_p - 1.5 < x < k_p + 1.5 \\ \frac{1}{N-3}, & k_p + 1.5 \leq x < N \end{cases} \tag{2.46}$$

With these assumptions, the the gross error probability is defined as $1 - p$ where $p = P\{Z = R_{k_{p-1}}\} + P\{Z = R_{k_p}\} + P\{Z = R_{k_{p+1}}\}$. Then an approximate lower bound (due to several assumptions) can be given as:

$$\text{ALB} \triangleq (1-p) \int_0^N (x - k_p)^2 f_{\text{gross}}(x) dx + p\,\text{CRB} \tag{2.47}$$

where ALB refers to the short hand notation for the phrase approximate lower bound.

In Figures 2.10 and 2.11, for different δ values, we give the simulation results to verify the theoretical gross error calculation for $N = 64$, $k_p = 15$ and $N = 32$, $k_p = 23$; respectively. In these figures, for different SNR values the RMSE of the AM algorithm and the $\sqrt{\text{ALB}}$ given in (2.47) are shown. As we mentioned earlier, the gross error is calculated for the $\delta = 0$ case. The error expression we found can be argued to be a lower bound on the gross error; since the best case is $\delta = 0$ for the detection of k_p. In this case, all the power of the signal of interest is collected at one single DFT bin. Hence, as $|\delta|$ increases, we have larger gross error terms at low SNR and to attain CRB, there is a need for extra signal power. For different δ's, this behaviour can be observed from Figures 2.10 and 2.11. Due to several assumptions in the derivation, we interpret ALB as a practical lower bound for the MSE analysis of AM method.

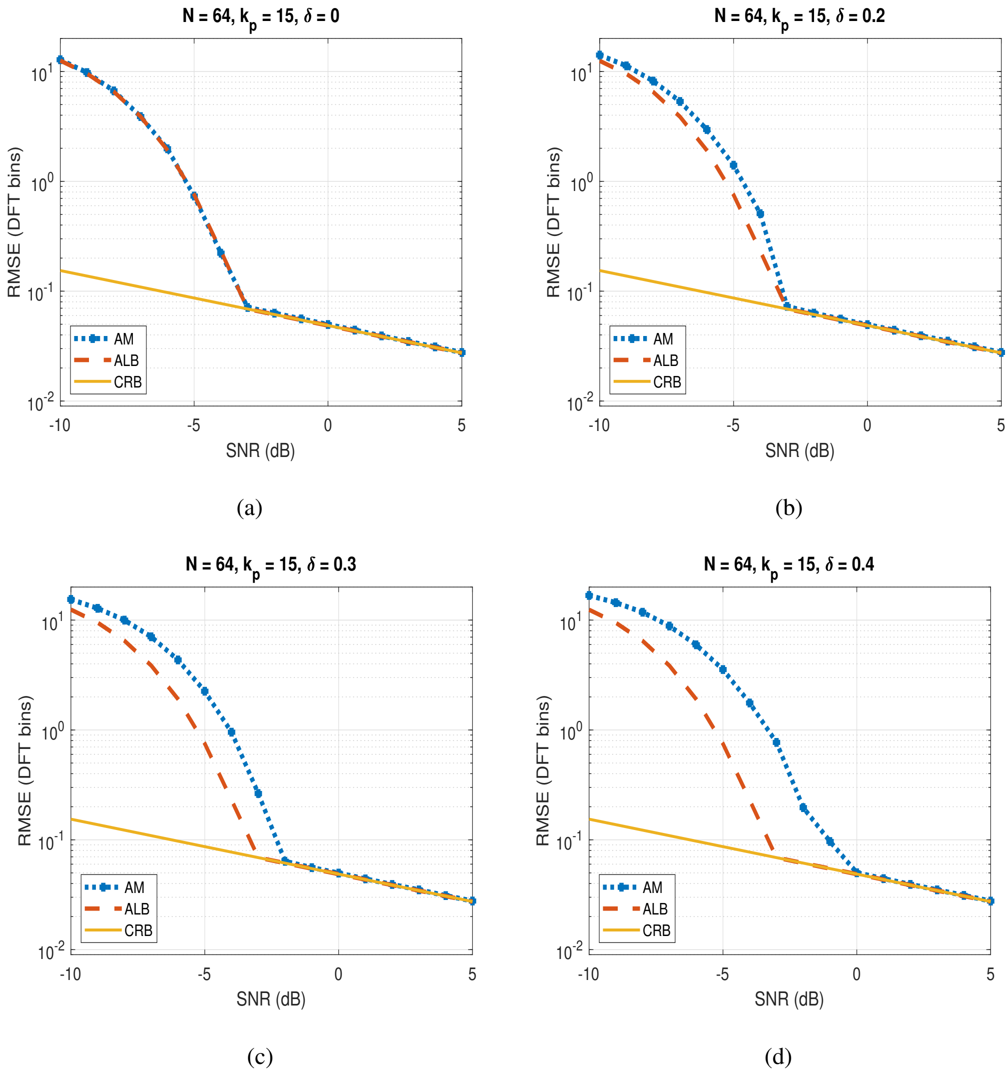

Figure 2.10: AM algorithm simulation results and approximate lower bound for different δ values where $N = 64$ and $k_p = 15$: (a) $\delta = 0$, (b) $\delta = 0.2$, (c) $\delta = 0.3$, (d) $\delta = 0.4$.

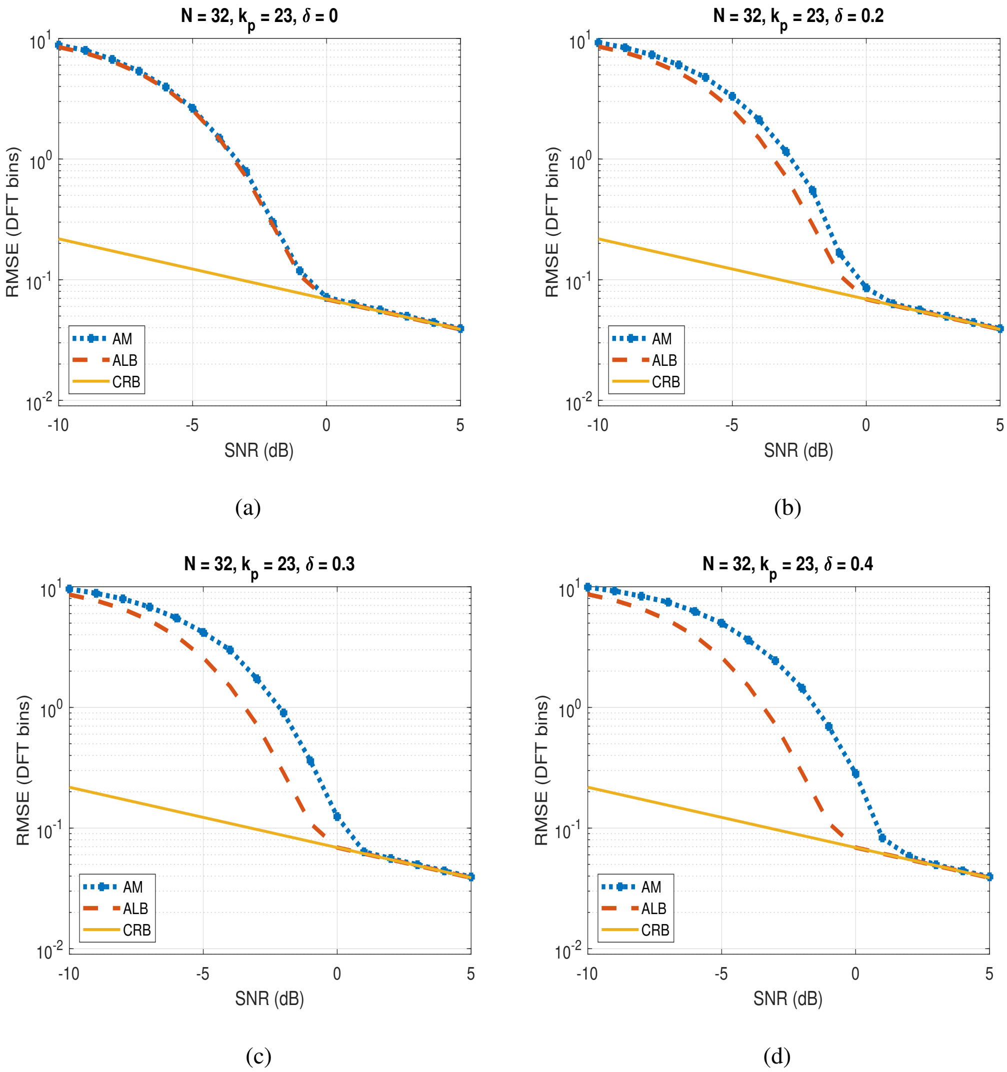

Figure 2.11: AM algorithm simulation results and approximate lower bound for different δ values where $N = 32$ and $k_p = 23$: (a) $\delta = 0$, (b) $\delta = 0.2$, (c) $\delta = 0.3$, (d) $\delta = 0.4$.

2.5.3 Asymptotic MSE Analysis at high SNR

The We present MSE analysis of AM method at high SNR. This analysis is also called fine error analysis in the literature. In equation (2.20), the invariant function of the AM algorithm is given. By representing the DFT of complex sinusoidal signal and the noise separately, the same relation can be written as,

$$\text{Ratio}_{\text{w/n}} = \frac{1}{2}\,\text{Real}\left\{\frac{\widetilde{R}[k_p+0.5]+\widetilde{R}[k_p-0.5]+W[k_p+0.5]+W[k_p-0.5]}{\widetilde{R}[k_p+0.5]-\widetilde{R}[k_p-0.5]+W[k_p+0.5]-W[k_p-0.5]}\right\} \tag{2.48}$$

where $\widetilde{R}[k] = \sum_{n=0}^{N-1} Ae^{j(2\pi fn+\phi)}e^{-\frac{j2\pi kn}{N}}$ and $W[k] = \sum_{n=0}^{N-1} w[n]e^{-\frac{j2\pi kn}{N}}$. As mentioned in the previous sections, after several iterations, δ estimate approaches to its true value, given that operational SNR is sufficiently high. This enable us to make following approximations,

$$\begin{aligned}\widetilde{R}[k_p+0.5]+\widetilde{R}[k_p-0.5] &= Ae^{j\phi}(1+e^{j2\pi\widetilde{\delta}})\frac{2-2e^{j\frac{2\pi}{N}\widetilde{\delta}}\cos(\pi/N)}{1-2e^{j\frac{2\pi}{N}\widetilde{\delta}}\cos(\pi/N)+e^{j\frac{4\pi}{N}\widetilde{\delta}}},\\ &\approx 2Ae^{j\phi} = S_1.\end{aligned} \tag{2.49}$$

$$\begin{aligned}\widetilde{R}[k_p+0.5]-\widetilde{R}[k_p-0.5] &= Ae^{j\phi}(1+e^{j2\pi\widetilde{\delta}})\frac{-2je^{j\frac{2\pi}{N}\widetilde{\delta}}\sin(\pi/N)}{1-2e^{j\frac{2\pi}{N}\widetilde{\delta}}\cos(\pi/N)+e^{j\frac{4\pi}{N}\widetilde{\delta}}},\\ &\approx 2Ae^{j\phi}\frac{-j\sin(\pi/N)}{1-\cos(\pi/N)},\\ &= -j2Ae^{j\phi}\frac{\cos(\pi/2N)}{\sin(\pi/2N)} = S_2.\end{aligned} \tag{2.50}$$

where $\widetilde{\delta} = \delta - \widehat{\delta} \approx 0$. As mentioned in Section 2.1, $W[k_p+0.5]$ and $W[k_p-0.5]$ are independent random variables with $W[k] \sim \mathcal{CN}(0, N\sigma_w^2)$. Also, real and imaginary parts of these random variables are independent with distribution $\mathcal{N}(0, \frac{N}{2}\sigma_w^2)$.

The equation (2.51) shows the derivation of the theoretical variance under high SNR assumption. It is important to note that the second order noise terms are ignored, that is $\frac{W_{0.5}^2-W_{-0.5}^2}{S_2^2} \approx 0$ and $\frac{(W_{0.5}-W_{-0.5}).^2}{S_2^2} \approx 0$, since they are negligible at high SNR.

$$
\begin{aligned}
\text{Ratio}_{\text{w/n}} =& \frac{1}{2}\,\text{Real}\left\{\frac{\widetilde{R}_{0.5}+\widetilde{R}_{-0.5}+W_{0.5}+W_{-0.5}}{\widetilde{R}_{0.5}-\widetilde{R}_{-0.5}+W_{0.5}-W_{-0.5}}\right\} = \frac{1}{2}\,\text{Real}\left\{\frac{S_1+W_{0.5}+W_{-0.5}}{S_2+W_{0.5}-W_{-0.5}}\right\} \\
=& \frac{1}{2}\,\text{Real}\left\{\frac{S_1/S_2+(W_{0.5}+W_{-0.5})/S_2}{1+(W_{0.5}-W_{-0.5}])/S_2}\times\frac{(1-(W_{0.5}-W_{-0.5})/S_2)}{(1-(W_{0.5}-W_{-0.5})/S_2)}\right\} \\
\approx& \frac{1}{2}\,\text{Real}\left\{\frac{S_1}{S_2}+\frac{W_{0.5}+W_{-0.5}}{S_2}-\frac{S_1(W_{0.5}-W_{-0.5})}{S_2^2}\right\} \\
=& \widetilde{\delta}+\frac{1}{2}\,\text{Real}\left\{\frac{W_{0.5}+W_{-0.5}}{S_2}-\frac{S_1(W_{0.5}-W_{-0.5})}{S_2^2}\right\} \\
=& \widetilde{\delta}+\frac{S_3}{A}\,\text{Real}\left\{je^{-j\phi}(W_{0.5}+W_{-0.5})\right\}+\frac{S_4}{A}\,\text{Real}\left\{e^{-j\phi}(W_{0.5}-W_{-0.5})\right\} \\
=& \widetilde{\delta}+\left(\frac{S_3\sin(\phi)+S_4\cos(\phi)}{A}\right)\text{Real}\left\{W_{0.5}\right\} \\
&+\left(\frac{S_3\sin(\phi)-S_4\cos(\phi)}{A}\right)\text{Real}\left\{W_{-0.5}\right\} \\
&+\left(\frac{-S_3\cos(\phi)+S_4\sin(\phi)}{A}\right)\text{Imag}\left\{W_{0.5}\right\} \\
&+\left(\frac{-S_3\cos(\phi)-S_4\sin(\phi)}{A}\right)\text{Imag}\left\{W_{-0.5}\right\}
\end{aligned} \tag{2.51}
$$

In (2.51), we use the following short-hand notations: $\widetilde{R}_p = \widetilde{R}[k_p+p]$, $W[k_p+p] = W_p = \sum_{k=0}^{N-1} w[n]e^{-j\frac{2\pi}{N}(k_p-k+\delta-\widehat{\delta}+p)}$, $S_3 = \frac{\sin(\frac{\pi}{2N})}{4\cos(\frac{\pi}{2N})}$ and $S_4 = \frac{\sin^2(\frac{\pi}{2N})}{4\cos^2(\frac{\pi}{2N})}$ and these random terms are independent (see equations (2.5), (2.6) and (2.7)).

The variance of the δ estimate is then the variance of random terms on the right hand side of (2.51). The variance can be calculated as:

$$
\begin{aligned}
\text{var}(\widehat{\delta}_{\text{AM}}) =& \left(\frac{2S_3^2}{A^2}+\frac{2S_4^2}{A^2}\right)\frac{N\sigma_w^2}{2} = \frac{(S_3^2+S_4^2)N}{\text{SNR}}, \\
=& \frac{(\tan^2(\frac{\pi}{2N})+\tan^4(\frac{\pi}{2N}))N}{16\text{SNR}}, \\
=& \frac{N\tan^2(\frac{\pi}{2N})\sec^2(\frac{\pi}{2N})}{16\text{SNR}}, \\
\approx& \frac{\pi^2}{64\text{SNR}N} = \frac{c}{A^2},
\end{aligned} \tag{2.52}
$$

where $c = \frac{\sigma_w^2\pi^2}{64N}$ and we take $\tan(\frac{\pi}{2N}) \approx \frac{\pi}{2N}$, $\sec(\frac{\pi}{2N}) \approx 1$ when $N \gg 1$.

The ratio between the CRB and the theoretical variance of the AM estimator is 1.0147 (see 2.53). This analysis shows that the asymptotic MSE of AM estimator is about

1.5 percent more than CRB:

$$\frac{\mathrm{var}(\widehat{\delta}_{\mathrm{AM}})}{\mathrm{CRB}} = \frac{\frac{\pi^2}{64\mathrm{SNR}N}}{\frac{6N}{(N^2-1)(2\pi)^2\mathrm{SNR}}} \approx 1.0147. \tag{2.53}$$

CHAPTER 3

FUNDAMENTAL FREQUENCY ESTIMATION OF PERIODIC SIGNAL WITH HARMONICS

This chapter gives the details on the fundamental frequency estimation of periodic signal with harmonics. In Section 3.1, the signal model is given. In Section 3.2, the Cramer-Rao bound, its asymptotic version and hybrid Cramer-Rao bound are given. In Section 3.3, the maximum likelihood estimator is derived. In Section 3.4, a discussion on the model order selection procedures is given. Finally, in Section 3.5, the proposed method, which is based on the fine-frequency estimator of Aboutanios-Mulgrew (AM) and a successive interference cancellation procedure, is given.

3.1 Signal Model

A group of harmonically related complex sinusoids, whose frequencies are integer multiples of fundamental frequency $\omega_0 = 2\pi f_0$, are observed under iid circularly symmetric zero mean, complex white Gaussian noise $w[n]$ with variance σ_w^2:

$$r[n] = \sum_{l=1}^{L} A_l e^{j(\omega_0 ln + \phi_l)} + w[n], \quad n = \{0, \dots, N-1\}. \tag{3.1}$$

Here N is the number of samples, A_l and ϕ_l are the amplitude and the phase of the l'th harmonic. The number of harmonics is L. L is also called the model order. We make the assumption that $\omega_0 < 2\pi/L$ to avoid aliasing/ambiguity problem. The frequency variable f_0 is the normalized frequency defined in $[0, 1/L)$ and can be expressed as $f_0 = \frac{(k_p+\delta)}{N}$ in terms of N-point DFT bins. Here, k_p is an integer in $[0, N/L-1/2)$ and δ is a real number in $(-0.5, 0.5)$. The noise samples $w[n]$ are iid complex Gaussian distributed, $w[n] \sim \mathcal{CN}(0, \sigma_w^2)$. The pseudo signal-to-noise ratio (PSNR) definition specific for this problem is [19]:

$$\text{PSNR} = \frac{\sum_{l=1}^{L} A_l^2 l^2}{\sigma_w^2}. \tag{3.2}$$

The observed samples in (3.1) can be represented as,

$$\begin{bmatrix} r[0] \\ r[1] \\ \vdots \\ r[N-1] \end{bmatrix} = \begin{bmatrix} 1 & \dots & 1 \\ e^{j\omega_0} & \dots & e^{j\omega_0 L} \\ \vdots & \ddots & \vdots \\ e^{j\omega_0 (N-1)} & \dots & e^{j\omega_0 L(N-1)} \end{bmatrix} \mathbf{a} + \mathbf{w}, \tag{3.3}$$

or in matrix-vector notation as

$$\mathbf{r} = \mathbf{Z}\mathbf{a} + \mathbf{w}, \tag{3.4}$$

where $\mathbf{r} \in \mathbb{C}^{N\times 1}$ is the observation vector, $\mathbf{Z} \in \mathbb{C}^{N\times L}$ is the Vandermonde matrix in (3.3), $\mathbf{a} = [A_1 e^{j\phi_1}\ A_2 e^{j\phi_2}\ \dots\ A_L e^{j\phi_L}]^T$ is the vector of complex amplitudes and $\mathbf{w} = \big[w[0]\ w[1]\ \dots\ w[N-1]\big]^T$ is the noise vector. The autocorrelation matrix $\mathbf{R}$ of $\mathbf{r}$ is,

$$\mathbf{R} = \mathbf{Z}\,\mathbb{E}\{\mathbf{a}\mathbf{a}^H\}\mathbf{Z}^H + \sigma_w^2 \mathbf{I}. \tag{3.5}$$

If the phase terms, $\{\phi_1, \dots, \phi_L\}$, are statistically independent and uniformly distributed on the interval $(-\pi, \pi]$, the expression in (3.5) can be written as

$$\mathbf{R} = \sum_{l=1}^{L} A_l^2 \mathbf{e}[l]\mathbf{e}[l]^H + \sigma_w^2 \mathbf{I}, \tag{3.6}$$

where $\mathbf{e}[l] = [1\ e^{j\omega_0 l}\ \dots\ e^{j\omega_0 l(N-1)}]^T$.

Given a single snapshot vector $\mathbf{r}$, the sample covariance matrix (the maximum likelihood estimate of the autocorrelation matrix for Gaussian vectors) can be expressed as

$$\widehat{\mathbf{R}} = \frac{1}{N-M+1} \sum_{n=0}^{N-M} \widetilde{\mathbf{r}}[n]\widetilde{\mathbf{r}}[n]^H, \tag{3.7}$$

where $\widetilde{\mathbf{r}}[n] = \big[r[n]\ r[n+1]\ \dots\ r[n+M-1]\big]^T$ and $\widehat{\mathbf{R}}$ is a $M \times M$ matrix . Note that to obtain a non-singular $\widehat{\mathbf{R}}$, M should be smaller than $\frac{N}{2}+1$ and also to resolve each harmonic component, M should be larger than the number of harmonics L.

3.2 Cramer-Rao Bound (CRB)

The non-random unknown parameter vector is given as $\boldsymbol{\psi} = [\omega_0 \; A_1 \; \phi_1 \; A_2 \; \phi_2 \; \ldots \; A_l \; \phi_l]^T$. The expression in (3.8) shows the elements of Fisher information matrix (FIM) and it is the simplified version of the Fisher information matrix for the Gaussian vectors [2]:

$$\begin{aligned} \mathbf{I}[\boldsymbol{\psi}]_{ij} &= 2\,\mathrm{Real}\left[\frac{\partial(\mathbf{Za})}{\partial\psi_i}^H \frac{1}{\sigma_w^2}\frac{\partial(\mathbf{Za})}{\partial\psi_j}\right], \\ &= \frac{2}{\sigma_w^2}\,\mathrm{Real}\left[\sum_{m=0}^{N-1}\frac{\partial(\mathbf{Za})[n,\boldsymbol{\psi}])}{\partial\psi_i}^{*}\frac{\partial(\mathbf{Za}[n,\boldsymbol{\psi}])}{\partial\psi_j}\right]. \end{aligned} \tag{3.8}$$

Here ψ_i is the i'th element of the vector $\boldsymbol{\psi}$ and $\mathbf{Za}[n,\boldsymbol{\psi}] = \sum_{l=1}^{L} A_l e^{j(\omega_0 l n+\phi_l)}$. Hence, we have

$$\frac{\partial(\mathbf{Za}[n,\boldsymbol{\psi}])}{\partial\boldsymbol{\psi}} = \begin{bmatrix} jn\sum_{l=1}^{L} lA_l e^{j(\omega_0 l n+\phi_l)} \\ e^{j(\omega_0 1 n+\phi_1)} \\ jA_1 e^{j(\omega_0 1 n+\phi_1)} \\ \vdots \\ e^{j(\omega_0 L n+\phi_L)} \\ jA_L e^{j(\omega_0 L n+\phi_L)} \end{bmatrix}. \tag{3.9}$$

Assuming that ω_0 is not close to 0 and N is large, FIM is approximately [43],

$$\mathbf{I}[\boldsymbol{\psi}] \approx \mathbf{S} = \frac{2}{\sigma_w^2}\begin{bmatrix} \gamma & 0 & A_1^2 1\frac{N(N-1)}{2} & \ldots & 0 & A_L^2 L\frac{N(N-1)}{2} \\ 0 & N & 0 & \ldots & 0 & 0 \\ A_1^2 1\frac{N(N-1)}{2} & 0 & A_1^2 N & \ldots & 0 & 0 \\ \vdots & \vdots & \vdots & \ddots & \vdots & \vdots \\ 0 & 0 & 0 & \ldots & N & 0 \\ A_L^2 L\frac{N(N-1)}{2} & 0 & 0 & \ldots & 0 & A_L^2 N \end{bmatrix}_{(2L+1)\times(2L+1)} \tag{3.10}$$

where $\gamma = \sum_{l=l}^{L} A_l^2 l^2 \frac{N(N-1)(2N-1)}{6}$. The matrix $\mathbf{S}$ is composed of the vector $\mathbf{h}$, diagonal matrix $\mathbf{D}$ and a scalar γ which can be represented as:

$$\mathbf{S} = \begin{bmatrix} \gamma & \mathbf{h}^H \\ \\ \mathbf{h} & \mathbf{D} \end{bmatrix}. \tag{3.11}$$

By using the matrix inversion lemma [1], the first element of the matrix $\mathbf{S}^{-1}$ can be calculated as,

$$[\mathbf{S}^{-1}]_{11} = (\gamma - \mathbf{h}^H \mathbf{D}^{-1} \mathbf{h})^{-1}. \tag{3.12}$$

Finally, the asymptotic Cramer-Rao Lower Bound (ACRB) for large N [43] for the fundamental frequency becomes,

$$\text{var}(\widehat{\omega}_0) \geq \left[\mathbf{I}^{-1}[\boldsymbol{\psi}]\right]_{11} \approx \frac{6\sigma_w^2}{N(N^2-1)\sum_{l=1}^{L} A_l^2 l^2}. \tag{3.13}$$

To convert this bound to the unit of N-point DFT bins, we scale the bound by $\frac{N^2}{(2\pi)^2}$, since $f = 1 \leftrightarrow \omega_0 = 2\pi \leftrightarrow N$'th DFT bin:

$$\begin{aligned} \text{var}(\widehat{f}_0) &\geq \left[\mathbf{I}^{-1}[\boldsymbol{\psi}]\right]_{11} / (2\pi)^2 \approx \frac{3\sigma_w^2}{2\pi^2 N(N^2-1)\sum_{l=1}^{L} A_l^2 l^2}, \\ \text{var}(\widehat{f}_0 N) &\geq N^2 \left[\mathbf{I}^{-1}[\boldsymbol{\psi}]\right]_{11} / (2\pi)^2 \approx \frac{3N\sigma_w^2}{2\pi^2 (N^2-1)\sum_{l=1}^{L} A_l^2 l^2}. \end{aligned} \tag{3.14}$$

In the presence of random nuisance parameters, whose values are of no interest, an exact calculation of CRB is often difficult. Some simpler, alternative bounds are studied in [44] to avoid the complications due to the nuisance parameters. In our model, the phase terms $\{\phi_1, \ldots, \phi_L\}$ are considered as random nuisance parameters which are statistically independent and uniformly distributed in the interval $(-\pi, \pi]$. The Hybrid Cramer Rao Bound (HCRB) is one of the bounds, looser than exact Cramer-Rao Bound (also called as posterior Cramer-Rao Bound) that can be used when nuisance parameters are present. To calculate HCRB, the expectation of the deterministic FIM matrix given by equation (3.8) is calculated with respect to the nuisance parameters first and then the matrix is inverted. Since we have $E\{e^{j\phi_l}\} = 0$ and $E\{e^{j\phi_l} e^{-j\phi_k}\} = \delta[l-k]$ where $k, l \in \{1, \ldots, L\}$; the expectation of each entry of FIM matrix given in (3.8) is identical to the entries of the asymptotic FIM in (3.10). Hence, the CRB for the non-random parameter setting as $N \to \infty$ (ACRB) and

HCRB with uniformly distributed phases are identical:

$$\mathrm{HCRB}(\widehat{\omega}_0) = \left[(\mathbb{E}_{\phi_1,\ldots,\phi_L}\{[\mathbf{I}[\boldsymbol{\psi}]]\})^{-1}\right]_{11} = \left[\mathbf{S}^{-1}[\boldsymbol{\psi}]\right]_{11} = \frac{6\sigma_w^2}{N(N^2-1)\sum_{l=1}^{L} A_l^2 l^2}. \tag{3.15}$$

With the PSNR definition in (3.2), HCRB reduces to

$$\mathrm{HCRB}(\widehat{\omega}_0) = \frac{6}{N(N^2-1)\mathrm{PSNR}}. \tag{3.16}$$

3.3 Maximum Likelihood Estimation (MLE)

For the complex white Gaussian noise model, the joint distribution of observations in (3.1) can be given as [19],

$$p(\mathbf{r};\boldsymbol{\psi}) = \frac{1}{(\pi\sigma_w^2)^N} \exp\left[-\frac{1}{\sigma_w^2}(\mathbf{r}-\mathbf{Za})^H(\mathbf{r}-\mathbf{Za})\right], \tag{3.17}$$

or more explicitly,

$$p(\mathbf{r};\boldsymbol{\psi}) = \frac{1}{(\pi\sigma_w^2)^N} \exp\left[-\frac{1}{\sigma_w^2}\sum_{n=0}^{N-1}\left|r[n]-\sum_{l=1}^{L}A_l e^{j(\omega_0 ln+\phi_l)}\right|^2\right]. \tag{3.18}$$

The maximum likelihood estimates (MLE) of the unknown parameters can be found by minimizing negative of the log-likelihood function given below:

$$\begin{aligned} J(\mathbf{r},\boldsymbol{\psi}) =& \sum_{n=0}^{N-1}\left|r[n]-\sum_{l=1}^{L}A_l e^{j(\omega_0 ln+\phi_l)}\right|^2, \\ =&(\mathbf{r}-\mathbf{Za})^H(\mathbf{r}-\mathbf{Za}). \end{aligned} \tag{3.19}$$

By minimizing (3.19) over the complex amplitude vector $\mathbf{a}$, we get,

$$\widehat{\mathbf{a}} = (\mathbf{Z}^H\mathbf{Z})^{-1}\mathbf{Z}^H\mathbf{r}, \tag{3.20}$$

and inserting the estimate $\widehat{\mathbf{a}}$ into negative log-likelihood expression, we have

$$\begin{aligned} J'(\mathbf{r},\widehat{\mathbf{a}},\omega_0) =&(\mathbf{r}-\mathbf{Z}\widehat{\mathbf{a}})^H(\mathbf{r}-\mathbf{Z}\widehat{\mathbf{a}}), \\ =&(\mathbf{r}-\mathbf{Z}(\mathbf{Z}^H\mathbf{Z})^{-1}\mathbf{Z}^H\mathbf{r})^H(\mathbf{r}-\mathbf{Z}(\mathbf{Z}^H\mathbf{Z})^{-1}\mathbf{Z}^H\mathbf{r}), \\ =&\mathbf{r}^H(\mathbf{I}-\mathbf{Z}(\mathbf{Z}^H\mathbf{Z})^{-1}\mathbf{Z}^H)^H(\mathbf{I}-\mathbf{Z}(\mathbf{Z}^H\mathbf{Z})^{-1}\mathbf{Z}^H)\mathbf{r}, \\ =&\mathbf{r}^H(\mathbf{P}_{\mathbf{Z}}^{\perp})^H\mathbf{P}_{\mathbf{Z}}^{\perp}\mathbf{r} = \mathbf{r}^H\mathbf{P}_{\mathbf{Z}}^{\perp}\mathbf{r} = ||\mathbf{P}_{\mathbf{Z}}^{\perp}\mathbf{r}||_2^2, \end{aligned} \tag{3.21}$$

where $\mathbf{P_Z} = \mathbf{Z}(\mathbf{Z}^H\mathbf{Z})^{-1}\mathbf{Z}^H$ is the projection matrix to the range space of $\mathbf{Z}$ and $\mathbf{P}_\mathbf{Z}^\perp = \mathbf{I} - \mathbf{Z}(\mathbf{Z}^H\mathbf{Z})^{-1}\mathbf{Z}^H$ is the projector to the orthogonal complement of range space of $\mathbf{Z}$. It is important to note that we make use of $(\mathbf{P}_\mathbf{Z}^\perp)^H = \mathbf{P}_\mathbf{Z}^\perp$ and $(\mathbf{P}_\mathbf{Z}^\perp)^2 = \mathbf{P}_\mathbf{Z}^\perp$ in this calculation. To get the fundamental frequency estimation, we minimize the expression in (3.21) or equivalently maximize $||\mathbf{P_Z r}||_2^2$, as shown below:

$$\begin{aligned}
\widehat{\omega}_0 &= \arg\max_{\omega_0} ||\mathbf{P_Z r}||_2^2 = \arg\max_{\omega_0} \mathbf{r}^H\mathbf{P_Z r}, \\
&= \arg\max_{\omega_0} \mathbf{r}^H\mathbf{Z}(\mathbf{Z}^H\mathbf{Z})^{-1}\mathbf{Z}^H\mathbf{r} \approx \arg\max_{\omega_0} \frac{||\mathbf{Z}(\omega_0)\mathbf{r}||_2^2}{N}, \\
&= \arg\max_{\omega_0} \frac{1}{N}\sum_{l=1}^{L}\left|\sum_{n=0}^{N-1} r[n]e^{-j\omega_0 ln}\right|^2.
\end{aligned} \tag{3.22}$$

In (3.22), an asymptotic ($N \to \infty$) approximation of $\mathbf{Z}^H\mathbf{Z} \approx N\mathbf{I}$ is used for simplification. Hence, the asymptotic ML estimate is the frequency for which the sum of the magnitude squares of the DTFT samples at the frequency and its harmonics is maximized; that is the frequency for which the maximum total power is achieved.

As a side note, for the same problem, an estimate for noise variance estimate can be given as,

$$\widehat{\sigma}_w^2 = \frac{1}{N}||\mathbf{r} - \mathbf{P_Z r}||_2^2. \tag{3.23}$$

By inserting the estimates in (3.17), we can write the log-likelihood expression as

$$\ln p(\mathbf{r}; \widehat{\boldsymbol{\psi}}) = -N\ln\pi - N\ln\widehat{\sigma}_w^2 - N. \tag{3.24}$$

In Appendix A, the specialization of the MUSIC and ESPRIT methods to the fundamental frequency estimation are described. The proposed method is compared with MLE, MUSIC and ESPRIT methods in the numerical results chapter.

3.4 Model Order Selection

Model order selection refers to the detection of the total number of harmonics L in the context of fundamental frequency estimation problem. To clarify the concept, if $L = 2$, then the input is considered to be a periodic signal with a fundamental frequency ω_0 and a single harmonic at the frequency $2\omega_0$. For the same input, if the model order L is mistakenly taken as 4, the fundamental frequency can be erroneously estimated as $\omega_0/2$; since the total signal power at the frequencies $\{\omega_0/2, \omega_0,\ 3\omega_0/2,\ 2\omega_0\}$ includes the total power at the true signal frequencies $\{\omega_0, 2\omega_0\}$. An automated model order selection procedure enables the resolution of such issues and also improves the low SNR performance of sub-optimal frequency estimators by disregarding the contributions of harmonics buried under noise due their small valued amplitudes.

The Akaike information criterion (AIC) [45], the minimum description length criterion (MDL) [46] and the MAP approach [47, 48] are examples of the most popular model order selection criteria [49]. Basically, AIC and MDL minimize the following expression to decide on model order:

$$J(l) = \underbrace{-\ln p(\mathbf{r}; \widehat{\boldsymbol{\psi}}_{ML}, L = l)}_{\text{negative log-likelihood}} + \underbrace{\gamma(L = l)\eta}_{\text{penalty term}}. \tag{3.25}$$

Here η is the penalty coefficient and the coefficient is equal to 1 for AIC and $0.5 \ln N$ for MDL. The coefficient γ is the total number of parameters in the signal model. In our model, we have $\gamma = 2L + 2$ unknown parameters (L amplitudes, L phases, the fundamental frequency and noise variance). Without any penalty terms, the maximum likelihood approach and other classical methods suffer from over-fitting problem, (an increase in the number of harmonics results in an increase in the log-likelihood value). With the penalty term, the inclusion of additional unknown parameters (overfitting) is penalized. In this study, we use MAP approach for model order selection. In MAP approach, the selection of the most probable model is based on posterior probability maximization where the posterior probability is written as $p(L = l|\mathbf{r})$ and $\mathbf{r}$ is the observation vector, $l \in \{1, \ldots, L_{\max}\}$ and $L_{\max}$ is the maximum possible model order:

$$\begin{aligned} \widehat{L} &= \arg\max_{l} p(L = l|\mathbf{r}) \\ &= \arg\max_{l} \frac{p(\mathbf{r}|L = l)p(L = l)}{p(\mathbf{r})}. \end{aligned} \tag{3.26}$$

By assuming that all models are equally probable, the selection criterion reduces to,

$$\widehat{L} = \arg\max_{l} p(\mathbf{r}|L = l). \tag{3.27}$$

As shown in [19], the model order selection via MAP method reduces to

$$\widehat{L}_{\text{MAP}} = \arg\min_{L} \underbrace{N \ln \widehat{\sigma}_w^2(L)}_{\text{log-likelihood}} + \underbrace{\frac{3}{2} \ln N + L \ln N}_{\text{penalty term}}, \tag{3.28}$$

where noise variance estimate $\widehat{\sigma}_w^2$ is given in (3.24). We note that MAP based approach and MDL for the model order selection are identical for this problem; however, this is not the case in general.

3.5 Proposed Method

In this section, the proposed estimator is presented. As shown in (3.1), the harmonic signal model can be considered as a superposition of multiple complex exponential signals. For models involving superposition of signals, RELAX algorithm (successive interference cancellation) is proposed in the literature [18]. With this method, the problem reduces to the parameter estimation problem of a single complex exponential signal provided that interference from other harmonics can be successfully cancelled.

The steps of RELAX algorithm for the case of $L = 3$ can be simply explained as follows:

- Step (1): Obtain estimates $\widehat{f}_1$ and $\widehat{A}_1$ by processing the input $r[n]$. Then, reconstruct and subtract the estimated sinusoidal component with parameters $\widehat{f}_1$ and $\widehat{A}_1$ from $r[n]$ and call the result $r_2[n]$.
- Step (2): Operate on $r_2[n]$ and obtain the estimates $\widehat{f}_2$ and $\widehat{A}_2$. Then, reconstruct and subtract the estimated sinusoidal component with parameters $\widehat{f}_2$ and $\widehat{A}_2$ from $r_2[n]$ and call the result $r_3[n]$.
- Step (3): Operate on $r_3[n]$ and obtain estimates $\widehat{f}_3$ and $\widehat{A}_3$.

In the successive interference cancellation schemes, the order of estimation plays an important role. Generally speaking, the estimation order starts from the strongest component in the superposition and moves towards the 2nd strongest and then to the 3rd strongest and so on. The goal is to reliably estimate and cancel each component sequentially so that the parameters of the weakest component in the superposition can be accurately estimated.

Different from this general set-up, the frequency parameters to be estimated in the problem of interest are related via a harmonic relation. Hence, there exists a deterministic constraint between non-random parameters to be estimated at each step of successive cancellation algorithm. This simplifies the estimation and interference cancellation procedures at each step.

Our goal is to extend the low complexity fine frequency methods given for the complex exponentials to the fundamental frequency estimation problem. The proposed method [39] estimates the frequencies of all harmonically related complex exponentials individually, after successively eliminating the interference due to other harmonics. Also, we make use of the deterministic relation between the frequencies of harmonics and suggest a fusion step to combine the frequency estimates generated in all steps of the method.

The proposed estimator is composed of two stages. The first stage obtains a coarse estimate, $\widehat{k}_{p_f}$. (The notation $\widehat{k}_{p_f}$ denotes the coarse part of the fundamental frequency.) First, N-point DFT of the input $r[n]$ is calculated $R[k] = \sum_{n=0}^{N-1} r[n] e^{-j\frac{2\pi}{N}kn}$ and the coarse frequency estimate is obtained by the maximum likelihood search, as in (3.22), over a coarse grid with only N points:

$$\widehat{k}_{p_f} = \underset{1 \le k \le \lfloor N/L \rfloor}{\arg\max} \sum_{l=1}^{L} |R[kl]|^2 . \tag{3.29}$$

To increase the accuracy of the first stage, DFT size can be increased. For example, $4N$-point DFT can be used. The performance increase in the first stage increases the performance of the estimator especially at low SNR region.

The second stage has two parts. In the first part, the first stage result $\widehat{k}_{p_f}$ is refined by using the available information in the data about the fundamental component. The refined frequency estimate is shown as $\widehat{s}_1 = \widehat{\omega}$. In the second part, the frequency estimates for higher order harmonics, that is $\{\widehat{s}_2, \ldots, \widehat{s}_L\}$ are generated. Under noiseless operation, the frequency estimates is to satisfy $\widehat{s}_k = k\widehat{s}_1$ for $k = \{1, \ldots, L\}$. The main difference between the first and second parts of the second stage is some operations (the complex amplitude estimation) are not repeated in the second part. The parts are indicated as “Second Stage - First Part” and “Second Stage - Second Part” in Algorithm Table 2.

In the second stage - first part, AM algorithm is applied to the DFT bin with index $k = \widehat{k}_{p_f}$. More specifically, the variable $\widehat{k}_p$ in AM algorithm (see Algorithm Table 1) is set as $\widehat{k}_{p_f}$ and the second stage of the AM algorithm is executed as it is. The estimate produced by AM algorithm is also denoted as $\widehat{s}_1$.

Once an estimate for the fundamental frequency is available, the complex amplitude vector $\mathbf{a}$ is estimated using the linear observation model in (3.3) via the least squares solution:

$$\widehat{\mathbf{a}} = (\mathbf{Z}^H(\widehat{s}_1)\mathbf{Z}(\widehat{s}_1))^{-1}\mathbf{Z}^H(\widehat{s}_1)\mathbf{r}. \tag{3.30}$$

Here $\mathbf{Z}$ is the Vandermonde matrix in (3.3).

Once an estimate for the fundamental frequency and the complex amplitudes are available, it is possible to reconstruct each harmonic. We follow the successive interference cancellation approach and re-run the AM algorithm after the reconstruction and cancellation of all harmonics except the fundamental one. The equation below shows the cancellation all harmonics except k'th one from the input:

$$r_k[n] = r[n] - \sum_{l=1, l\neq k}^{L} \widehat{a}_l e^{j\frac{\widehat{s}_k}{k}ln}, \quad n = \{0, \dots, N-1\}. \tag{3.31}$$

In the second stage - first part, the fundamental component is kept and all higher order harmonics are cancelled by setting $k = 1$ in (3.31). The estimate $\widehat{s}_k$ in (3.31) is the estimated frequency of the k'th harmonic. The steps of estimation-reconstruction-cancellation are repeated to improve the estimates for a given number of iterations, as shown in Algorithm Table 2.

The second stage - second part is almost identical to the earlier part. The main differences are the frequency estimates correspond to the frequencies of higher order harmonics which are shown as $\{\widehat{s}_2, \dots, \widehat{s}_L\}$ and the complex amplitude estimate vector is not calculated, that is the result in the first stage, given by (3.30), is used to save computation. To apply the AM algorithm on the k'th harmonic, the spectrum sample with the frequency $k\widehat{s}_1 \in [0, 2\pi)$ is the utilized as the initial estimate. More specifically, the AM algorithm parameter $\widehat{k}_p$ in Step 2 of AM method in Algorithm Table 1 is set as the index of the DFT bin closest to $k\widehat{s}_1$, that is $\widehat{k}_p = \text{round}(k\widehat{s}_1\frac{N}{2\pi})$. Here $\text{round}(\cdot)$ is the rounding operation to the closest integer and $\frac{N}{2\pi}$ factor is the unit conversion factor from radian per sample to the N-point DFT bins. Also, the initial fine frequency estimate $\widehat{\delta}^{(0)}$, which is set as 0 in Step 3 of Algorithm Table 1, is set as the decimal part of $k\widehat{s}_1$ after the conversion to the units of DFT bins, $\widehat{\delta}^{(0)} = k\widehat{s}_1\frac{N}{2\pi} - \widehat{k}_p$.

After the completion of the second stage, we have a total of L estimates for the location of the fundamental and harmonic frequencies in the spectrum. Next, we combine these estimates by taking into account the deterministic relation between true values of harmonics, namely $s_k = k \times \omega_0$, $k = \{1, \ldots, L\}$.

The estimation result for the k'th harmonic frequency can be represented as $\widehat{s}_k = k\omega_0 + n_k$ where ω_0 is the fundamental frequency and n_k is the noise component (estimation error) with zero mean and $(\frac{2\pi}{N})^2 \times \frac{\pi^2\sigma_w^2}{64A_k^2N}$ variance at high SNR conditions (see (2.52)). As discussed in Section 2.1, the spectrum samples which are separated by an integer number of DFT bins are independent random variables. If the separation is of fractional bins than the spectrum samples are correlated. In spite of this fact, we ignore the possible correlation between estimates and assume that the frequency estimates are corrupted with a zero mean and known variance *uncorrelated* noise. With this assumption, it is possible to use Best Linear Unbiased Estimator (BLUE) [2] for the fusion of estimates:

$$\widehat{\omega}_0 = \frac{\mathbf{m}^T\mathbf{K}^{-1}\widehat{\mathbf{s}}}{\mathbf{m}^T\mathbf{K}^{-1}\mathbf{m}}. \tag{3.32}$$

Here $\mathbf{m} = [1\ 2\ \ldots\ L]^T$ and $\mathbf{K}$ is the covariance matrix of vector $\widehat{\mathbf{s}} = [\widehat{s}_1\ \widehat{s}_2\ \ldots\ \widehat{s}_L]^T$. The covariance matrix $\mathbf{K}$ is a diagonal matrix, with the uncorrelated noise assumption, and its k'th diagonal is the variance of noise for the k'th harmonic estimate which is $(\frac{2\pi}{N})^2 \times \frac{\pi^2\sigma_w^2}{64A_k^2N} = c/A_k^2 \propto 1/A_k^2$ according to the high SNR analysis given in (2.52). By simple manipulation, we can express the final estimate as,

$$\widehat{\omega}_0 \triangleq \frac{A_1^2\widehat{s}_1 + 2A_2^2\widehat{s}_2 + \ldots + LA_L^2\widehat{s}_L}{A_1^2 + 2^2A_2^2 + \ldots + L^2A_L^2}. \tag{3.33}$$

Here A_k is the true amplitude of the k'th harmonic which is an unknown. We suggest to utilize the magnitude of the k'th complex amplitude estimate in (3.30) ($|\widehat{a}_k|$) instead of the true values (A_k) in the fusion operation.

The MSE of the fundamental frequency estimate after fusion can be given as:

$$\begin{aligned}
\mathrm{var}(2\pi\widehat{f}_0) =& \mathrm{var}\left(\frac{A_1^2\widehat{s}_1 + 2A_2^2\widehat{s}_2 + \ldots + LA_L^2\widehat{s}_L}{A_1^2 + 2^2A_2^2 + \ldots + L^2A_L^2}\right), \\
=& \frac{\frac{A_1^4c}{A_1^2} + \frac{2^2A_2^4c}{A_2^2} + \ldots + \frac{L^2A_L^4c}{A_L^2}}{(A_1^2 + 2^2A_2^2 + \ldots + L^2A_L^2)^2}, \\
=& \frac{c \times \mathrm{PSNR}}{\mathrm{PSNR}^2} = \frac{\pi^4}{16\mathrm{PSNR}N^3}.
\end{aligned} \tag{3.34}$$

The theoretical estimator variance is 1.0147 times bigger than ACRB in (3.13).

In Figure 3.1, the simulation results are given for different scenarios. The details of scenarios are given in the figure label. The performance curve labelled as “Proposed Method (fundamental only)” (red curve) represents the performance of the estimator when the fusion rule is not implemented. Here the estimate $\widehat{s}_1$ is taken as the final estimate. The blue curve labelled “Proposed Method (Fusion)” illustrates the performance improvement provided by the fusion rule. For the SNR range given in this figure, only 2 iterations are sufficient for the AM algorithm (see Section 2.5.1) and for the harmonic cancellation stage, again 2 iterations are used. The figure shows that RMSE of the proposed estimator is on the order of ACRB and the fusion rule improves the performance significantly by utilizing the power of higher order harmonics.

As a side note, we would like to mention that the method is described by considering that the fundamental component is the strongest component of the periodic signal. If this is not the case, the suggested method, as described, performs poorly. In such cases, the initial frequency and the complex amplitude estimation should be done by using the strongest harmonic component.

Figure 3.2 shows the effect of missing harmonics on the performance. The results show that as long as two consecutive harmonics are present, the estimator works properly. Figure 3.2(b) shows the case of $A_1 = A_4 = 0$, which is the case of missing fundamental component. The numerical results chapter of this thesis also includes several other comparisons.

Algorithm 2: Proposed Method

Input : $r[n]$: N samples of noisy set of complex sinusoids having frequencies that are multiples of the fundamental frequency.

Output: $\widehat{\omega}_0 = \frac{2\pi}{N}(\widehat{k}_{p_f} + \widehat{\delta})$ rad./sample

First Stage:

$R[k]$ =fft$(r[n], N)$ (N-point FFT calculation).

$\widehat{k}_{p_f} = \underset{1 \leq k \leq \lfloor N/L \rfloor}{\arg\max} \sum_{l=1}^{L} |R[kl]|^2$.

Second Stage - First Part:

for $i = 1$: maximum iteration

    Apply AM algorithm to the bin $\widehat{k}_p = \widehat{k}_{p_f}$ and get $\widehat{s}_1 = \widehat{\omega}$. (see Algorithm 1)

    Construct the matrix **Z** using the frequency estimate $\widehat{s}_1$ (use 3.4)

    Estimate the complex amplitudes of the harmonics (use 3.30)

    Reconstruct and subtract all harmonics expect the first one from $r[n]$. (use 3.31)

end for

return $\widehat{s}_1$ and the vector $\widehat{\mathbf{a}}$

Second Stage - Second Part:

for $k = 2 : L$

    for $i = 1$: maximum iteration

        Apply AM algorithm to the bin closest to $k\widehat{s}_1$ and get $\widehat{s}_k = \widehat{\omega}$. (see Algorithm 1)

        Reconstruct and subtract all harmonics expect the k'th one from $r[n]$. (use 3.31)

    end for

    return $\widehat{s}_k$

end for

return $[\widehat{s}_2 \ldots \widehat{s}_{L-1}\ \widehat{s}_L]^T$

Fusion Operation:

Apply the fusion rule on the vector $\widehat{\mathbf{s}} = [\widehat{s}_1\ \widehat{s}_2\ \ldots\ \widehat{s}_{L-1}\ \widehat{s}_L]^T$ by using $\widehat{\mathbf{a}}$. (use 3.33)

Return $\widehat{\omega}_0 = \frac{2\pi}{N}(\widehat{k}_{p_f} + \widehat{\delta})$

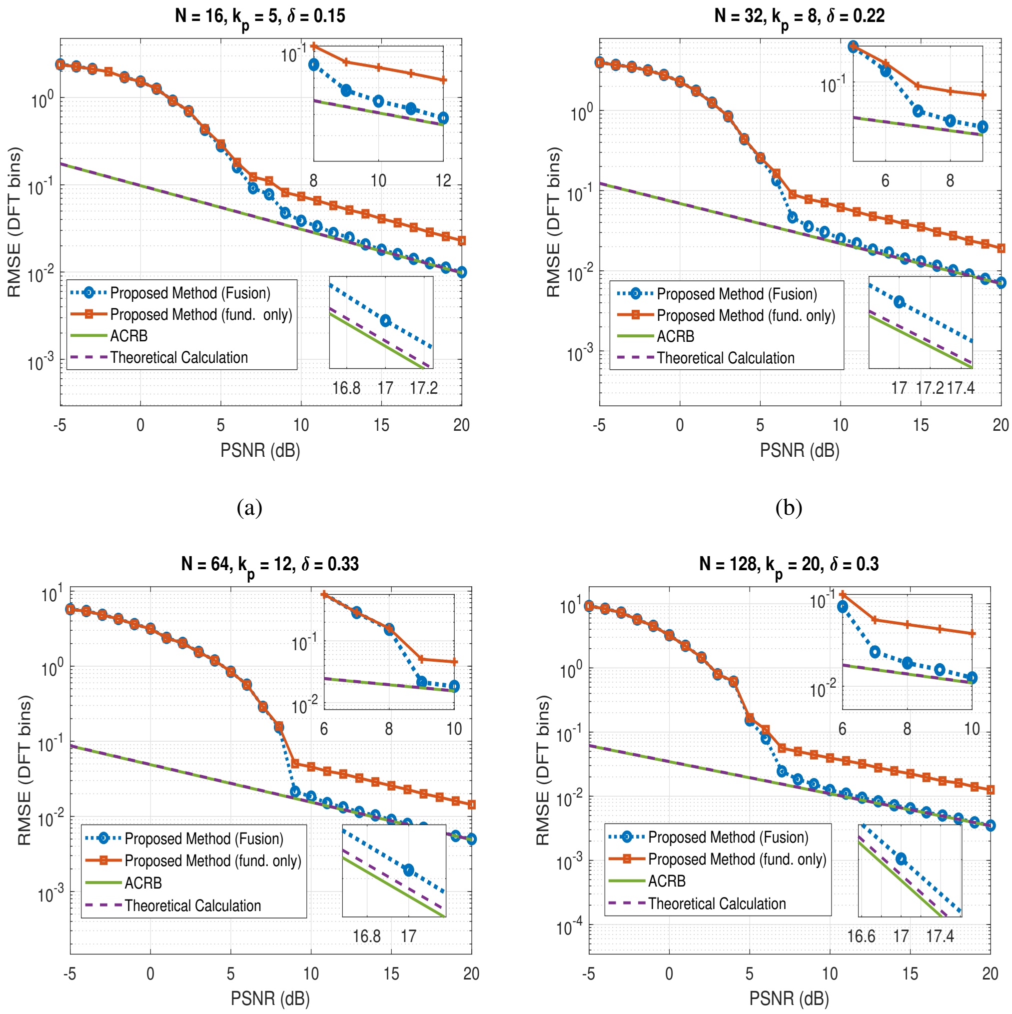

(a) (b) (c) (d)

Figure 3.1: Performance of the Proposed Estimator: (a) $f_0 = \frac{5+0.15}{16}$, $L = 2$ and $A_1 = A_2$, (b) $f_0 = \frac{8+0.22}{32}$, $L = 3$ and $A_1 = A_2 = 2A_3$, (c) $f_0 = \frac{12+0.33}{64}$, $L = 4$ and $A_1 = A_2 = 2A_3 = 4A_4$, (d) $f_0 = \frac{20+0.3}{128}$, $L = 5$ and $A_1 = A_2 = 2A_3 = 2A_4 = 4A_5$.

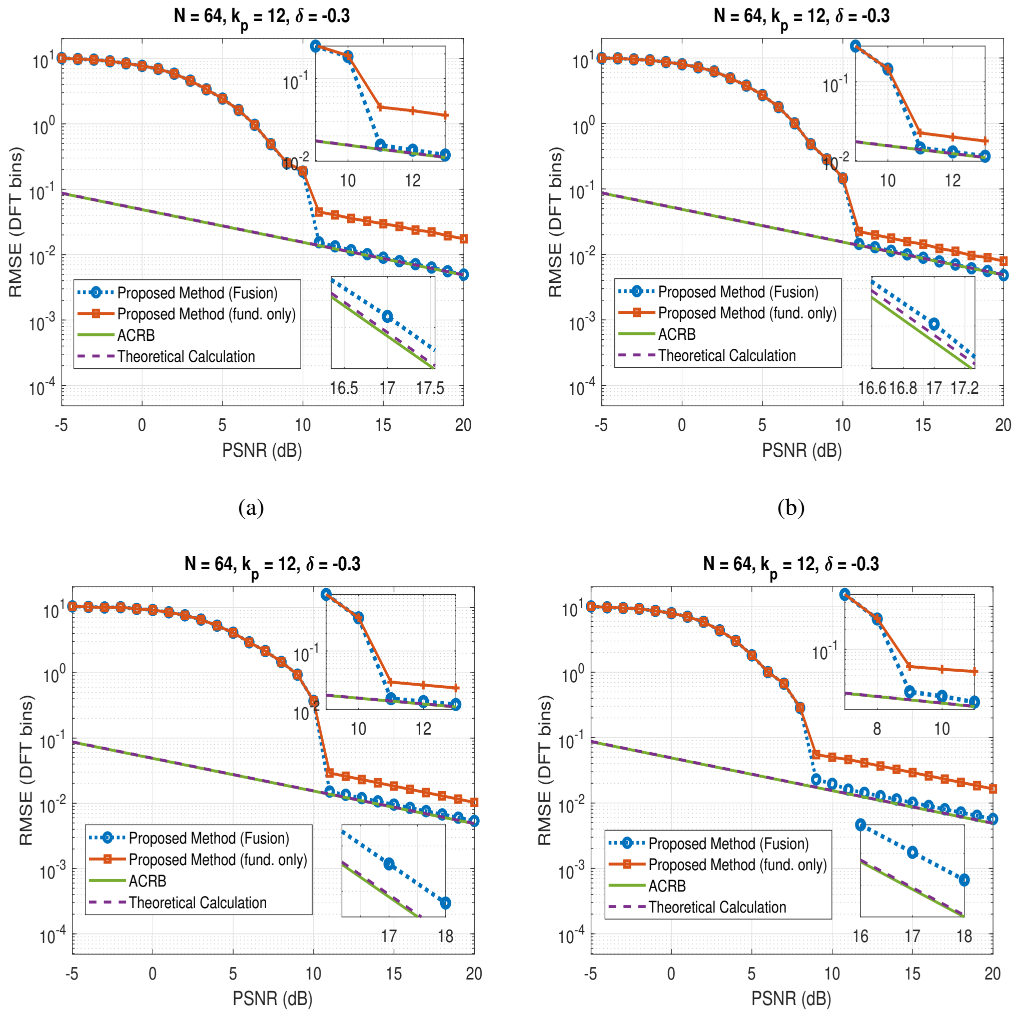

(a) (b)

(c) (d)

Figure 3.2: Performance of the Proposed Estimator: $f_0 = \frac{12-0.3}{64}$ and $L = 4$ (a) $A_1 = A_2 = A_4$ and $A_3 = 0$, (b) $A_2 = A_3$ and $A_1 = A_4 = 0$, (c) $A_2 = A_3 = A_4$ and $A_1 = 0$, (d) $A_1 = A_3 = A_4$ and $A_2 = 0$.

CHAPTER 4

DIRECTION OF ARRIVAL ESTIMATION PROBLEM FOR PERIODIC SIGNALS WITH HARMONICS

Direction of arrival estimation (DOA) is a problem of array signal processing with applications in radar signal processing, wireless communication and several other applications involving tracking and localization of signal sources. Conventional DOA estimation literature can be categorized into two based on the signal bandwidth as narrowband and wideband DOA estimation. In this chapter, we study the DOA estimation problem for a special class of signals which is the periodic signals with several harmonics. The study is well suited for the DOA estimation of acoustic signals. As an illustrative example, we may consider the problem of angular localization of a musician playing an instrument in a multipath-free environment. The incoming signal, say the sound of a violin, in a short-time window can be considered as a sum of several harmonics in relation with the physics of the instrument. The fundamental frequency, typically, corresponds to the frequency of the note shown in the music sheets; but, there are several higher harmonics generated by the instrument making the sound of each instrument uniquely different from each other[1]. Results of this chapter are applicable to the angular localization of such sources. Similarly, in some underwater applications, the signal of interest can be of periodic nature, such as the propeller noise of vessels. The suggested method is also applicable for some underwater signal processing applications. The conventional approach for the detection and DOA estimation of such signal sources is based on the strongest harmonic component. Different from the conventional approach, we examine the DOA estimation problem by taking into account the harmonic structure of the signal.

[1] You can get more information on the harmonic structure of string instruments from `https://newt.phys.unsw.edu.au/jw/strings.html`.

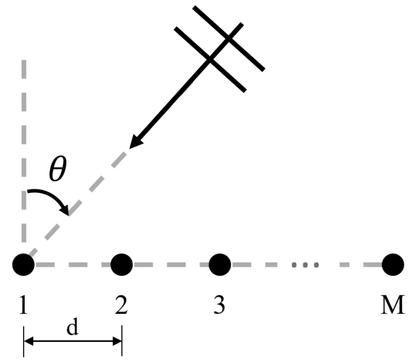

Figure 4.1: Uniform Linear Array Structure.

The direction of arrival estimation problem can be interpreted as the spatial frequency estimation problem. Our main goal in this chapter is to apply the efficient frequency estimation method given in earlier chapters to the spatial frequency estimation setting. We consider uniform linear array (ULA) structure with M identical and omnidirectional sensors and consider a single incoming periodic signal with several harmonics originated in the far field region.

In this chapter, we first review the basics of array signal processing to clarify the spatial frequency concept and then extend the discussion to the sources with several harmonics. Some pre-processing methods and their effect on the harmonic structure are discussed. Cramer-Rao bounds for the systems utilizing higher order harmonics and conventional systems utilizing only the fundamental component are compared.

4.1 DOA Estimation with Uniform Linear Array: Monochromatic Wave

Uniform linear array (ULA) with M elements is an array of M equidistant sensors placed on a line as shown in Figure 4.1. Each sensor receives the delayed version of the incoming signal. For the configuration shown in Figure 4.1, the delay between two consecutive sensors is $d\sin(\theta)/c$ where d is the sensor spacing, c is the propagation speed of the signal and θ is the angle of incoming wave measured from boresight. In this section, we examine the case of monochromatic wave, that is the case of $s(t) = A(t)\exp^{j\Omega_c t}$ where $A(t)$ is the complex amplitude which is considered to be constant, $A(t) \approx Me^{j\phi}$, during the processing interval under the narrowband assumption.

The signal received by the kth sensor can be expressed as

$$r_k(t) = s(t - \tau_k), \quad k = \{1, \dots, M\} \tag{4.1}$$

where τ_k is the delay due to signal propagation from the emitter to the kth sensor. The delay τ_k can be expressed as

$$\tau_k = \tau_1 - \frac{(k-1)d\sin(\theta)}{c}, \quad k = \{1, \dots, M\}. \tag{4.2}$$

where τ_1 is the delay from the emitter to the first sensor.

One can construct $M \times 1$ dimensional snapshot vector $\mathbf{r}(t)$ by concatenating the sensor outputs of the same time instant, as shown below:

$$\mathbf{r}(t) = \begin{bmatrix} r_1(t) \\ r_2(t) \\ \vdots \\ r_M(t) \end{bmatrix} = \begin{bmatrix} s(t-\tau_1) \\ s(t-\tau_2) \\ \vdots \\ s(t-\tau_M) \end{bmatrix} = e^{j\Omega_c(t-\tau_1)} \begin{bmatrix} A(t-\tau_1) \\ A(t-\tau_2)e^{j\Omega_c d\sin(\theta)/c} \\ \vdots \\ A(t-\tau_M)e^{j(M-1)\Omega_c d\sin(\theta)/c} \end{bmatrix}. \tag{4.3}$$

If the incoming signal is a narrowband signal, $A(t - \tau_k) \approx A(t - \tau_1)$ for $k = \{2, \dots, M\}$; then the snapshot vector becomes

$$\mathbf{r}(t) = A(t-\tau_1)e^{j\Omega_c(t-\tau_1)} \begin{bmatrix} 1 \\ e^{j\Omega_c d\sin(\theta)/c} \\ \vdots \\ e^{j(M-1)\Omega_c d\sin(\theta)/c} \end{bmatrix} = s(t-\tau_1) \begin{bmatrix} 1 \\ e^{j\Omega_c d\sin(\theta)/c} \\ \vdots \\ e^{j(M-1)\Omega_c d\sin(\theta)/c} \end{bmatrix}. \tag{4.4}$$

The narrowband assumption requires the product of signal bandwidth W and the maximum signal propagation time across the elements of the array ΔT (the propagation time across the diameter of the array) to be much smaller than 1, that is $W \times \Delta T \ll 1$ ($\Delta T = (M-1)d/c$ for ULA). In other words, with the narrowband assumption, the amplitude $A(t)$ of message bearing signal varies so slow that its variation over the time-interval of signal propagation across the elements of the array can be ignored. Equivalently, the diameter of the array can be considered to be so small that the incoming wave is intercepted by the elements of the array almost simultaneously.

By introducing the wavelength $\lambda = c/f_c$ where $f_c = \Omega_c/2\pi$, and wavenumber $k = 2\pi/\lambda$, the snapshot vector can also be written as

$$\mathbf{r}(t) = s(t-\tau_1)\begin{bmatrix} 1 \\ e^{jkd\sin\theta} \\ \vdots \\ e^{j(M-1)kd\sin\theta} \end{bmatrix} = r_1(t)\begin{bmatrix} 1 \\ e^{jkd\sin\theta} \\ \vdots \\ e^{j(M-1)kd\sin\theta} \end{bmatrix} = r_1(t)\begin{bmatrix} 1 \\ e^{j\omega^s} \\ \vdots \\ e^{j\omega^s(M-1)} \end{bmatrix}. \tag{4.5}$$

Here $\omega^s = kd\sin(\theta)$ is the spatial frequency. From (4.5), we note that the elements of the snapshots vector $\mathbf{r}(t)$ are identical in magnitude, but differ in phase. The direction of arrival estimation problem with this model corresponds to the estimation of the phase progression over the elements of the snapshot vector. From (4.5), we see that for ULA, the phase progression between two consecutive sensors (elements of snapshot vector) is $kd\sin(\theta)$ radians, that is $kd\sin(\theta)$ radians per d meters measured over the straight line that ULA is placed. We interpret the phase progression as a spatial frequency of $\omega^s = kd\sin(\theta)$. We adopt the notation of ω^s to be compatible with earlier discussions on the frequency estimation; in spite of the practice of using wavenumber vector $\mathbf{k}$ notation for the same concept.

We note that to estimate DOA parameter θ uniquely, it is important not to have spatial aliasing, i.e. the grating lobes in beamforming terminology. For this reason, the spatial frequency should be in the range of $[-\pi, \pi]$. This requirement induce an additional constraint on inter-element spacing of the antenna array. The inter element spacing should be equal or smaller than $\lambda/2$, i.e $d \leq \lambda/2$. When this condition is satisfied, there is no ambiguity in the DOA estimation and the estimates are limited to the interval $[-90°, 90°]$.

4.2 DOA Estimation with Uniform Linear Array: Periodic Wave with Multiple Harmonics

This section extends the earlier results for the monochromatic wave to general periodic waves with harmonics. It is assumed that the incoming wave can be written in the following form:

$$s(t) = \sum_{l=1}^{L} \alpha_l e^{jl\Omega_0 t}. \tag{4.6}$$

Here L is the total number of harmonics, Ω_0 is the fundamental frequency in radians per second and α_l is the complex-valued Fourier series coefficient of the periodic waveform.

The previous discussion given for the monochromatic wave can be considered as the special case of $s(t)$ in (4.6) for $L = 1$. Repeating the same arguments given for a monochromatic wave for all harmonics $l = \{1, \ldots, L\}$, we can extend the snapshot vector expression in (4.4) and (4.5) to

$$\mathbf{r}(t) = \sum_{l=1}^{L} \alpha_l e^{jl\Omega_0(t-\tau_1)} \begin{bmatrix} 1 \\ e^{jl\Omega_0 d\sin(\theta)/c} \\ \vdots \\ e^{j(M-1)l\Omega_0 d\sin(\theta)/c} \end{bmatrix} = \sum_{l=1}^{L} \alpha_l e^{jl\Omega_0(t-\tau_1)} \begin{bmatrix} 1 \\ e^{jl\omega^s} \\ \vdots \\ e^{j(M-1)l\omega^s} \end{bmatrix}. \tag{4.7}$$

Here $\omega^s = kd\sin(\theta)$ is the fundamental spatial frequency. The main assumption in this extension is the validity of narrowband approximation for all harmonics. It is easy to see that if the narrowband assumption is satisfied for the K'th harmonic; it is guaranteed to be satisfied for all harmonics with a smaller index $k < K$. Hence, it is sufficient to check the narrowband assumption for the harmonic component with the maximum frequency to verify the assumption.

In many applications, to increase the estimation accuracy, several snapshot vectors are collected, $\{\mathbf{r}(t_1), \mathbf{r}(t_2), \ldots, \mathbf{r}(t_N)\}$. Typically, the set of snapshots are first temporally processed in order to increase the operational SNR. The temporal processing for the maximum SNR improvement under white noise conditions is known to be the matched filtering operation. The matched filtering operation for signal $s(t)$ given in (4.6) corresponds to Fourier transformation and this operation can be implemented via a temporal-DFT operation. Considering (4.7), let's assume that N snapshot vectors are generated by uniformly sampling operation, that is $\mathbf{r}[n] = \mathbf{r}(nT_s)$ for $n = \{1, \ldots, N\}$ where T_s is the sampling period. Taking the Fourier transform in the temporal direction, that is taking the Fourier transform of N samples of collected by each sensor and concatenating the Fourier transform outputs at the frequency ω, we get:

$$\mathrm{DTFT}_N\{\mathbf{r}[n]\}(\omega) = \sum_{l=1}^{L} \alpha_l \mathrm{DTFT}_N\{e^{jl\Omega_0(nT_s-\tau_1)}\}(\omega) \begin{bmatrix} 1 \\ e^{jl\omega^s} \\ \vdots \\ e^{j(M-1)l\omega^s} \end{bmatrix}. \tag{4.8}$$

Here, $\mathrm{DTFT}_N\{\cdot\}(\Omega)$, with some abuse of notation, denotes the discrete-time Fourier transform of N-point input evaluated at the spectrum sample ω. If we examine the extreme cases, for $N = 1$, that is for a single snapshot vector, (4.8) is identical to (4.7). As $N \to \infty$, $\mathrm{DTFT}_N\{e^{jl\Omega_0(nT_s)}\}(\omega)$ approaches $2\pi\delta(\omega - l\Omega_0 T_s)$. Hence, as $N \to \infty$; we have

$$\lim_{N\to\infty} \mathrm{DTFT}_N\{\mathbf{r}[n]\}(\omega) = 2\pi \sum_{l=1}^{L} \alpha_l e^{-jl\Omega_0\tau_1}\delta(\omega - l\Omega_0 T_s) \begin{bmatrix} 1 \\ e^{jl\omega^s} \\ \vdots \\ e^{j(M-1)l\omega^s} \end{bmatrix}. \tag{4.9}$$

The case of $N \to \infty$ shows that harmonics can be isolated after DTFT operation, that is one and at most one term of the summation in (4.9) is non-zero, by the temporal Fourier transform operation as $N \to \infty$.

In this study, we assume that a total of N snapshots are made available and as a pre-processing operation, a temporal DTFT over N snapshots are calculated as in (4.8). We interpret the DTFT output given in (4.8) evaluated at $\omega = \omega_0 \triangleq \Omega_0 T_s$, given below,

$$\mathrm{DTFT}_N\{\mathbf{r}[n]\}(\omega_0) = \sum_{l=1}^{L} A_l \begin{bmatrix} 1 \\ e^{jl\omega^s} \\ \vdots \\ e^{j(M-1)l\omega^s} \end{bmatrix} \tag{4.10}$$

as the input to the spatial frequency estimation algorithm to be described next. Here

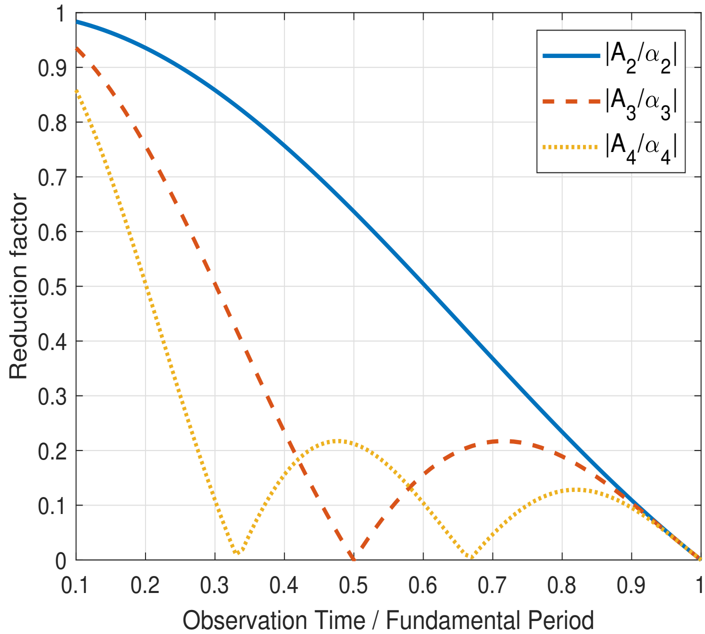

Figure 4.2: Reduction factor of second, third and fourth harmonics ($\omega_0 = 2\pi/200$).

$A_l = \frac{\alpha_l}{N}\text{DTFT}_N\{e^{jl\Omega_0(nT_s-\tau_1)}\}(\omega_0) = \frac{\alpha_l}{N}e^{-jl\Omega_0\tau_1}\text{DTFT}_N\{e^{jl\omega_0 n}\}(\omega_0)$ is the complex amplitude of l'th harmonic after pre-processing.

To study the effect of suggested preprocessing operation, we introduce a reduction factor definition for the pre-processign operation:

$$\text{Reduction Factor}_l(\omega_0, N) \triangleq \left|\frac{A_l}{\alpha_l}\right| = \frac{1}{N}\left|\frac{1-e^{j\omega_0 N(l-1)}}{1-e^{j\omega_0(l-1)}}\right| = \frac{1}{N}\left|\frac{\sin(\omega_0 N(l-1)/2)}{\sin\left(\omega_0(l-1)\right)/2}\right|. \tag{4.11}$$

The reduction factor can be interpreted as the magnitude ratio of harmonics in spatial (A_l) and temporal dimensions (α_l). It can be easily verified that $A_l/\alpha_l = 1$, that is, the fundamental component is not attenuated by pre-processing.

Figure 4.2 shows the reduction factor for a time-domain signal whose fundamental period is 200 samples, ($\omega_0 = \Omega_0 T_s = 2\pi/200$). The x-axis of this figure indicates the ratio of number of samples at the pre-processing stage (N) to the fundamental period of the signal, which is 200 samples in this case. To better explain, if $N = 100$ samples are combined in the pre-processing stage; this combination corresponds to the x-axis point of 0.5 in Figure 4.2. We can observe from Figure 4.2 that, for this case, the third harmonic completely vanishes after pre-processing; while the second harmonic is reduced by a factor of ≈ 0.64. Hence, with a relatively low number of snapshots at the pre-processing stage, say observation time to fundamental period ratio is less than 0.2, the spatial frequency estimation problem becomes a fundamental frequency estimation with possibly significant harmonic amplitudes. We note that the reduction factor definition in (4.11) is a variable of ω_0 and N for a given harmonic order l. When $\omega_0 \ll 1$, the reduction factor is not strong function of ω_0. Hence, if the time-domain signal is sampled such that its fundamental period is hundreds of samples after sampling; the reduction factor values for this signal are almost identical to ones given in Figure 4.2.

4.3 Direction of Arrival Estimation for Periodic Signals

In Section 4.2, the direction of arrival estimation of periodic signals is studied and it has been shown that the problem of direction of arrival, after a pre-processing stage, reduces to a fundamental frequency estimation problem. The expression in (4.10) shows the pre-processing output in the absence of noise. In the presence of noise, we can follow the same steps and get the following expression for the pre-processing output,

$$r_{\text{DTFT}}[m] = \sum_{l=1}^{L} A_l e^{j(\omega^s lm+\phi_l)} + w[m], \quad m = \{0, \ldots, M-1\}. \tag{4.12}$$

Here M is the number of sensors, L is the total number of harmonics, $r_{\text{DTFT}}[m]$ is the m'th element of the pre-processing output vector $\text{DTFT}_N\{\mathbf{r}[n]\}(\omega_0)$ given in (4.10). The variable m denotes the sensor index and $\omega^s = kd\sin\theta$ is the spatial frequency to be estimated, since the pre-processing operation is a linear operation, the Gaussian noise at the input of the pre-processing block remains Gaussian distributed at the output of the block. The term indicated with $w[m]$ in (4.12) shows the resultant additive Gaussian noise after pre-processing. Noise is assumed to be circularly symmetric complex Gaussian distributed with zero mean and variance σ_w^2, as before.

It can be seen from (4.12) that the problem of spatial frequency estimation is identical to the fundamental frequency estimation that has been previously studied in earlier chapters. Hence, we suggest applying the method given in Section 3.5 for the estimation of ω^s. Once, ω^s is estimated as $\widehat{\omega}_s$; the DOA estimate is generated via

$\widehat{\theta} = \sin^{-1}(\widehat{\omega}_s/(kd))$ which reduces to $\widehat{\theta} = \sin^{-1}(\widehat{\omega}_s/\pi)$ for ULA with $d = \lambda/2$. The CRB for $\widehat{\theta}$ can be easily calculated from the CRB of $\widehat{\omega}_s$,

$$\text{var}(\widehat{\omega}_s) \geq \frac{6\sigma_w^2}{M(M^2-1)\sum_{l=1}^{L} A_l^2 l^2}, \tag{4.13}$$

via CRB$(g(x)) =$ CRB$(x)(\frac{\partial g}{\partial x})^2$ relation from [2], by taking $g(x) = 2\pi d \sin(x)/\lambda$ as

$$\text{var}(\widehat{\theta}) \geq \frac{6\sigma_w^2 \lambda^2}{(2\pi)^2 d^2 M(M^2-1)\cos(\theta)^2 \sum_{l=1}^{L} A_l^2 l^2} \ (\text{radian}^2). \tag{4.14}$$

In Figure 4.3, the square root of CRB is shown with respect to PSNR for different angles and total number of sensors. As expected, the CRB values are smaller for setups with higher number of sensors (M) and when the target is located closer to the boresight. It should be remembered that the 3 dB beamwidth of ULA is $\frac{\lambda}{Md\cos\theta}$ radians for a target located at the angle θ. The denominator term in the 3 dB beamwidth expression, that is $Md\cos\theta$, corresponds to the extend of the aperture when projected towards the direction of incoming wave. In Figure 4.4, the ratio of root CRB to 3 dB beamwidth is shown. The normalization operation removes the dependency of the target angle on CRB and it can be seen that an accuracy on order of 1/100'th of 3 dB beamwidth is possible beyond 10 dB PSNR value.

Conventional DOA estimation systems do not take into account the signal power in higher harmonics. For communication/localization systems in radio-frequency (RF) bands, the transmitted spectrum can be indeed very narrowband. In many cases, the center-frequency and the instantaneous bandwidth ratio can be on the order of tens or more. For such systems, the information bearing signal can be considered as a monochromatic wave and conventional DOA estimation approaches are essentially developed for this setup. We note that the CRB expression for the conventional systems with no harmonics is the special case of (4.14) for $A_2 = A_3 = \ldots = A_L = 0$.

For underwater and free-space acoustic applications, the power in the harmonics can be significant in some applications. Figure 4.5 gives a CRB comparison of systems using only fundamental component and all available harmonics. For illustration simplicity, we consider the case of $L = 3$ harmonics and take $A_1 = 1$ and A_2, A_3 as free variables are in the range $[0, 1]$. For a DOA system utilizing only the fundamental frequency, the sum in the denominator of the CRB expression in (4.14) becomes

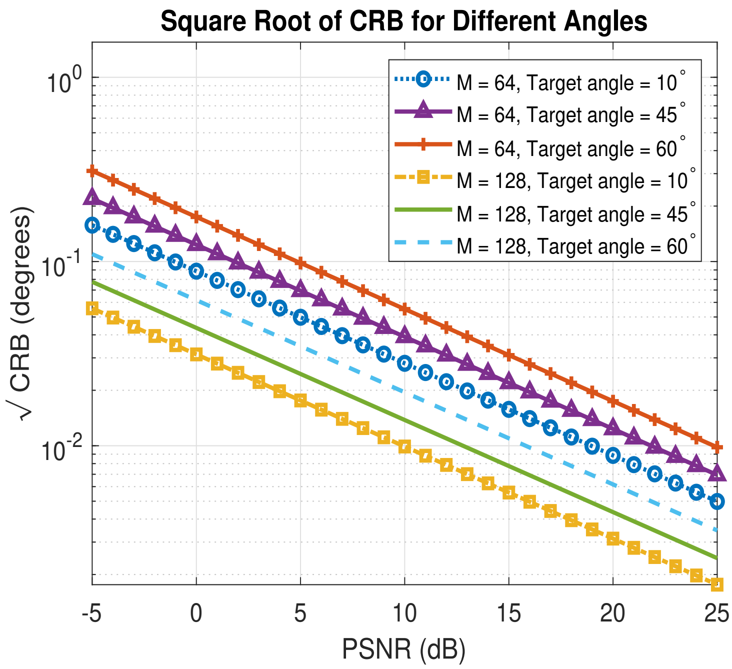

Figure 4.3: Square root of CRB for different target angles and total number of sensors ($d = \lambda/2$).

$\sum_{l=1}^{L} A_l^2 l^2 = 1$. While for a DOA system, utilizing all three harmonics, we have $1 + 4A_2^2 + 9A_3^2$. Hence, a conventional system utilizing only the power in the fundamental frequency requires $10\log_{10}(1 + 4A_2^2 + 9A_3^2)$ dB more power to reach the CRB of system using all three harmonics. Figure 4.5 shows the additional power (in dB) for the conventional system to reach the CRB of system using all three harmonics.

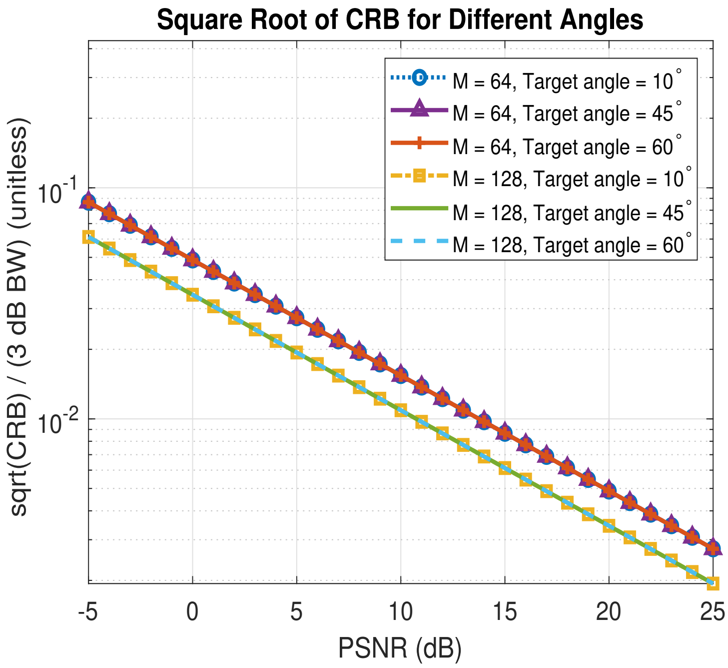

Figure 4.4: Square Root of CRB normalized to 3 dB beamwidth of ULA array for different target angles and total number of sensors ($d = \lambda/2$).

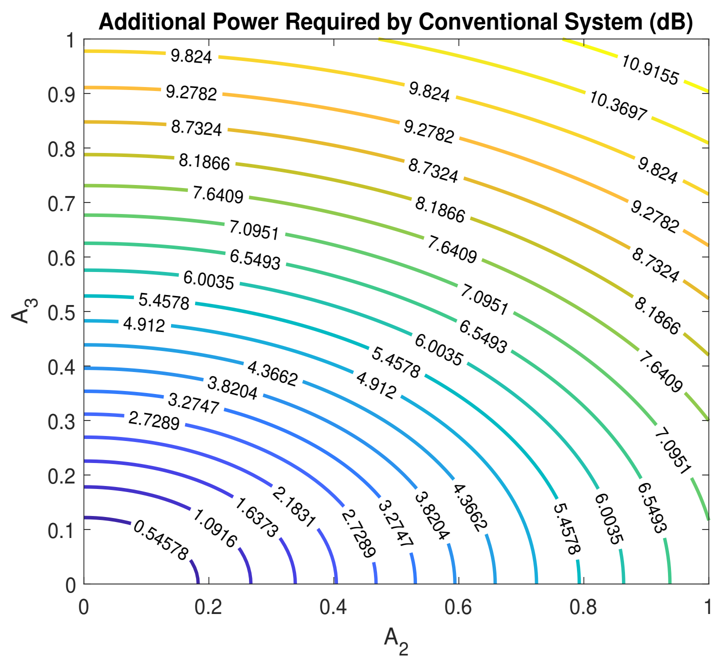

Figure 4.5: Additional power in dB required by the conventional DOA system ($A_1 = 1, A_2 = A_3 = 0$) to operate at the CRB of the system utilizing three harmonics ($A_1 = 1, A_2 \in [0, 1], A_3 \in [0, 1]$)

CHAPTER 5

NUMERICAL RESULTS

In this chapter, the simulation results of the proposed estimator are provided in comparison with some conventional methods. MLE in (3.21), MUSIC and ESPRIT (see Appendices A.1 and A.2) methods are selected to represent the conventional methods. In these simulation results, HCRB/ACRB is illustrated as a lower bound on the performance (see Section 3.2). Comparisons are given in three sets. In the first set, a performance comparison is given for the basic version of the suggested method without model order selection. In the second set, the effect of model order selection is examined. In the third set, a performance comparison for the spatial frequency estimation problem, that is the direction of arrival estimation problem, is given.

Before giving the details on the performance comparisons, we would like to briefly mention the computational complexity of methods in comparison. In Table 5.1, the computation time of the MATLAB implementation of algorithms is given for PSNR of 20 dB and $N = 64$ via averaging over 10000 realizations. We are providing this table to give an idea about the complexity of the suggested method. It can be seen that the suggested method requires 4 to 10 times less central processing unit (CPU) time than other methods. Of course, the CPU times can change depending on the implementation; but it should be evident that, also considering the steps of the suggested method, the suggested method is as efficient as, if not much more efficient, other methods in comparison.

We should note that while producing the simulation results in MATLAB, it is handy to implement proposed method and the MLE by using a matrix for multiple realizations without using a 'for loop', since MATLAB has convenient functions that enables to apply same operation on each row or each column of a matrix such as 'fft' function.

Table 5.1: Computation Time

$N = 64$	Proposed Method	MLE	MUSIC	ESPRIT
$L = 3$	0.0017 sec	0.013 sec	0.0125 sec	0.012 sec
$L = 4$	0.0022 sec	0.016 sec	0.0135 sec	0.012 sec
$L = 5$	0.0028 sec	0.020 sec	0.0140 sec	0.012 sec

However, in MUSIC and ESPRIT, we need to make covariance matrix estimation and eigenvalue decomposition for each realization separately and it is not easy to utilize matrix notation on MATLAB while implementing aforementioned subspace based methods. While generating Table 5.1, matrix implementation is not used to have fair computation time comparison. However, the RMSE vs. PSNR curves of MLE and proposed method presented at following sections are generated by forming a matrix contains each realization for a given PSNR. On the other hand, every operation in MUSIC and ESPRIT is done separately for each realization and this makes the CPU time required for MUSIC and ESPRIT far more larger.

We would like to reiterate that the main purpose of this study is to provide a simple method for the fundamental frequency estimation problem working as good as, or almost as good as more complicated methods in the literature. Table 5.1 is given to provide some evidence to the complexity aspect of this goal.

5.1 Performance Comparison Without Model Order Selection

In Figures 5.1 and 5.2 give the performance comparison for different number of harmonics and harmonic amplitudes. A total of 8 cases are shown and a performance comparison is given in terms of RMSE vs. PSNR sketches. In these comparisons, the number of samples and the fundamental frequency are selected as $N = 64$ and $f_0 = \frac{10+0.2}{64}$, respectively.

The main differences between the scenarios are the number of harmonics (L) and the combination of the harmonic amplitudes $(A_1, \ldots, A_L)$ as presented in the figure labels. It should be noted that A_l denotes the magnitude of the lth harmonic. The phase of harmonics are taken as independent identically distributed (iid) uniform random variables distributed in $[0, 2\pi)$ at each Monte Carlo run.

We know that the gap between the ACRB and the DFT based methods (the proposed method and MLE) is slightly affected by the number of samples. Besides, the fundamental frequency is not a major parameter that impacts the performance of DFT based methods if the harmonics are resolvable. Hence, simulation results for different N and f_0 values are similar to the ones given in this section.

Examining Figures 5.1 and 5.2, DFT based methods are superior than sub-space methods at low PSNR. It is known that subspace based methods are sub-optimal and it is not easy to utilize the harmonic relation between the sinusoidal components to estimate fundamental frequency, since noise subspace eigenvectors $(\mathbf{G})$ in MUSIC does not guarantee whether the fundamental frequency and its harmonics are orthogonal to noise space especially at low PSNR. In a similar way, ESPRIT suffers from this problem while estimating the signal subspace eigenvectors. As observed from the Figures 5.1(a), 5.1(b) and 5.1(c), when the magnitude of the sinusoidal component which has the fundamental frequency $(A_1 e^{j(\omega_0 n + \phi_1)})$ is greater or at least equal to largest harmonic amplitude $(A_1 \geq \max\{A_2, A_3, \ldots A_L\})$, performance of the subspace methods are better when we compare their performances with remaining 5 cases. However, it is easier to make use of harmonic relation for DFT based estimators, that is MLE and the proposed estimator.

For DFT based methods, the PSNR value which estimator starts to track the ACRB differs for different scenarios. There are two reasons. First reason is the poor power distribution among sinusoidal components. Remember that PSNR is defined as PSNR $= \frac{\sum_{l=1}^{L} A_l^2 l^2}{\sigma_w^2}$. However, the coarse frequency estimation stage relies on basically maximizing the relation, $\sum_{l=1}^{L} A_l^2$ (see 3.22). Hence, for a fixed PSNR, as the distribution of power among harmonics changes, the cases with fewer harmonics or the cases with majority power located at low indexed harmonic components helps the operation of first stage that maximizes $\sum_{l=1}^{L} A_l^2$. Hence, if the majority of total power is distributed to low ordered harmonics, the estimators track ACRB at lower PSNR values. We can examine the simulation results in Figure 5.1(a) with Figures 5.1(b) and 5.2(a) to see this effect. In numerical results presented in Figures 5.1(a) and Figure 5.1(b), the total number of harmonics are equal to 2 and 3, respectively. We can see that having a third harmonic component causes poorer detection of the fundamental frequency at coarse search and this results in starting to track ACRB at a higher PSNR value (Figure 5.1(a) at 2 dB PSNR and Figure 5.1(b) at 4 dB PSNR). When we compare the results in Figure 5.1(a) and 5.2(a), the amplitudes are $A_1 = 2A_2$ and $5A_1 = A_2$, respectively. Even if the number of harmonics are the same, having the strongest sinusoidal component at the fundamental frequency improves the performance of the proposed estimator at low SNR region. For these two cases, the required PSNR values to track the ACRB are 2 dB and 15 dB, respectively.

The second effect on the tracking PSNR value can be explained by a case example given in Figures 5.2(b) and 5.2(c) (respectively, harmonic amplitude relations are $5A_1 = A_2 = A_3$ and $5A_1 = 5A_2 = A_3$). In Figure 5.2(c), the third frequency component $(A_3 e^{j(\omega_0 3n+\phi_1)})$ has the greatest magnitude and at low PSNR, first two frequency components remain hidden under noise level. This causes two possible set of frequency sets which are $(\omega_0,\ 2\omega_0,\ 3\omega_0)$ and $(3\omega_0,\ 6\omega_0,\ 9\omega_0)$. However, In Figure 5.2(b), magnitudes of second and third frequencies increase together as the PSNR increases and the ambiguity disappears sooner. This results in late tracking of ACRB, that is at a higher PSNR value for the case illustrated in Figure 5.2(c) (Figure 5.2(b) tracking starts at 7 dB PSNR and Figure 5.2(c) at 16 dB PSNR).

The same result can be observed by comparing the results in Figures 5.2(c) and 5.2(d) with magnitude relations $5A_1 = 5A_2 = A_3$ and $5A_1 = 5A_2 = A_3 = A_4$. Even if there is a one extra harmonic term in Figure 5.2(d), having two strong sinusoidal components improves the detection performance at low PSNR and respectively, at PSNR values 16 dB and 11 dB, RMSE's for these two cases are on the order of ACRB.

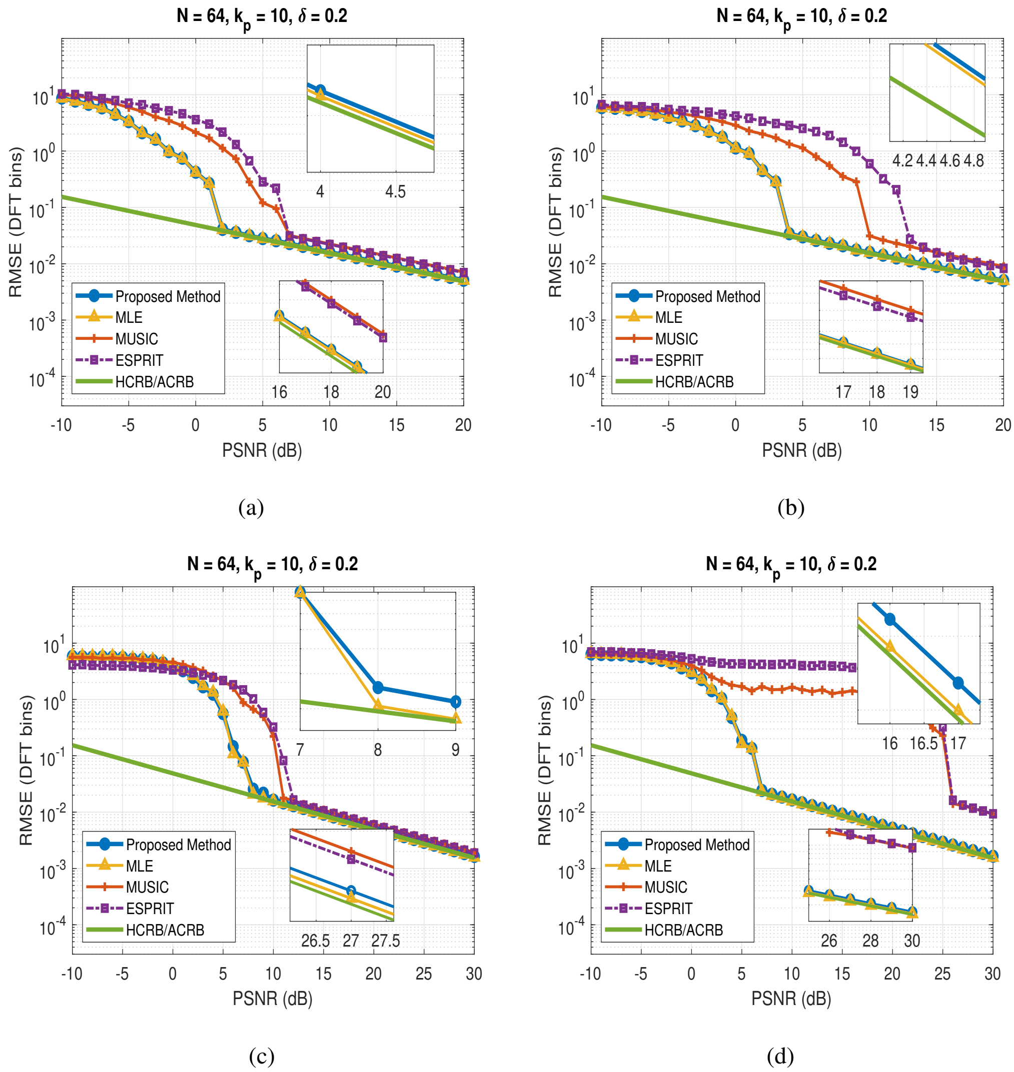

Figure 5.1: RMSE comparison of the proposed method with other methods where $f_0 = \frac{10+0.2}{64}$: (a) $L = 2$ and $A_1 = 2A_2$, (b) $L = 3$ and $A_1 = 2A_2 = 4A_3$, (c) $L = 4$ and $A_1 = A_2 = A_3 = A_4$, (d) $L = 3$ and $A_1 = 10A_2 = A_3$.

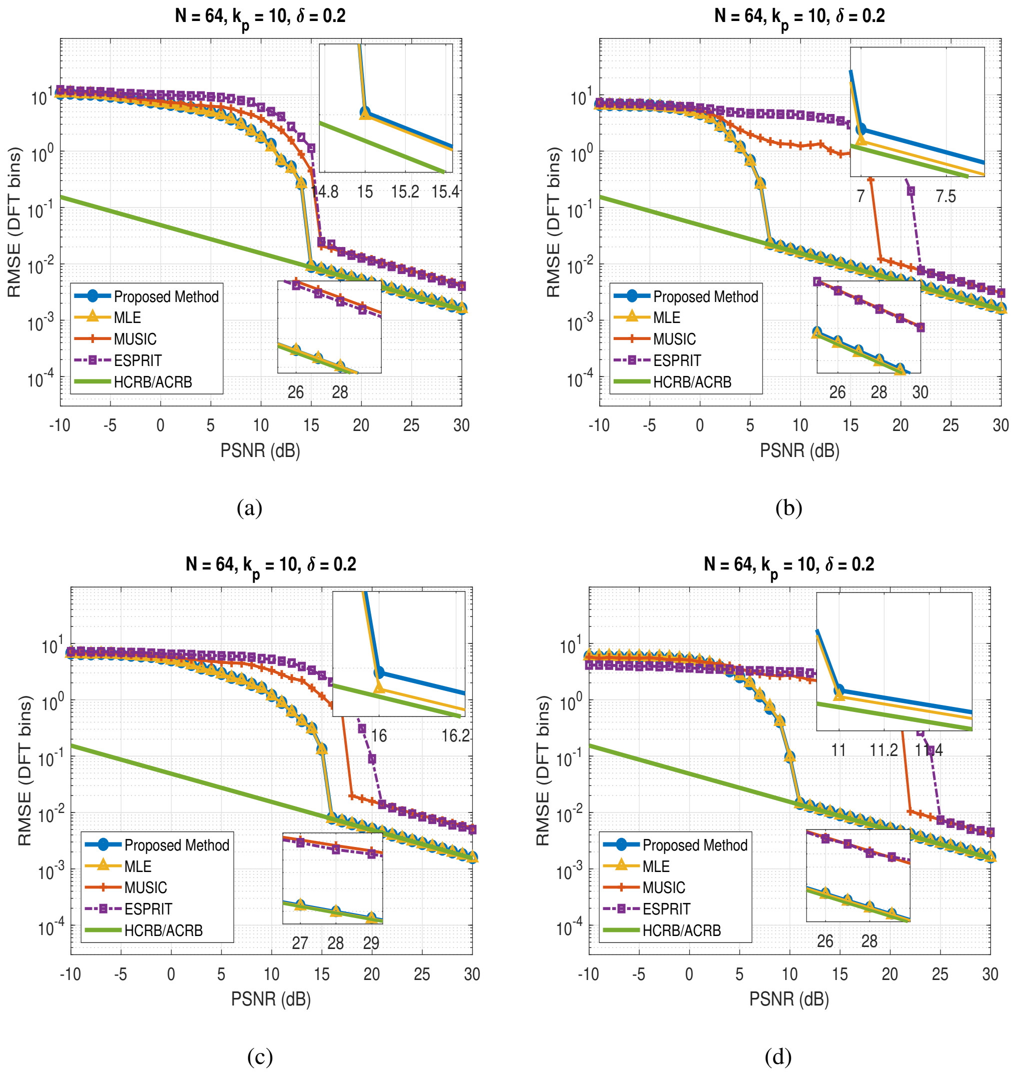

Figure 5.2: RMSE comparison of the proposed method with other methods where $f_0 = \frac{10+0.2}{64}$: (a) $L = 2$ and $5A_1 = A_2$, (b) $L = 3$ and $5A_1 = A_2 = A_3$, (c) $L = 3$ and $5A_1 = 5A_2 = A_3$, (d) $L = 4$ and $5A_1 = 5A_2 = A_3 = A_4$.

5.2 Performance Comparison With Model Order Selection

In this section, the performance of the suggested method is compared with the conventional methods when model order, the total number of harmonics L, is also estimated from data in additional to the frequency. Results given in Chapter 5.1 assume a fixed model order of L which is the true value for the total number of harmonics. Different from earlier study, we assume that L is also an unknown of the problem in this section.

To examine the effect of model order comparison, MDL, HMUSIC and ESTER model selection rules are implemented for respectively DFT-based estimators (MLE and proposed method), MUSIC and ESPRIT. These model order selection rules are discussed in Section 3.4, Appendices A.1 and A.2 respectively. We would like to underline that the model order selection not only generalizes the application range of an algorithm; but can also improve the performance of sub-optimal detectors. As illustrated later, in same scenarios, it is possible achieve better performance by using a different model order than the true model order for some estimators at low SNR conditions. When all harmonics are at a similar power, the information on frequency value can be said to be equally distributed among harmonics. Yet, enforcing the utilization of a harmonic with a little information value, due to low harmonic amplitude, in the estimation process without a proper precaution can lead to poor results. Model order selection enables to use lower model orders at low SNR operational conditions for sub-optimal estimators. Hence, the information in higher order harmonics can be neglected if the information is not very much distinguishable from the noise. We underline that this effect is strictly limited to sub-optimal estimator such as proposed detector, MUSIC and ESPRIT at low SNR operational conditions. An optimal estimator is to utilize any information, however it is noisy, in the estimation process in a correct manner. Unfortunately, the theory of non-random parameter estimation involves only asymptotically optimal results; hence even MLE, which is considered as the benchmark estimator, at low SNR can be positively affected with the model order selection.

Figures 5.3, 5.4, 5.5 and 5.6, give numerical results of the comparisons. In each of these figures, the top sub-figure, labelled as (a), is the performance results with the model order selection; and the bottom sub-figure, labelled as (b), is for a fixed model order of L. In these four figures, we have 4 different cases and on purpose, low power harmonics exist to observe the performance improvement of the model order selection. All numerical experiment parameters are given in respective figure labels.

In all figures, we observe that performance of subspace based methods are positively affected in a dramatic way by the model order selection, since at low PSNR, the noise and signal subspace estimates can get rid of unnecessary (low information bearing) dimensions which are kept under fixed model order operation. Besides, in MLE and proposed method, the main problem is the poor performance of coarse search. For example, in the case illustrated in Figure 5.3, we have two sinusoidal components which are the fundamental frequency and the first harmonic. The magnitude of the harmonic component is so small that it has no significant contribution to the performance up to PSNR $=$ 15 dB. By wrongly choosing the model order as $L = 1$ at low PSNR, the low powered harmonic is essentially ignored. When fixed model order condition, that is $L = 2$, is enforced; the coarse search results in two possible frequency sets, in general: $(\omega_0, 2\omega_0)$ and $(\omega_0/2, \omega_0)$ and selecting the coarse search result as $\omega_0/2$ results in irrecoverable error (gross error). However, by using MAP, only one sinusoidal component (fundamental frequency) is selected and other component is essentially ignored. This leads to a better performance at low SNR. Hence, the model order selection does not only generalize the application range of the suggested method, but also improves its low SNR performance in some cases.

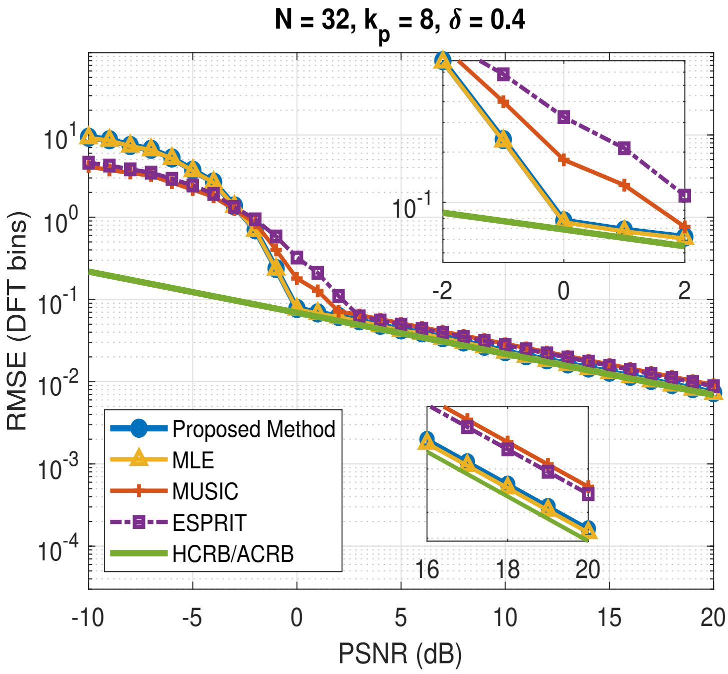

(a)

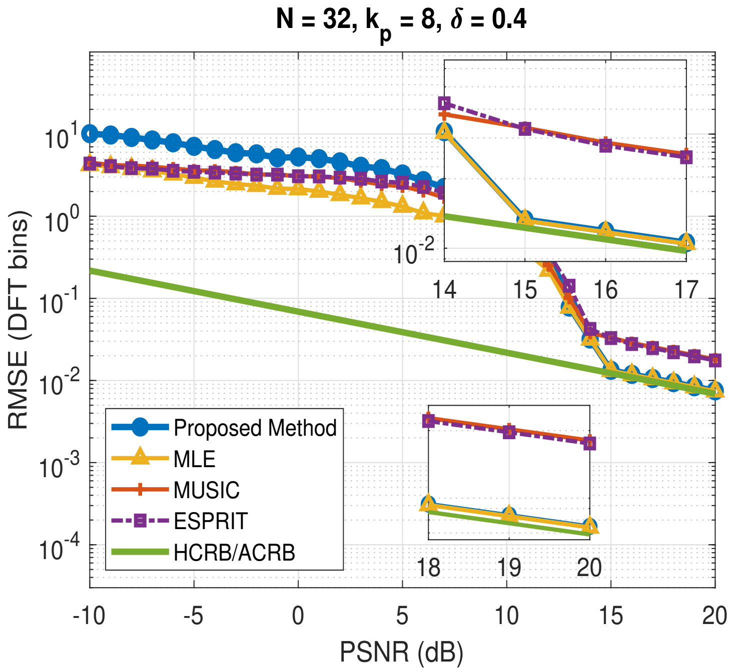

(b)

Figure 5.3: RMSE comparison of the proposed method with other methods where $f_0 = \frac{8+0.4}{32}$, $L = 2$ and $A_1 = 5A_2$: (a) model order selection is made, (b) model order is given.

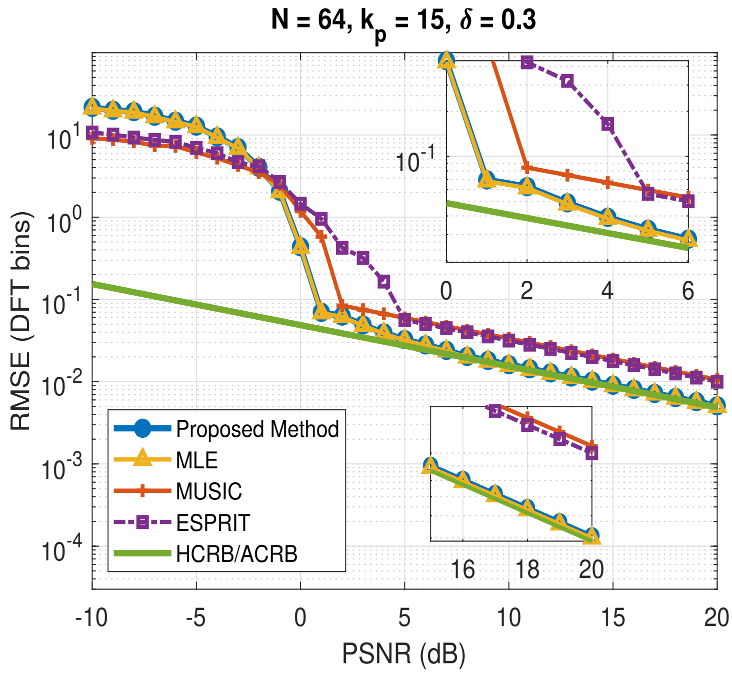

(a)

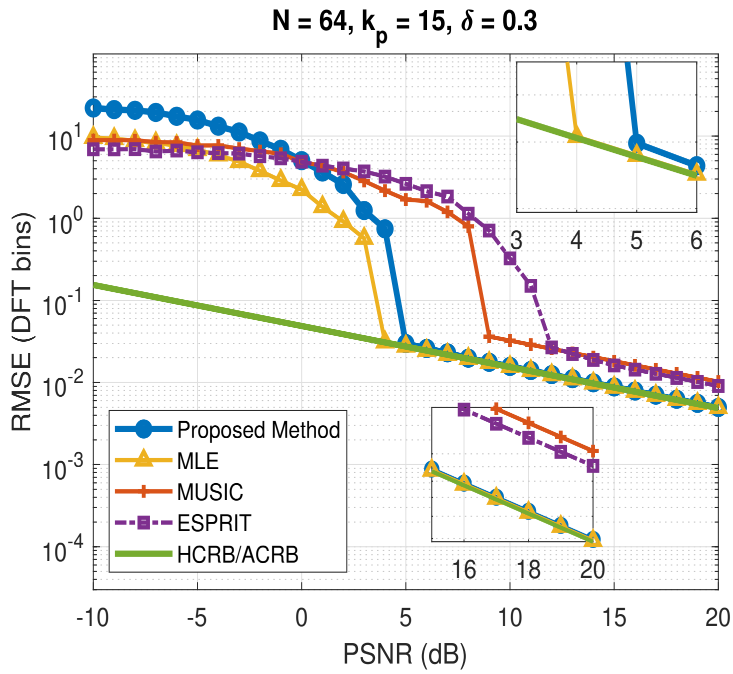

(b)

Figure 5.4: RMSE comparison of the proposed method with other methods where $f_0 = \frac{15+0.3}{64}$, $L = 3$ and $A_1 = 2A_2 = \frac{10}{3}A_3$: (a) model order selection is made, (b) model order is given.

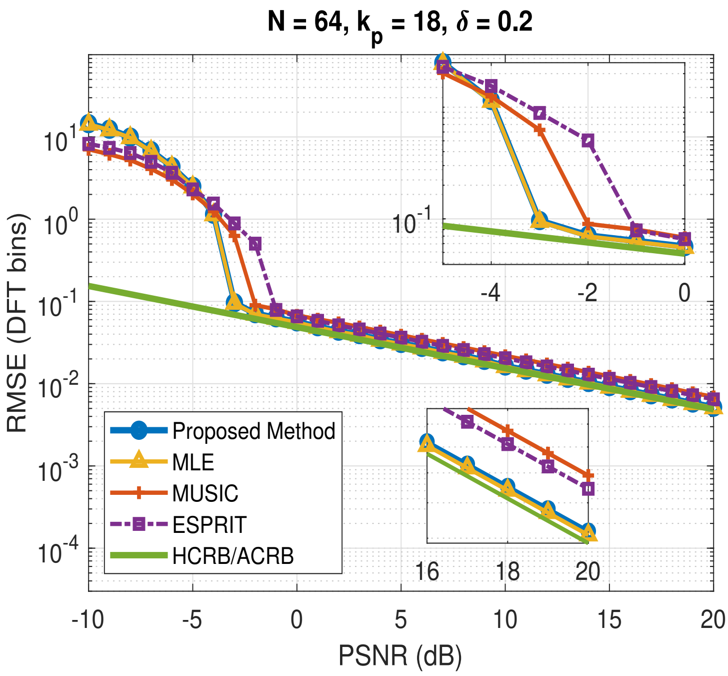

(a)

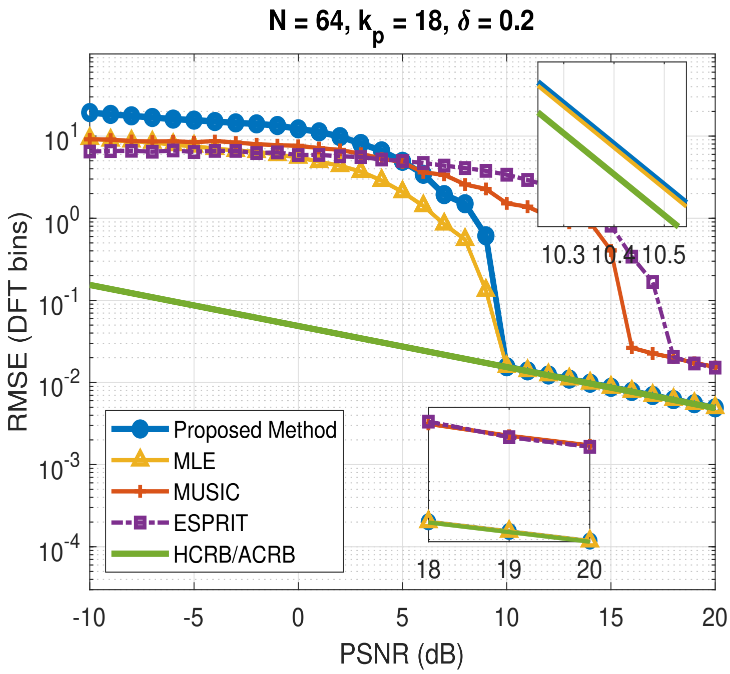

(b)

Figure 5.5: RMSE comparison of the proposed method with other methods where $f_0 = \frac{18+0.2}{64}$, $L = 3$ and $A_1 = 5A_2 = 10A_3$: (a) model order selection is made, (b) model order is given.

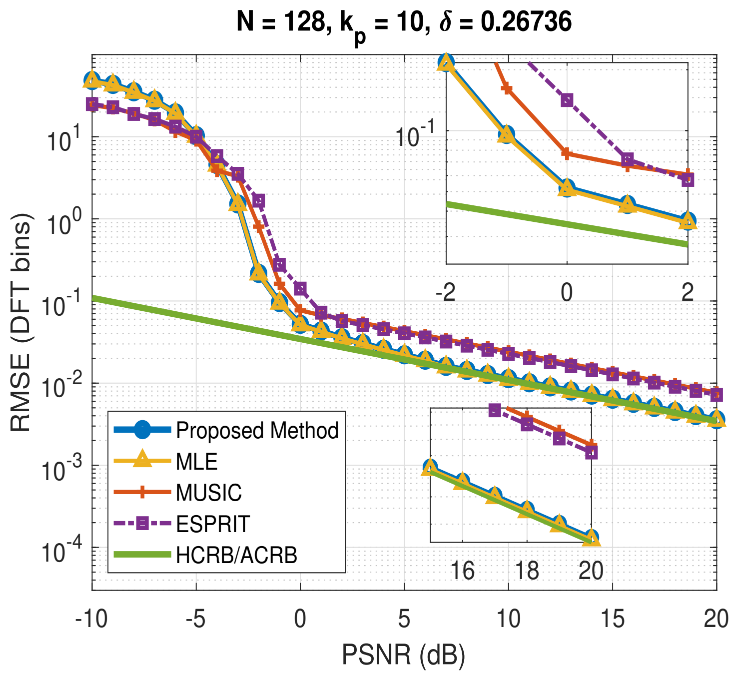

(a)

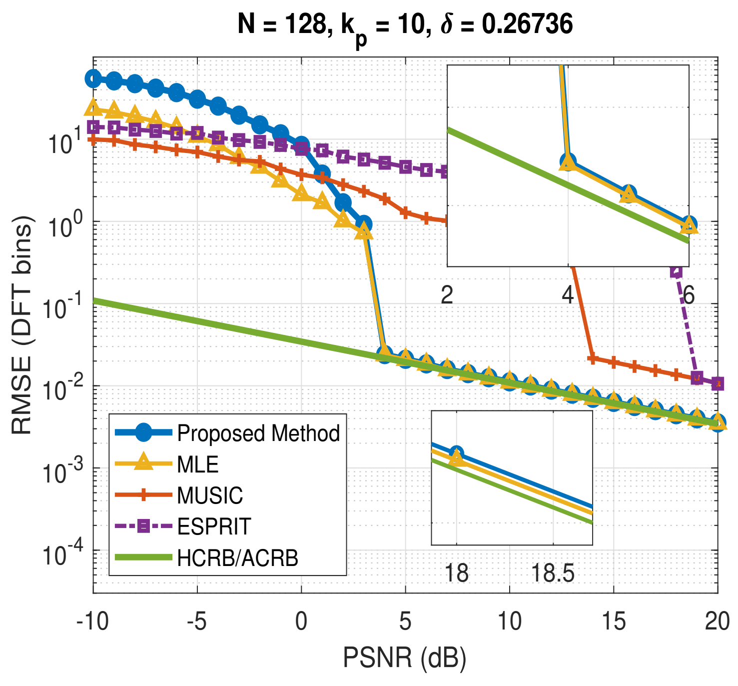

(b)

Figure 5.6: RMSE comparison of the proposed method with other methods where $f_0 = \frac{10+0.26736}{128}$, $L = 4$ and $A_1 = 2A_2 = \frac{10}{3}A_3 = 10A_4$: (a) model order selection is made, (b) model order is given.

5.3 Performance Comparison for Spatial Frequency Estimation

We present the performance comparison of the proposed method with the conventional methods that estimate DOA from the fundamental component. The methods labeled as “MLE (fundamental only)” and “AM (fundamental only)” show the performance of the maximum likelihood and the AM methods, respectively, under the assumption that the input is composed of only fundamental component, i.e. free of harmonics. Hence, the conventional methods operate in mismatch conditions in the presence of harmonics. Neglecting the harmonic components has two important impacts. The first one is the interference generated by the ignored harmonics over the fundamental component. The second one is the reduction in PSNR due to not harnessing the available signal power in harmonics. As expected, the first impact becomes important at high PSNR; while the other becomes important at low PSNR. The numerical comparisons in this section aims to study these effects for different operating conditions.

Figure 5.7 gives the results of a comparison with $M = 64$ sensors for the target angle of 20 degrees. In this comparison, the harmonic amplitudes are related according to $A_1 = 2A_2 = 4A_3$. In 4-6 dB PSNR range of Figure 5.7, the gap between conventional methods and ACRB is large due to the neglected power in harmonic components. This loss is about 4 dB in this example. At high PSNR, the interference of harmonics on the fundamental frequency results in an error floor. In other words, as PSNR increases the interference due to higher order harmonic results in an estimator bias for the conventional methods. This is due to the mismatch of operational conditions and conventional estimator assumptions.

In Figure 5.7, two versions of the proposed method are shown. The proposed method without model order selection (MOS) takes the model order (total number of harmonics) as the true model, which is 3 in this example. The other method, called the proposed method with model order selection, estimates the model order in addition to the DOA. In the high PSNR region of Figure 5.7, the proposed method without model order selection (blue curve) tracks the ACRB better than other methods. With this method, the interference cancellation and harnessing all available power in harmonics yield improved performance. However, at low PSNR, enforcing the model order

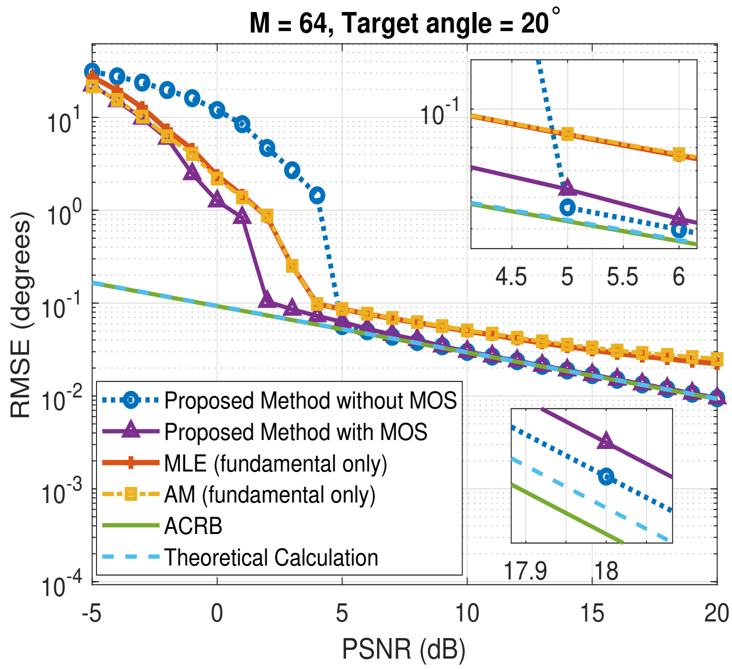

Figure 5.7: Performance comparison of proposed method with conventional methods where $\omega^s = \pi \sin(20°) = 2\pi \frac{10.9446}{64}$, $L = 3$ and $A_1 = 2A_2 = 4A_3$.

as 3 generates spurious fits to the noisy data and the performance of the suggested method becomes poorer than the conventional ones utilizing only the fundamental component. On the other hand, the proposed method with model order selection also selects the model order as 1 (fundamental only) at very low PSNR values and successfully incorporates additional harmonics into estimation procedure as PSNR increases. Hence, the suggested method with its successful model order estimation yields a better performance at all SNR values.

We would like to remind that the antenna spacing of $d = \lambda/2$ does not create any grating lobes or angle ambiguities in beamforming. Here λ corresponds to the wavelength of the propagating wave. For the periodic waves with harmonics, we assume that the antenna spacing of $d = \lambda/2$ is set for the wavelength corresponding to the fundamental harmonic. Hence, the spatial frequencies of higher order harmonics can be folded or aliased. Yet, the folding of spatial frequencies does not create an ambiguity on the final estimate due to the presence of ambiguity-free estimation for the fundamental component. Higher-order harmonics can be considered to refine the estimate generated unambiguously from the fundamental component.

Figures 5.8 and 5.9 show the cases for the target angle of 50 and -60 degrees, respectively, where the frequency folding/aliasing occurs. To illustrate the ambiguity removal in these figures, if the peak location of coarse search (first stage) is at the 25'th bin, then the second harmonic should be at the 50'th bin and the third harmonic should be at the 75'th bin. If $M = 64$, that is there are only 64 bins; the third harmonic is folded to the 11'th bin, since $75 \equiv 11 \mod 64$. Hence, a sufficiently accurate estimate of the fundamental spatial frequency, generated by the first stage of the suggested method, correctly resolves the ambiguities for higher order harmonics. Then, by successfully fusing the DOA estimates generated from each harmonic after interference cancellation; an estimator closely tracking the performance bound for a wide range of SNR values can be constructed.

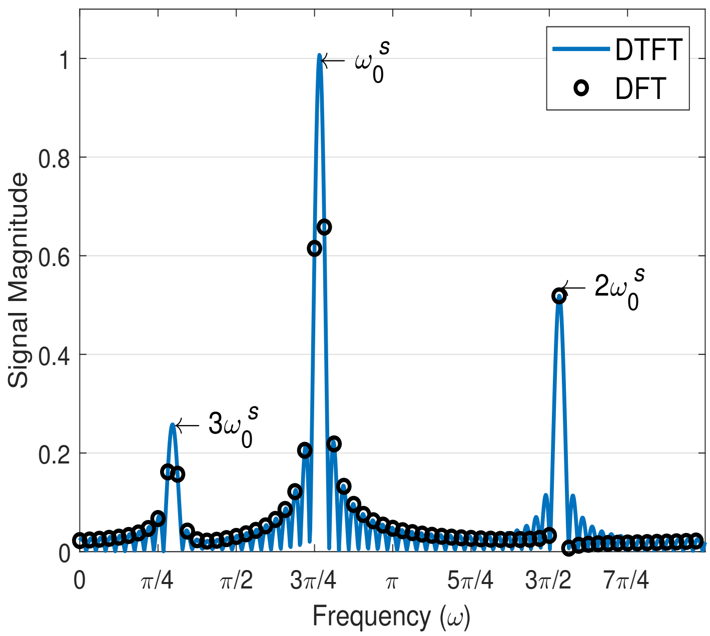

(a)

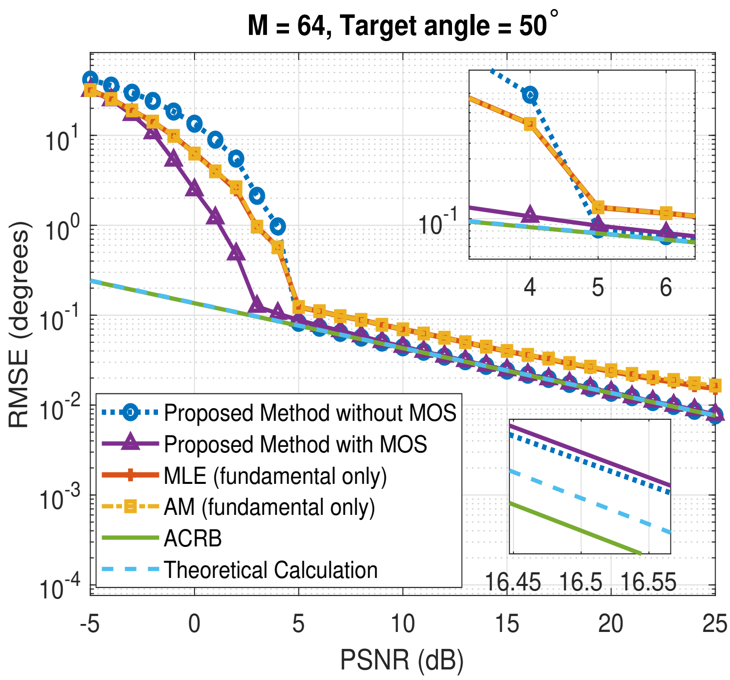

(b)

Figure 5.8: Performance comparison of proposed method with conventional methods under spatial aliasing for DOA estimate where $\omega^s = \pi\sin(50°) = 2\pi\frac{24.5134}{64}$, $L = 3$ and $A_1 = 2A_2 = 4A_3$: (a) DFT and DTFT spectra of the observed signal, (b) Performance comparison.

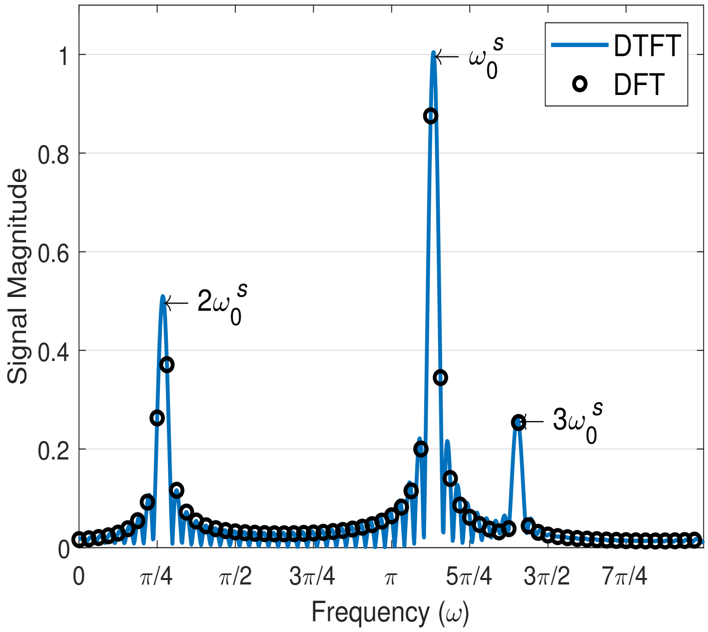

(a)

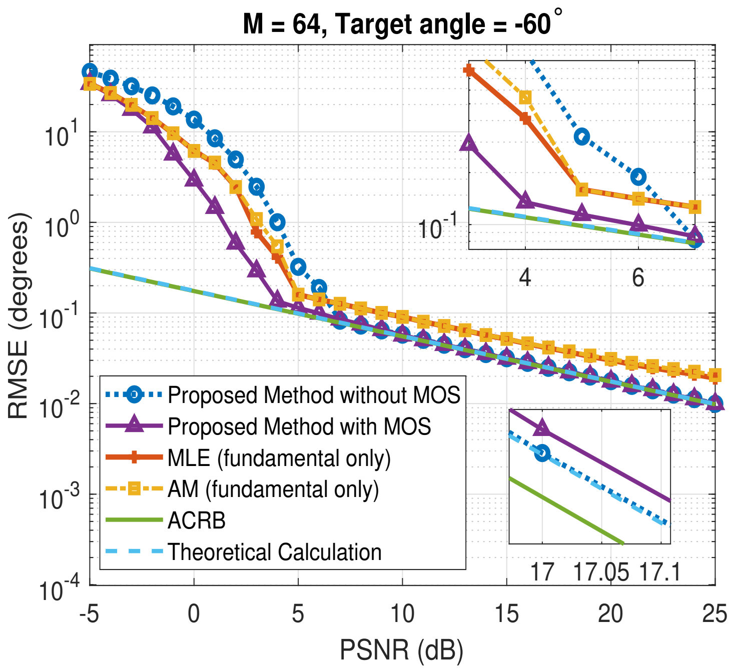

(b)

Figure 5.9: Performance comparison of proposed method with conventional methods under spatial aliasing for DOA estimate where $\omega^s = \pi \sin(-60°) = 2\pi \frac{36.2872}{64}$, $L = 3$ and $A_1 = 2A_2 = 4A_3$: (a) DFT and DTFT spectra of the observed signal, (b) Performance comparison.

CHAPTER 6

CONCLUSION

This thesis studies the problem of fundamental frequency estimation of a periodic signal with multiple harmonics. A computationally efficient method for the solution is given. The method is shown to track the Cramer-Rao bound with a SNR penalty of $10\log_{10}(1.02) = 0.086$ dB in the high SNR region. The suggested method is based on a similarly efficient fine-frequency estimation method, both in computational and statistical sense, known as the Aboutanios-Mulgrew (AM) method. AM method is given for the frequency estimation of single tone complex exponential signals. For the problem of interest, AM method is utilized to estimate the frequency of each harmonic in the framework of successive interference cancellation. The suggested method is also applied to a direction of arrival estimation (DOA) problem.

The literature on the fundamental frequency estimation is rich and several well known spectrum estimation methods, such as MUSIC and ESPRIT, have already been extended to this problem [19]. This thesis study can be considered as the extension of the fine-frequency estimation methods [5–14] to the same problem. Here, we use the AM method in the estimation of harmonic frequencies; any other fine-frequency estimators can also be utilized.

As we mentioned in Section 5.2, the model order selection improves the performance of the given algorithms dramatically at low SNR. However, for high SNR, this operation doesn't improve the performance and only increases the computation. Hence, as a future work, a fused technique can be developed, that is at low SNR, model order selection is implemented to increase the performance and at high SNR, if the model order is given, we don't need any model order selection. In this approach, the main problems are the specification of the low and high SNR values and the boundary of these regions. In [50], sinusoid detection in course frequency estimation stage and the model order selection are performed after calculation of a threshold. The DFT samples with sufficiently high magnitudes which are larger than the threshold are considered as candidates for the frequency of interest and this threshold is calculated so that a fixed probability of false alarm is provided (Neymann–Pearson criterion). The necessity of the noise variance estimation is the main concern in this approach. However, this concept can be a starting point for the mentioned fusion technique for model order estimation. Also, the penalty term of the MAP approach derived in [19] can gives us an idea for the specification of the undesired harmonics in the course frequency estimation stage.

The proposed method is a computationally efficient method. However, as the number of harmonics increases, the number of 'for loops' increases linearly to get an individual estimate of each harmonic (see Algorithm Table 2). The possible improvement of the proposed method is the joint estimation of the frequencies of all harmonics in a single 'for loop'. For this purpose, the successive interference calculation procedure should be updated accordingly. Also, when the multiple periodic signals with harmonics are observed, the multiple fundamental frequency estimation problem for all periodic signals can be a possible extension of this study. For this purpose, the coarse frequency estimation step should be updated. The harmonic summation strategy over a coarse grid given in (3.29) can be modified to get rough fundamental frequency estimates of each periodic signal, that is instead of only taking the maximum summation result in (3.29), for example, the second and third maximum summation results can be taken as the rough fundamental frequency estimates of second and third periodic signal. In addition to this, the interference cancellation should be implemented carefully by taking into account the adverse situations, such as overlapping harmonics of different periodic signals.

Possible extensions of this study can be the tracking of "periodic" signals with time-varying Fourier series coefficients. This is a highly practical problem of music signal processing, since tones generated by the instruments attenuate in time, overlap with other tones etc. An almost identical problem arises in underwater acoustics. More specifically, the problem of tracking ships or underwater vehicles based on the noise generated by their propellers, that is the passive ranging, direction of arrival and tracking problems, can be studied within this context. Another possible extension of this study can be the frequency estimation under non-uniform sampling. In radar signal processing, non-uniform sampling methods are of interest to handle the blind speed problem and to avoid jamming. An efficient method for this problem can be considered as a possible future work of this study.

REFERENCES

[1] P. Stoica and R. Moses, *Spectral Analysis of Signals*. Upper Saddle River, NJ: Pearson Prentice Hall, 2005.

[2] S. M. Kay, *Fundamentals of Statistical Signal Processing, Volume 1: Estimation Theory*. Prentice Hall, 1993.

[3] R. Roy and T. Kailath, “ESPRIT-estimation of signal parameters via rotational invariance techniques,” *IEEE Transactions on Acoustics, Speech, and Signal Processing*, vol. 37, pp. 984–995, July 1989.

[4] R. Schmidt, “Multiple emitter location and signal parameter estimation,” *IEEE Transactions on Antennas and Propagation*, vol. 34, pp. 276–280, March 1986.

[5] E. Jacobsen and P. Kootsookos, “Fast, accurate frequency estimators,” *IEEE Signal Process. Mag.*, vol. 24, pp. 123–125, May 2007.

[6] C. Candan, “A method for fine resolution frequency estimation from three DFT samples,” *IEEE Signal Process. Lett.*, vol. 18, no. 6, pp. 351–354, 2011.

[7] C. Candan, “Analysis and further improvement of fine resolution frequency estimation method from three DFT samples,” *IEEE Signal Process. Lett.*, vol. 20, no. 9, pp. 913–916, 2013.

[8] E. Aboutanios and B. Mulgrew, “Iterative frequency estimation by interpolation on Fourier coefficients,” *IEEE Trans. Signal Process.*, vol. 53, pp. 1237–1242, April 2005.

[9] L. Fan and G. Qi, “Frequency estimator of sinusoid based on interpolation of three DFT spectral lines,” *Elsevier Signal Processing*, vol. 144, pp. 52–60, 2018.

[10] J.-R. Liao and S. Lo, “Analytical solutions for frequency estimators by interpolation of DFT coefficients,” *Elsevier Signal Processing*, vol. 100, pp. 93–100, 2014.

[11] D. Belega and D. Petri, "Frequency estimation by two- or three-point interpolated Fourier algorithms based on cosine windows," *Elsevier Signal Processing*, vol. 117, pp. 115–125, 2015.

[12] B. G. Quinn, "Estimating frequency by interpolation using Fourier coefficients," *IEEE Trans. Signal Process.*, vol. 42, no. 5, pp. 1264–1268, 1994.

[13] M. D. Macleod, "Fast nearly ML estimation of the parameters of real or complex single tones or resolved multiple tones," *IEEE Trans. Signal Process.*, vol. 46, no. 1, pp. 141–148, 1998.

[14] U. Orguner and C. Candan, "A fine-resolution frequency estimator using an arbitrary number of DFT coefficients," *Elsevier Signal Processing*, vol. 105, pp. 17–21, 2014.

[15] C. Candan and U. Çelebi, "Invariant function approach for gridless and non-iterative maximum likelihood parameter estimation and its application to frequency estimation of real-valued sinusoids," *Elsevier Signal Processing*, (under review), 2020.

[16] S. Ye, J. Sun, and E. Aboutanios, "On the estimation of the parameters of a real sinusoid in noise," *IEEE Signal Process. Lett.*, vol. 24, pp. 638–642, May 2017.

[17] S. Djukanoviċ, "An accurate method for frequency estimation of a real sinusoid," *IEEE Signal Process. Lett.*, vol. 23, pp. 915–918, July 2016.

[18] Jian Li and P. Stoica, "Efficient mixed-spectrum estimation with applications to target feature extraction," *IEEE Transactions on Signal Processing*, vol. 44, pp. 281–295, Feb 1996.

[19] M. Christensen and A. Jakobsson, *Multi-Pitch Estimation*. Morgan & Claypool, 2009.

[20] M. Noll, "Pitch determination of human speechby harmonic product spectrum, the harmonic sum, and a maximum likelihood estimate," *Proc. Symposium on Computer Processing Communications*, vol. 32, pp. 779–797, 1969.

[21] D. Hermes, "Measurement of pitch by subharmonic summation," *IPO Annual Progress Report*, vol. 21, pp. 24–33, 1986.

[22] J. Tabrikian, S. Dubnov, and Y. Dickalov, "Maximum a-posteriori probability pitch tracking in noisy environments using harmonic model," *IEEE Transactions on Speech and Audio Processing*, vol. 12, no. 1, pp. 76–87, 2004.

[23] M. G. Christensen, J. H. Jensen, A. Jakobsson, and S. H. Jensen, "On optimal filter designs for fundamental frequency estimation," *IEEE Signal Processing Letters*, vol. 15, pp. 745–748, 2008.

[24] M. G. Christensen, P. Stoica, A. Jakobsson, and S. Holdt Jensen, "Multi-pitch estimation," *Signal Processing*, vol. 88, no. 4, pp. 972 – 983, 2008.

[25] A. Nehorai and B. Porat, "Adaptive comb filtering for harmonic signal enhancement," *IEEE Trans. Acoust. Speech Signal Process.*, vol. 34, pp. 1124–1138, 1986.

[26] V. Pisarenko, "The retrieval of harmonics from a covariance function," *Geophysical Journal of the Royal Astronomical Society*, vol. 33, pp. 347 – 366, 04 2007.

[27] M. G. Christensen, P. Vera-Candeas, S. D. Somasundaram, and A. Jakobsson, "Robust subspace-based fundamental frequency estimation," in *2008 IEEE International Conference on Acoustics, Speech and Signal Processing*, pp. 101–104, 2008.

[28] M. G. Christensen, A. Jakobsson, and S. H. Jensen, "Multi-pitch estimation using harmonic music," in *2006 Fortieth Asilomar Conference on Signals, Systems and Computers*, pp. 521–524, 2006.

[29] M. G. Christensen, S. H. Jensen, S. V. Andersen, and A. Jakobsson, "Subspace-based fundamental frequency estimation," in *2004 12th European Signal Processing Conference*, pp. 637–640, Sep. 2004.

[30] J. Zhang, M. Christensen, J. Dahl, S. Jensen, and M. Moonen, "Robust implementation of the MUSIC algorithm," in *Acoustics, Speech, and Signal Processing, 1988. ICASSP-88., 1988 International Conference on*, pp. 3037–3040, 04 2009.

[31] M. G. Christensen, A. Jakobsson, and S. H. Jensen, "Fundamental frequency estimation using the shift-invariance property," in *2007 Conference Record of the*

Forty-First Asilomar Conference on Signals, Systems and Computers, pp. 631–635, Nov 2007.

[32] R. Badeau, B. David, and G. Richard, "A new perturbation analysis for signal enumeration in rotational invariance techniques," *IEEE Transactions on Signal Processing*, vol. 54, pp. 450–458, Feb 2006.

[33] J. Papy, L. De Lathauwer, and S. Van Huffel, "A shift invariance-based order-selection technique for exponential data modelling," *IEEE Signal Processing Letters*, vol. 14, pp. 473–476, July 2007.

[34] B. N. Bhaskar, G. Tang, and B. Recht, "Atomic norm denoising with applications to line spectral estimation," *IEEE Transactions on Signal Processing*, vol. 61, no. 23, pp. 5987–5999, 2013.

[35] G. Tang, B. N. Bhaskar, and B. Recht, "Near minimax line spectral estimation," *IEEE Transactions on Information Theory*, vol. 61, no. 1, pp. 499–512, 2015.

[36] G. Tang, B. N. Bhaskar, P. Shah, and B. Recht, "Compressed sensing off the grid," *IEEE Transactions on Information Theory*, vol. 59, no. 11, pp. 7465–7490, 2013.

[37] Z. Yang and L. Xie, "On gridless sparse methods for line spectral estimation from complete and incomplete data," *IEEE Transactions on Signal Processing*, vol. 63, no. 12, pp. 3139–3153, 2015.

[38] Z. Yang and L. Xie, "Exact joint sparse frequency recovery via optimization methods," *IEEE Transactions on Signal Processing*, vol. 64, no. 19, pp. 5145–5157, 2016.

[39] U. Celebi and C. Candan, "A computationally efficient fine frequency estimation method for harmonic signals," in *2020 28th Signal Processing and Communications Applications Conference (SIU)*, pp. 1–4, 2020.

[40] R. G. Gallager, "Circularly-Symmetric Gaussian random vectors," 2008. `https://www.rle.mit.edu/rgallager/documents/CircSymGauss.pdf`.

[41] A. V. Oppenheim and R. W. Schafer, *Discrete-Time Signal Processing*. USA: Prentice Hall Press, 3rd ed., 2009.

[42] K. E. Atkinson, *Theoretical Numerical Analysis: A Functional Analysis Framework.* New York:Springer, 2000.

[43] M. G. Christensen, A. Jakobsson, and S. H. Jensen, "Joint high-resolution fundamental frequency and order estimation," *IEEE Transactions on Audio, Speech, and Language Processing*, vol. 15, pp. 1635–1644, July 2007.

[44] F. Gini and R. Reggiannini, "On the use of Cramer-Rao-like bounds in the presence of random nuisance parameters," *IEEE Trans. on Communications*, vol. 48, pp. 2120–2126, Dec 2000.

[45] H. Akaike, "A new look at the statistical model identification," *IEEE Transactions on Automatic Control*, vol. 19, pp. 716–723, December 1974.

[46] J. Rissanen, "Modeling by shortest data description," *Automatica*, vol. 14, p. 465–478, 1978.

[47] P. M. Djuric, "A model selection rule for sinusoids in white Gaussian noise," *IEEE Transactions on Signal Processing*, vol. 44, pp. 1744–1751, July 1996.

[48] P. M. Djuric, "Asymptotic map criteria for model selection," *IEEE Transactions on Signal Processing*, vol. 46, pp. 2726–2735, Oct 1998.

[49] P. Stoica and Y. Selen, "Model-order selection: a review of information criterion rules," *IEEE Signal Processing Magazine*, vol. 21, pp. 36–47, July 2004.

[50] S. Djukanović and V. Popović-Bugarin, "Efficient and accurate detection and frequency estimation of multiple sinusoids," *IEEE Access*, vol. 7, pp. 1118–1125, 2019.

[51] D. Kundu and S. Nandi, *Statistical Signal Processing: Frequency Estimation*. Springer Publishing Company, Incorporated, 2012.

[52] Y. Hua and T. K. Sarkar, "Matrix pencil method for estimating parameters of exponentially damped/undamped sinusoids in noise," *IEEE Transactions on Acoustics, Speech, and Signal Processing*, vol. 38, no. 5, pp. 814–824, 1990.

[53] P. Shah, B. N. Bhaskar, G. Tang, and B. Recht, “Linear system identification via atomic norm regularization,” in *2012 IEEE 51st IEEE Conference on Decision and Control (CDC)*, pp. 6265–6270, 2012.

[54] V. Chandrasekaran, B. Recht, P. A. Parrilo, and A. S. Willsky, “The convex geometry of linear inverse problems,” *Foundations of Computational Mathematics*, vol. 12, p. 805–849, Oct 2012.

[55] B. Dumitrescu, *Positive Trigonometric Polynomials and Signal Processing Applications*. Springer Publishing Company, Incorporated, 2007.

[56] Z. Yang, J. Li, P. Stoica, and L. Xie, “Sparse methods for direction-of-arrival estimation,” in *Academic Press Library in Signal Processing*, vol. 7, ch. 11, pp. 509–581, Academic Press, 2018.

[57] S. Boyd, N. Parikh, E. Chu, B. Peleato, and J. Eckstein, “Distributed optimization and statistical learning via the alternating direction method of multipliers,” *Foundations and Trends in Machine Learning*, vol. 3, pp. 1–122, 01 2011.

APPENDIX A

SUBSPACE METHODS FOR FUNDAMENTAL FREQUENCY ESTIMATION

Subspace methods decompose the observation space into signal and noise spaces. Signal and noise spaces are derived upon the processing of the auto-correlation matrix of the input. The most well known subspace methods are MUSIC and ESPRIT for the frequency estimation, [1]. The main advantage of subspace methods is their application to multiple source/signal problems does not require any more computational resources than a single source/signal problem. On the other hand, the maximum likelihood method suffers from the multi-dimensional search problem when more than one source is present. Even though the subspace methods are computationally less demanding for multi-source problems, they are sub-optimal and require an accurate estimate of the input auto-correlation matrix. In this section, we present some subspace methods for the fundamental frequency estimation problem and also discuss the model order estimation procedures in relation with these methods.

A.1 MUSIC Method

Multiple Signal Classification (MUSIC) [4] relies on the noise subspace estimate. For a single snapshot vector, the subspace decomposition can be done with the autocorrelation matrix estimation as in (3.7), followed by its eigenvalue decomposition. The resultant eigenvectors can be represented as $\mathbf{U} = [\mathbf{u}_1, \mathbf{u}_2, \ldots \mathbf{u}_M]$ where $\mathbf{u}_l$ is the eigenvector that corresponds to the l'th eigenvalue value λ_l. We assume that eigenvalues are sorted in descending order. With the prior information on the total number of harmonics (L), the MUSIC algorithm reduces to

$$\widehat{\omega}_0 = \arg\max_{\omega_0} \frac{1}{||\mathbf{Z}^H(\omega_0)\mathbf{G}||_F}, \tag{A.1}$$

where the matrix $\mathbf{G} = [\mathbf{u}_{L+1}, \mathbf{u}_{L+1}, \ldots \mathbf{u}_M]$ is the noise subspace matrix and $||\cdot||_F$ is the Frobenius norm. The matrix $\mathbf{G}$ is formed by the eigenvectors corresponding to the smallest eigenvalues, $\{\lambda_{L+1}, \lambda_{L+2}, \ldots, \lambda_M\}$.

By using the Cauchy-Schwarz inequality, the normalization term can be added to the cost function in (A.1) so that the number of harmonics and the fundamental frequency can be estimated jointly. The harmonically constrained MUSIC (HMUSIC [29]) method can be written as follows,

$$[\widehat{\omega}_0, \widehat{L}] = \arg\max_{\omega_0, L} \frac{LM(M-L)}{||\mathbf{Z}^H(\omega_0, L)\mathbf{G}(L)||_F^2}, \tag{A.2}$$

where,

$$||\mathbf{Z}^H(\omega_0)\mathbf{G}||_F^2 \leq ||\mathbf{Z}^H(\omega_0)||_F^2 ||\mathbf{G}||_F^2 = LM(M-L). \tag{A.3}$$

and $\mathbf{Z}$ is $M \times L$ Vandermonde matrix.

It is important to note that it is possible to implement MUSIC algorithm without a grid search via what is called the root-MUSIC method. In article [30], a comparison of MUSIC and root-MUSIC is given and MUSIC algorithm is shown to outperform the root-MUSIC.

A.2 ESPRIT Method

ESPRIT stands for the Estimation of Signal Parameters via Rotational Invariance Technique. In the literature, there are several variations of the ESPRIT [3]. The common steps of these variations are signal subspace estimation, generation of an invariant equation by using a symmetry in the signal model and the solution of the invariant equation for the frequency estimation.

Differently from MUSIC, ESPRIT operates with the signal subspace. The eigenvectors of the estimated autocorrelation matrix which have L most significant eigenvalues form the signal subspace matrix $\mathbf{S} = [\mathbf{u}_1, \mathbf{u}_2, \ldots \mathbf{u}_L]$. The relation between signal subspace matrix and Vandermonde matrix $\mathbf{Z}$ defined in (3.4) can be represented as

$\mathbf{S} = \mathbf{ZB}$. We know that range space of Vandermonde and signal subspace matrix are same and the matrix $\mathbf{B}$ is uniquely determined when $L \leq M$. By using the shift invariance property of the matrix $\mathbf{Z}$, we have the relation $\overline{\mathbf{Z}} = \underline{\mathbf{Z}}\mathbf{D}$ where $\overline{\mathbf{Z}}$ and $\underline{\mathbf{Z}}$ are respectively generated by removing the first and last row of the Vandemonde matrix $\mathbf{Z}$ and $\mathbf{D} = [e^{j\omega_0}\ e^{j\omega_0 2}\ \ldots\ e^{j\omega_0 L}]^T$. By simple mathematical manipulations, we can get $\overline{\mathbf{S}} = \underline{\mathbf{S}}\mathbf{D}'$ where $\mathbf{D}' = \mathbf{B}^{-1}\mathbf{DB}$. The matrix $\mathbf{D}'$ can be estimated as $(\underline{\mathbf{S}}^H\underline{\mathbf{S}})^{-1}\underline{\mathbf{S}}^H\overline{\mathbf{S}}$ and its eigenvalues give the frequency estimates, $[e^{j\widehat{\omega}_0}\ e^{j\widehat{\omega}_0 2}\ \ldots\ e^{j\widehat{\omega}_0 L}]$.

The ESTER [32] method is one of the model order estimation methods developed for ESPRIT. The method can be expressed as follows:

$$\begin{aligned}\widehat{L} =& \arg\min_L ||\overline{\mathbf{S}}(L) - \underline{\mathbf{S}}(L)\mathbf{D}'||_2^2 \\ =& \arg\min_L ||\overline{\mathbf{S}}(L) - \underline{\mathbf{S}}(L)[\underline{\mathbf{S}}^H(L)\underline{\mathbf{S}}(L)]^{-1}\underline{\mathbf{S}}^H(L)\overline{\mathbf{S}}(L)||_2^2.\end{aligned} \tag{A.4}$$

SAMOS [33] is another ESPRIT based model order estimation technique:

$$\widehat{L} = \arg\min_L \frac{1}{L}\sum_{i=L+1}^{2L} \gamma_i. \tag{A.5}$$

Here $\{\gamma_i\}_{i=1}^{2L}$ are singular values of the matrix $[\underline{\mathbf{S}}(L)\ \overline{\mathbf{S}}(L)]$ sorted in the descending order.

In article [32], a performance comparison of ESTER and SAMOS is given. Even though, a similar performance for two methods is expected; it has been observed that ESTER allows a wider range of candidate orders. It has been also noted that ESTER is much more efficient to implement. In another study, it has been claimed that for the fundamental frequency estimation problem ESPRIT outperforms MUSIC at high SNR; but, MUSIC performs better at low SNR [31]. A detailed performance comparison of these methods is given in the numerical results chapter of this thesis.

APPENDIX B

ATOMIC NORM DENOISING

In this study, the main concern is the frequency estimation of periodic signals. In recent works, atomic norm techniques [34–38] that utilize the sparsity of the superimposed sinusoidal signals are proposed for the frequency estimation and the main goal is to get optimal frequency estimates by resolving grid mismatch problem. These gridless methods can super-resolve the close frequencies and the number of sinusoidal components slightly increases the computational complexity. In these methods, after denoising the noisy observed signal $(\mathbf{y} = \mathbf{x} + \mathbf{w})$ with atomic norm optimization, the gridless frequency estimation techniques, such as Prony's method [51] and and its variations [3, 4, 52], are applied on the denoised signal $(\widehat{\mathbf{x}})$ to get a frequency estimate. Also, the concept of dual problem and the dual norm of the atomic norm are valuable tools for the determining the frequencies [34]. In [53–56], more detailed information about the sparse representation, atomic norm and other related topics can be obtained.

The fine frequency estimation methods and the atomic norm based techniques are two branches of frequency estimation literature with similar goals. However, a comparison of these approaches are not available in the literature. In this part of the study, we present performance comparison of these two approaches with a simple scenario.

B.1 Atomic Norm Denoising with Alternating Direction Method of Multipliers (ADMM)

In [34, 35], the method of Alternating Direction Method of Multipliers (ADMM) is provided to solve the semi-definite program for the atomic norm denoising problem, since ADMM is known as a reasonably fast method for solving the semi-definite programs [57]. The atomic denoising problem can be expressed with the following semi-definite program,

$$\begin{aligned} \text{minimize}_{t,\mathbf{u},\mathbf{x},\mathbf{Z}} \quad & \tfrac{1}{2}\|\mathbf{x}-\mathbf{y}\|_2^2 + \tfrac{\tau}{2}\left(t+u_1\right), \\ \text{subject to} \quad & \mathbf{Z} = \begin{bmatrix} T(\mathbf{u}) & \mathbf{x} \\ \mathbf{x}^H & t \end{bmatrix} \text{ and } \mathbf{Z} \succeq 0. \end{aligned} \tag{B.1}$$

Here $\mathbf{y} = \mathbf{x} + \mathbf{w}$ is the noisy observed signal, $\mathbf{x}$ is the signal of interest vector with length N. The mapping $T(\mathbf{u}) : \mathbb{C}^N \to \mathbb{C}^{N\times N}$ creates a Hermitian Toeplitz matrix out of its input vector $\mathbf{u}$. For the solution of this semidefinite program, [35] provides a efficient algorithm based upon the ADMM and dualize the equality constraint via an Augmented Lagrangian:

$$\begin{aligned} \mathcal{L}_\rho(t,\mathbf{u},\mathbf{x},\mathbf{Z},\mathbf{\Lambda}) &= \frac{1}{2}\|\mathbf{x}-\mathbf{y}\|_2^2 + \frac{\tau}{2}\left(t+u_1\right) \\ &+ \left\langle \mathbf{\Lambda}, \mathbf{Z} - \begin{bmatrix} T(\mathbf{u}) & \mathbf{x} \\ \mathbf{x}^H & t \end{bmatrix} \right\rangle + \frac{\rho}{2}\left\| \mathbf{Z} - \begin{bmatrix} T(\mathbf{u}) & \mathbf{x} \\ \mathbf{x}^H & t \end{bmatrix} \right\|_F^2 . \end{aligned} \tag{B.2}$$

The update steps of ADMM for line spectral estimation [35]:

$$\begin{aligned} \left(t^{l+1},\mathbf{u}^{l+1},\mathbf{x}^{l+1}\right) &\leftarrow \arg\min_{t,\mathbf{u},\mathbf{x}} \mathcal{L}_\rho\left(t,\mathbf{u},\mathbf{x},\mathbf{Z}^l,\mathbf{\Lambda}^l\right), \\ \mathbf{Z}^{l+1} &\leftarrow \arg\min_{\mathbf{Z}\geq 0} \mathcal{L}_\rho\left(t^{l+1},\mathbf{u}^{l+1},\mathbf{x}^{l+1},\mathbf{Z},\mathbf{\Lambda}^l\right), \\ \mathbf{\Lambda}^{l+1} &\leftarrow \mathbf{\Lambda}^l + \rho\left(\mathbf{Z}^{l+1} - \begin{bmatrix} T\left(\mathbf{u}^{l+1}\right) & \mathbf{x}^{l+1} \\ (\mathbf{x}^{l+1})^H & t^{l+1} \end{bmatrix}\right). \end{aligned} \tag{B.3}$$

The updates with respect to $t, \mathbf{x}$, and $\mathbf{u}$ can be computed in closed form:

$$\begin{aligned} t^{l+1} &= Z^l_{n+1,n+1} + \left(\Lambda^l_{n+1,n+1} - \frac{\tau}{2}\right)/\rho, \\ \mathbf{x}^{l+1} &= \frac{1}{2\rho+1}\left(\mathbf{y} + 2\rho\mathbf{z}_1^l + 2\boldsymbol{\lambda}_1^l\right), \\ \mathbf{u}^{l+1} &= \mathbf{W}\left(T^*\left(\mathbf{Z}_0^l + \mathbf{\Lambda}_0^l/\rho\right) - \frac{\tau}{2\rho}\mathbf{e}_1\right). \end{aligned} \tag{B.4}$$

Here the mapping $T^* : \mathbb{C}^{N\times N} \to \mathbb{C}^N$ is the adjoint of the mapping T, that is by summing the elements of main diagonal and the off-diagonals of the input matrix which is assumed as Hermitian Toeplitz matrix, the vector with length N is taken as an output and $\mathbf{W}$ is the normalization diagonal matrix with entries;

$$\mathbf{W}_{ii} = \begin{cases} \frac{1}{N} & , i = 1, \\ \\ \frac{1}{2(N-i+1)} & , i > 1, \end{cases} \tag{B.5}$$

and the partitions are given as follows:

$$\mathbf{Z}^l = \begin{bmatrix} \mathbf{Z}_0^l & \mathbf{z}_1^l \\ \\ (\mathbf{z}_1^l)^H & Z_{n+1,n+1}^l \end{bmatrix} \text{ and } \mathbf{\Lambda}^l = \begin{bmatrix} \mathbf{\Lambda}_0^l & \boldsymbol{\lambda}_1^l \\ \\ (\boldsymbol{\lambda}_1^l)^H & \Lambda_{n+1,n+1}^l \end{bmatrix}. \tag{B.6}$$

The $\mathbf{Z}$ update is simply the projection onto the positive definite cone;

$$\mathbf{Z}^{l+1} := \arg\min_{\mathbf{Z}\succeq 0} \left\| \mathbf{Z} - \begin{bmatrix} T\left(\mathbf{u}^{l+1}\right) & \mathbf{x}^{l+1} \\ \\ (\mathbf{x}^{l+1})^H & t^{l+1} \end{bmatrix} + \mathbf{\Lambda}^l/\rho \right\|_F^2. \tag{B.7}$$

Projecting a matrix $\mathbf{Z}$ onto the positive definite cone is accomplished by forming an eigenvalue decomposition of $\mathbf{Z}$ and setting all negative eigenvalues to zero.

To summarize, the update for $(t, \mathbf{u}, \mathbf{x})$ requires averaging the diagonals of a matrix (which is equivalent to projecting a matrix onto the space of Toeplitz matrices), and hence operations that are $O(N)$. The update for $\mathbf{Z}$ requires projecting onto the positive definite cone and $O\left(N^3\right)$ operations. The update for $\mathbf{\Lambda}$ is simply addition of symmetric matrices. These steps are taken exactly from the article in [35] and the MATLAB code is given in Section B.3. In the MATLAB implementation, we have a correction in one of the steps of the ADMM implementation given in [35]. After checking the derivation steps, we have corrected the normalization matrix $\mathbf{W}$ as follows:

$$\mathbf{W}_{ii} = \begin{cases} \frac{1}{N} & , i = 1, \\ \\ \frac{1}{N-i+1} & , i > 1. \end{cases} \tag{B.8}$$

After denoising operation with ADMM algorithm, the Prony's method is applied on the denoised signal $(\widehat{\mathbf{x}})$ for the frequency estimation and MATLAB implementation is given in Section B.3.

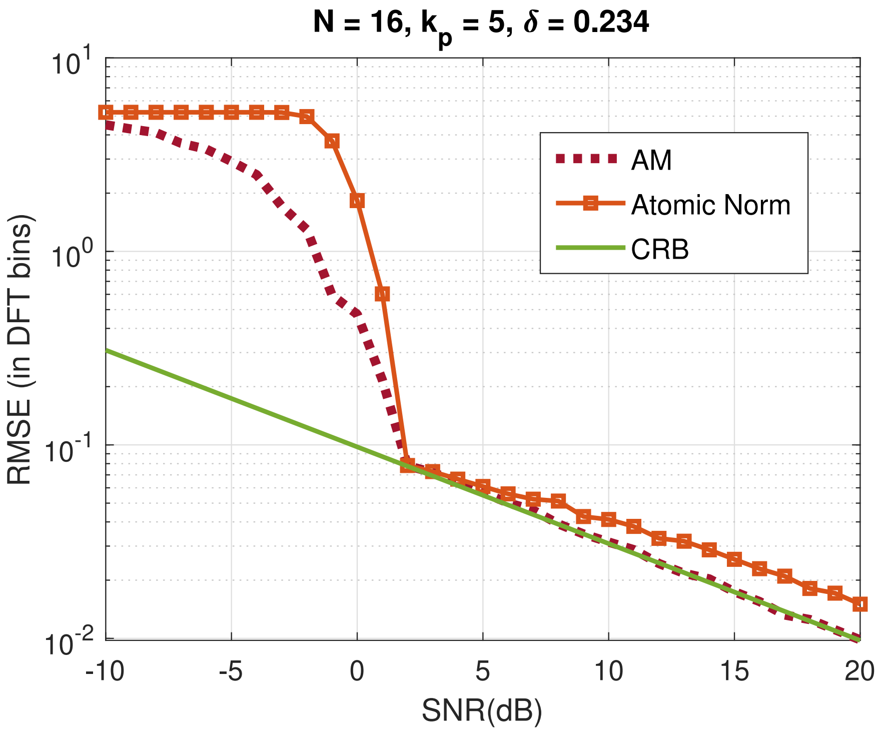

Figure B.1: RMSE and SNR plots for AM and ADMM with Prony's Method with frequency $\omega = \frac{2\pi(5+0.2345)}{16}$.

B.2 Numerical Result

In Figure B.1, performance comparison of the AM algorithm with atomic norm based method given in Section B.1. In this comparison, we have only one sinusoidal component and the number of samples and the frequency are selected as $N = 16$ and $f = \frac{2\pi(5+0.2345)}{16}$, respectively and for the ADMM method, 10000 iterations are used. Also, RMSE's are calculated over 1000 realizations. The performance of the atomic norm based method is inferior than AM method in this scenario. However, it is possible to increase the performance by using more successful frequency estimator methods instead of Prony's method and in this study, we are not interested in performance comparison. The main interest is the computational load of ADMM algorithm. Here, we compare the computation time of two methods on a simple problem to give an idea about their computation load.

In ADMM algorithm, at each iteration, an eigenvalue decomposition is required and the determining the number of iterations required for the denoising operation is not a simple task. In AM algorithm, we know that 2-3 iterations are sufficient to reach CRB for large SNR range (see Section 2.5.1), but in ADMM algorithm, we need lots of iterations and the number of iterations is more than 100 iterations in general. In MATLAB, for one realization, computation time of the AM algorithm is 7×10^{-5} seconds with the settings given for Figure B.1 and the computation time of the ADMM algorithm for only one iteration is 3×10^{-4} seconds and, for example, with 100 iterations, the computation time is around 3×10^{-2} seconds. Simply, the required CPU time for a single estimate generation is on the order of 1000 times more for atomic norm based methods in comparison to the AM method. However, we should note that in the atomic norm based methods, localizing the frequencies using the dual problem [34, 35] is an important concept which makes the model order selection insignificant and provides super-resolution of the close frequencies. Also, when the multiple sinusoidal signals are observed, in AM algorithm, we need to apply successive interference cancellation procedures to get individual frequency estimates of the sources. However, atomic norm based methods are proposed for such scenarios and it is possible to obtain frequencies with slight increase in computation. Yet, the eigenvalue value decomposition is a costly operation and it takes place in each iteration of ADMM based solvers which need lots of iterations.

B.3 MATLAB Implementation

MATLAB implementation of atomic norm denoising with ADMM for frequency estimation is given in Section B.1 [35].

```
function freqest_Atomic_Prony_ = frequency_est_Atomic_norm(y,SNR,maxiter,L)
%frequency_est = frequency_est_Atomic_norm(y,SNR,maxiter)
%
% Returns the frequency estimates for L complex sinusoidal
% signals observed under AWGN.
%
% Implements the method given in
%      "Near Minimax Line Spectral Estimation
%                   APPENDIX A
%   Alternating Direction Method of Multipliers For AST"
% Authors of the article are Gongguo Tang, Badri Narayan Bhaskar
%                 and Benjamin Recht.
% The given ADMM algorithm given in APPENDIX A implemented by
% Cagatay Candan and Utku Çelebi.
%
% Inputs:
%     y:    N x 1 matrix where each column contains an observation
%              vector of N samples
%     maxiter: maximum number of iterations for ADMM algorithm
%     SNR: Signal to noise ratio given for the calculation of
%          accelerated convergence rate (tau)
%     L : number of signals
% Output:
%     freqest_Atomic_Prony: L estimated frequencies with the unit of
%                           N-point DFT bins, i.e. a real number in [0,N]
%                           where N is number of samples
%
%                 To convert est_fused to radian per samples, use
%                             omega  = 2*pi/N*freqest_Atomic_Prony;
%August 2020
N = length(y);
tau = 2*sqrt(N*log(N))*sqrt(1/SNR);
rho = 2;
u = [1; zeros(N-1,1)];
t = 1; x = y;
Z = eye(N+1); Lambda = eye(N+1);
%dum = N:-1:1; dum(1) = 2*N; W = diag(1/2./dum); % in Appendix A
 dum = N:-1:1; dum(1) = N  ; W = diag(1./dum);   % Appendix A correction
% ADMM algorithm for atomic norm denoising
for iter = 1:maxiter
    tnew = Z(end,end) + (Lambda(end,end) - tau/2)/rho;
    xnew = 1/(2*rho+1)*(y + 2*rho*Z(1:end-1,end) + 2*Lambda(1:end-1,end));
    unew = W*(Tadj( Z(1:end-1,1:end-1) + Lambda(1:end-1,1:end-1)/rho )...
           - tau/2/rho*[1;zeros(N-1,1)]);

    dum1 = [toeplitz(unew) xnew; xnew' tnew]; dum = dum1 - Lambda/rho;
    [eigvec,eigval]=eig(dum);
    eigval = real(diag(eigval)); %ignore imaginary part
    eigval(eigval<0) = 0;
    Znew = eigvec*diag(eigval)*eigvec';

    Lambdanew = Lambda + rho*(Znew - dum1);
    Z = Znew; Lambda = Lambdanew;
end;
% Estimation of L frequencies with Prony's method
[Num,Den]=prony(x,L-1,L); q = roots(Den);
% Frequencies in terms of N-Point DFT bins
freqest_Atomic_Prony = mod(angle(q)*180/pi,360)/360*N;
freqest_Atomic_Prony = sort(freqest_Atomic_Prony,'ascend').';
%%
function out = Tadj(A)
N = size(A,1);
out = zeros(N,1);
for ind=1:N,
    out(ind) = sum(diag(A,ind-1));
end;
```